Final report on the ISTC project № 2088p

"THEORETICAL AND EXPERIMENTAL RESEARCH OF CAPABILITIES OF MHD TECHNOLOGY TO CONTROL GAS FLOW WITH NON-EQUILIBRIUM IONIZATION"

The work is performed in Hypersonic Systems Research Institute
of holding company "Leninetz"
St. Petersburg, Russia

2002

REPORT DOCUMENTATION PAGE

Form Approved OMB No. 0704-0188

1. REPORT DATE *(DD-MM-YYYY)*	2. REPORT TYPE	3. DATES COVERED *(From – To)*
10-05-2002	Final Report	02-Jul-01 - 02-Jul-04

4. TITLE AND SUBTITLE

Theoretical and experimental research of capabilities of MHD technology to control gas flow with non-equilibrium ionization

5a. CONTRACT NUMBER
ISTC Registration No: 2088p

5b. GRANT NUMBER

5c. PROGRAM ELEMENT NUMBER

6. AUTHOR(S)

Dr. Alexander Leonidovich Kuranov

5d. PROJECT NUMBER

5d. TASK NUMBER

5e. WORK UNIT NUMBER

7. PERFORMING ORGANIZATION NAME(S) AND ADDRESS(ES)

Leninetz Holding Company, NIPGS
212, Moskovsky Prospekt
St. Petersburg 196066
Russia

8. PERFORMING ORGANIZATION REPORT NUMBER

N/A

9. SPONSORING/MONITORING AGENCY NAME(S) AND ADDRESS(ES)

EOARD
PSC 802 BOX 14
FPO 09499-0014

10. SPONSOR/MONITOR'S ACRONYM(S)

11. SPONSOR/MONITOR'S REPORT NUMBER(S)
ISTC 00-7033

12. DISTRIBUTION/AVAILABILITY STATEMENT

Approved for public release; distribution is unlimited.

13. SUPPLEMENTARY NOTES

14. ABSTRACT

This report results from a contract tasking Leninetz Holding Company, NIPGS as follows: The purpose of the project is the theoretical and experimental research of capabilities of using of MHD technology to control gas flow with non-equilibrium ionization. Cold gas flows will be considered, where thermal ionization of gas flow is negligible. The analysis of various methods of ionization will be carried out, and mathematical models of an ionizer and MHD generator will be developed. Requirements to ionizer, MHD generator and flow parameters at which self-sustained operational mode of ionizer and MHD generator is realized will be formulated. Possibilities of using of MHD control in gas-dynamical systems will be considered. Traditional use of MHD transformation of energy to produce electric power is well understood both theoretically and experimentally nowadays. Nontraditional use of MHD to control flow parameters and hence performance of gas-dynamical systems that include MHD system as a subsystem is not well understood. MHD interaction acts as bulk force and power upon flow and allows varying flow parameters. In this case no mechanical parts are used to control the flow parameters. Therefore, this method of control can be considered as a perspective one for gas-dynamical system with a fixed geometry especially for high enthalpy flows. As a possible range of application for MHD control, two types of gas-dynamical system can be considered: a) gas-dynamical systems which must ensure variable parameters of flow at outlet of system with fixed parameters at inlet of one and b) gas-dynamical systems which must ensure limited range of variation for some flow parameters at outlet of system with variable parameters at inlet. The main requirement to realize MHD influence on flow is flow conductivity. In most gas-dynamical systems thermal ionization of flow is inappreciable and therefore it is necessary to use methods of non-equilibrium plasma creation. Various methods of flow ionization will be analyzed in the project. To ensure autonomous regime of system of MHD control self-sustained operational mode of ionizer and MHD generator is considered. Power spent on flow ionization is expected to be less than power produced by MHD generator for this operational mode.
In process of implementation of the project the next activities will be carried out: theoretical research of methods of non-equilibrium plasma creation; development of mathematical model of an ionizer; numerical calculations of electrical conductivity of plasma; determination of range of parameters, at which self-sustained operational mode of an ionizer and MHD generator exists; development of mathematical models of gas-dynamical systems which include ionizer and MHD generator as subsystems in quasi-1-D and 2-D approaches; numerical calculations of flow-fields in the gas-dynamical systems; determination of conditions at which MHD control appreciably modifies characteristics of investigated systems; development and creation of experimental model of ionizer; experimental testing and modification of mathematical model of ionizer; theoretical research of influence of configuration of magnetic field and various types of MHD generator on flow-field and performance of gas-dynamical system; formulating recommendations to the choice of parameters of ionizer and MHD generator to provide maximal influence on flow-field in gas-dynamical system; development, creation and test of model which includes MHD system for flow control.

15. SUBJECT TERMS
EOARD, Physics, Fluid Mechanics

16. SECURITY CLASSIFICATION OF:			17. LIMITATION OF ABSTRACT	18, NUMBER OF PAGES	19a. NAME OF RESPONSIBLE PERSON
a. REPORT	b. ABSTRACT	c. THIS PAGE			Wayne Donaldson
UNCLAS	UNCLAS	UNCLAS	UL		19b. TELEPHONE NUMBER *(Include area code)* +44 (0)20 7514 4299

CONTENTS

Report on the project № 2088p

"THEORETICAL AND EXPERIMENTAL RESEARCH OF CAPABILITIES OF MHD TECHNOLOGY TO CONTROL GAS FLOW WITH NON-EQUILIBRIUM IONIZATION"

1. INTRODUCTION

The purpose of the project is theoretical and experimental research of capabilities of using of MHD technology to control gas flow with non-equilibrium ionization. This report is devoted to theoretical investigation of the problem.

"Cold" gas flows are considered, such that thermal ionization of gas flow is negligible. The analysis of various methods of ionization is carried out, and mathematical models of an ionizer and MHD generator are developed. Requirements to ionizer, MHD generator and flow parameters at which self-sustained operational mode of ionizer and MHD generator is realized are formulated. Possibilities of using of MHD control in gas-dynamical systems are considered.

Traditional using of MHD transformation of energy to produce electric power is well understood both theoretically and experimentally nowadays. Nontraditional using of MHD to control flow parameters and hence performance of gas-dynamical systems, which include MHD system as a subsystem, is not well understood. MHD interaction acts as bulk force and power upon flow and allows varying flow parameters. In this case no mechanical parts are used to control the flow parameters. So this method of control can be considered as a perspective one for gas-dynamical system with a fixed geometry especially for high enthalpy flows. The main requirements to realize MHD influence on flow are the flow conductivity ensuring. In the most of gas-dynamical systems thermal ionization of flow is inappreciable and therefore it is necessary to use methods of non-equilibrium plasma creation. To ensure autonomous regime of system of MHD control self-sustained operational mode of ionizer and MHD generator is considered. For the operational mode power spent on flow ionization is less than power produced by MHD generator.

As a possible range of application for MHD control, two types of gas-dynamical system can be considered: a) gas-dynamical systems which must ensure variable parameters of flow at outlet of system with fixed parameters at inlet of one and b) gas-dynamical systems which must ensure limited range of variation for some flow parameters at outlet of system with variable parameters at inlet.

In the project we consider application of MHD systems for scramjet control.

2. MODEL OF MHD GENERATOR WITH NONEQUILIBRIUM CONDUCTIVITY.

One of the potential applications of MHD generator with non-equilibrium conductivity is flow control in scramjet, which allows us to improve scramjet performance. Scramjet with MHD control under "AJAX" concept use MHD generators that are located upstream the combustion chamber. Thus static temperature of gas in the MHD generators must be not greater than two thousand degrees of Kelvin. Equilibrium ionization of gas at these conditions is negligible, so to provide noticeable MHD effect we must use methods of nonequilibrium plasma creation. For this purpose it is possible to use different types of gas discharge, microwave radiation or beams of fast charged particles. In all the methods we need

some energy to be put in flow. It is evidently that non-equilibrium conductivity can be realized when energy spent on flow ionization is less than energy produced by MHD generator. Such operational mode of MHD generator and ionizer is called self-sustained operational mode. One of the main requirements to ionizer is minimal power spent to producing of necessary conductivity of flow. Analysis of known methods of ionization shows that electron beam is optimal ionizer from the point of view of minimization of the power spent on ionization. According to [1], electrons with the energies greater than 1 keV spend only W_i=34 eV to produce electron and ion pair in air. Ionization cost W_i in this case only few times greater than the ionization energy of molecules of air. High-voltage pulses discharge, according to [2], for the ratio of electric field strength to the gas number density $E/N>5\cdot10^{-15}$ $V\cdot cm^2$, is characterized by ionization cost $W_i\approx 66eV$. In principle this discharge can be considered as alternative to e-beam.

Table 1

Electron concentration and conductivity in air plasma sustained by e-beam with current density $j_b=0.1A/cm^2$, (computations of [3]).

e-beam energy (keV)	Pressure (atm)	Temperature (°K)	n_e , $10^{13}cm^{-3}$	σ, mho/m
10	0.013	300	0.68	23.1
		600	0.54	33.4
		1000	0.45	44.4
	0.066	300	1.2	10.7
		600	1.0	16.1
		1000	0.91	22.5
	0.132	300	1.5	7.07
		600	1.3	11.6
		1000	1.2	16.2
50	0.013	600	0.26	19.8
	0.066	600	0.50	9.6
	0.132	600	0.64	6.7
100	0.013	600	0.20	15.9
	0.066	600	0.38	7.8
	0.132	600	0.47	5.3
200	0.013	600	0.16	13.5
	0.066	600	0.31	6.7
	0.132	600	0.38	4.5

To calculate non-equilibrium conductivity of flow in channel of MHD generator with e-beam ionizer in [3] it was developed model of ionization of air. In the model more than 40 plasma components and more than 230 reactions of the plasma components were taking into account. Part of results computed in [3] is presented in the Table 1. MHD generator with non-equilibrium conductivity is a part of complicated system – scramjet with MHD systems. In order to analyze the complex system in a wide range of parameters variation, to formulate requirements for MHD generator and ionizer, to determine optimal operational regimes of the subsystems we need to develop simpler model of ionization of air. Results from [3] will be used to obtain simple approximation function to calculation of concentration of electrons and

conductivity of flow. Also we will consider simple model of low ionized plasma consisting of neutral molecules, electrons, negative and positive ions with corresponding number densities: n, n_e, n_-, n_+. Set of kinetic equations for the plasma components concentration is the next:

$$\begin{aligned}
\frac{\partial n_e}{\partial t} &= I + k_d \cdot n \cdot n_e - k_a N_{O_2}^2 n_e - \beta n_+ n_e \\
\frac{\partial n_+}{\partial t} &= I - \beta_{ii} n_+ n_- - \beta n_+ n_e \\
\frac{\partial n_-}{\partial t} &= k_a N_{O_2}^2 n_e - k_d N_{O_2} \cdot n_- - \beta_{ii} n_+ n_-
\end{aligned} \tag{1}$$

where I is e-beam induced ionization rate, N_{O_2} – is concentration of oxygen molecules in air, k_a and k_d are the rate constants of attachment and detachment of electrons respectively, β and β_{ii} are the rate constants for electron-ion and ion-ion recombination respectively. These constants are functions of gas temperature T_g and electron temperature T_e. In calculations we use dependencies from papers [4, 5]. Basic reactions and corresponding rate coefficients are shown below:

$$\begin{aligned}
e + O_2^+ &\to O + O \\
e + N_2^+ &\to N + N
\end{aligned} \tag{2}$$

with $\beta = 2 \cdot 10^{-7} \sqrt{300/T_e}\, cm^3 / s$.

$$A^+ + B^-(+M) \to A + B(+M) \tag{3}$$

with $\beta_{ii} = 2 \cdot 10^{-7} \sqrt{300/T_g} \left[1 + 10^{-18} \cdot n \cdot \left(300/T_g \right)^2 \right] cm^3 / s$. Process (3) is two or three body ion-ion recombination, where A^+ and B^- are positive and negative ions respectively.

$$e + 2O_2 \to O_2^- + O_2 \tag{4}$$

with $k_a = 1.4 \cdot 10^{-29} \left(\frac{300}{T_e} \right) \exp\left(-\frac{600}{T_g} \right) \exp\left(\frac{700\left(T_e - T_g\right)}{T_e T_g} \right) cm^6 / s$

$$O_2^- + O_2 \to e + 2O_2, \tag{5}$$

with $k_d = 8.6 \cdot 10^{-10} \exp\left(-\frac{6030}{T_g} \right) \left[1 - \exp\left(-\frac{1570}{T_g} \right) \right] cm^3 / s$

Ionization rate I is determined in terms of e-beam characteristics by the ratio:

$$I = \frac{q_i}{W_i} \equiv \frac{\left(j_b / e\right) \rho Y\left(E_b\right)}{W_i} \tag{6}$$

where j_b – is the e-beam current density, E_b – is the energy of electron, Y is the electron stopping power,

Concentration of electron in nonequilibrium plasma sustained by e-beam can be calculated numerically from the set of equations (1). To estimate energy balance in MHD generator with non-equilibrium ionization we consider spatially homogeneous and steady state plasma. Conductivity of plasma is determined by the following ratio

$$\sigma = e^2 n_e \big/ \left(m_e n k_c \right), \tag{7}$$

where m_e is the electron mass, k_c is the electron scattering rate constant. The rate constant k_c is determined by the ratio: $k_c = \overline{g_{en}}\left(T_e\right) \cdot \overline{Q_{en}}\left(T_e\right)$, where $\overline{g_{en}}$ is averaged relative velocity of electrons, $\overline{Q_{en}}$ is averaged transport cross-section of electron collisions.

In the case when dissociative recombination (2) is dominant process in the set of equations (1) the electron concentration n_e can be approximately determined by the ratio:

$$n_e \approx \sqrt{\frac{q_i}{W_i \beta}} \tag{8a}$$

Ionization fraction in the case is determined by the ratio

$$\frac{n_e}{n} \approx \sqrt{\frac{q_i / n^2}{W_i \beta}} \tag{8b}$$

To obtain simple formulas for calculation of electron concentration and determine the range of their applicability we use three approaches:

The first approach:

Electron concentration is determined numerically as a solution of the set of equations (1) with rate coefficients determined in (2-5).

The second approach:

The electron concentration will be determined by approximation function, which is similar to (8a): $n_e = a_1 \cdot \left(q_i\right)^{b_1}$, where coefficients a_1 and b_1 are fitting parameters.

The third approach:

The ionization fraction will be determined by approximation function, which is similar to (8b): $n_e / n = a_2 \cdot \left(q_i / n^2\right)^{b_2}$, where coefficients a_2 and b_2 are fitting parameters. The fitting parameters a_i and b_i for the second and the third approaches are determined by the least-squares method by comparing the numerical results from [3] with approximation functions proposed above.

Electron concentration and plasma conductivity in MHD generator located in scramjet are the functions of e-beam parameters and flow parameters. We have investigated several configurations for scramjet. Configuration of scramjet for Mach designed number M_d=10 and total turning angle θ_N=15° is shown in Fig.1. Characteristic cross-sections of scramjet are denoted in the figure. Flow parameters are calculated numerically in 2-D Euler approach (chapter 4 of the project). To provide estimations of conductivity in channel (cross-section 3) flow parameters are averaged across the channel. Results presented in Fig.16 (chapter 3) were used in calculations. The basic characteristic of ionizer is power spent on ionization. So we characterize e-beam by integral parameter q_i, which is expressed through parameters of e-beam and flow by the ratio: $q_i = \left(j_b / e\right) \rho Y\left(E_b\right)$. Fig 2 shows dependencies of q_i upon e-beam current density in characteristic cross-sections of scramjet for flight Mach number M_∞=8 with free-stream dynamic pressure 40kPa. One can see that change the cross-section location from first to third position causes the q_i value to be increased.

Fig.3 shows dependencies of electron concentration calculated in [3] upon q_i magnitude. Approximation function (red line) obtained for the results is given by the ratio:

$$n_e = 1.124 \cdot 10^{12} \sqrt{q_i} \cdot cm^{-3}, \tag{9}$$

where q_i is expressed in W/cm^3. Function (9) coincides with function (8a) at corresponding value of parameter β=1.455·10^{-7}cm^{3}s^{-1}, maximal deviation of results of [3] from the approximation function is less than 30%. It follows from Fig.3 that the deviations are systematic. Thus using of function (9) in out of calculated ranges can result in more serious deviation. Blue lines in Fig.3 are steady state solutions of (1). In the calculations we suppose that T_e=T_g. These curves are in good agreement with results of [3]. Thus the second approach (formula (9)) can be used to rough estimations of electron concentration in the case when plasma parameters not dramatically differ from parameters in the Fig.3. The first approach needs to be used to calculate electron concentration more precisely.

Fig.4 shows dependencies of ionization fraction of air plasma upon factor q_i / n^2. Approximation function (red line) obtained for the results is given by the ratio:

$$\frac{n_e}{n} = 1.17 \cdot 10^{-5} \cdot \left(10^{34} \cdot q_i / n^2\right)^{0.6}, \tag{10}$$

where q_i is expressed in W/cm^3, n in cm^{-3}. Approximation function (10) is distinguished from the function (8b) by the index of power. Function (10) more precisely, than function (9), agrees with numerical results of [3]. Maximal deviation of results of [3] from approximation function (10) is less than 9%. Blue lines in Fig.4 are steady state solutions of (1). It follows from Fig.4 that all dependencies of ionization fraction are practically coincides in the range $3 \cdot 10^{-6} \le n_e / n \le 3 \cdot 10^{-5}$.

To determine range of applicability of formula (10) (the third approach) to calculation of electron concentration in MHD generator located in scramjet we have computed n_e in the first approach for all possible locations of MHD generator in scramjet, denoted in the Fig.1, in the range of flight Mach numbers M_∞=*6÷10* at free stream dynamic pressure 40kPa. All obtained results are involved in the area restricted by the blue lines, which are shown in the Fig.5. Red line is result obtained in the third approach (formula (10)). It follows from Fig.5 that all dependencies of ionization fraction are neighbour in the range of $0.02 < \left(q_i / n^2\right) \cdot 10^{34} < 20$. In this range the formula (10) can be used with high reliability to analyze characteristics of MHD generator with non-equilibrium conductivity.

Obtained results allow us to estimate power characteristics of the MHD generator. Power density produced by MHD generator with nonequilibrium conductivity q_g is determined by the ratio:

$$q_g = k\left(1-k\right)\sigma\left(q_i\right)B^2 v^2, \tag{11}$$

where k is the load factor, B is the magnetic induction, v is the flow velocity. Fig.6 shows dependencies of power density produced by MHD generator except for power density put into flow ionization (q_g-q_i) as a function of q_i and B. One can see that there are limiting values of magnetic induction B=B_{cr} for which $q_g \ge q_i$. Increase of value q_i causes the critical magnetic induction to be increased. Increase of magnetic induction at fixed q_i causes the power produced by MHD generator to be increased. Dependence of (q_g-q_i) on the q_i value is not monotonic. There is optimal value of q_i, for which (q_g-q_i) has maximum at given value of magnetic induction.

To determine limits at which self-sustained operational mode of ionizer and MHD generator exists we need to compare two values: the power spent on flow ionisation q_i, and the power produced by MHD generator q_g. It is evidently from formulae (7,10,11) that q_g is not linear function of q_i. In this case for any given parameters of B and v there are range of q_i, which provide self-sustained operational mode for MHD generator and ionizer. At fixed value of q_i we can determine critical value (or limiting value) of magnetic induction B_{cr} for which $q_g=q_i$. Self-sustained operational mode of MHD generator and ionizer ($q_g \geq q_i$) is realized when $B>B_{cr}$. We have calculated conductivity for various values of q_i in approaches considered above. Function of critical magnetic induction upon power spent on flow ionization $B_{cr}(q_i)$ is determined by solving the evident equation $q_i = k(1-k)\sigma(q_i)B_{cr}^2(q_i)v^2$. Dependencies of critical magnetic inductions upon q_i/n^2 obtained in different approaches for various values of flight Mach number are shown in the Fig.7. MHD generator is located in cross-section 2 of scramjet. It is easy to see that critical magnetic induction is monotone increasing function of ratio q_i/n^2. Increase of flight Mach number leads to decrease of the critical magnetic induction. The critical magnetic inductions calculated both in the second and in the third approaches are less than one for the first approach. In the range of $0.1<q_i/n^2<10$ the deviations for different approaches are insignificant. In the range of small values of power spent on flow ionization ($q_i/n^2<0.01$) the second approach belittles value of critical magnetic induction noticeably. It is consequence of electron attachment processes, which cannot be taken into account in the second approach in principle. Nevertheless the second approach provides good agreement with numerical results obtained in the first approach in wide range of parameter q_i/n^2 variation. Besides, in the second approach we obtain simple analytical formula for critical value of magnetic induction :

$$B_{cr} = \sqrt{m_e n k_c \sqrt{q_i W_i \beta} \Big/ \left(k\left(1-k\right)e^2 v^2\right)} \qquad (12a)$$

This formula gives us opportunity to understand dependence of the critical magnetic induction on the pivotal parameters. At fixed value of magnetic induction we will use another notion namely the critical power density spent on flow ionization with corresponding notation q_{cr}. In the second approach it can be obtained by converting expression (12a).

$$q_{cr} = \frac{1}{W_i \beta}\left(\frac{k(1-k)e^2B^2v^2}{m_e k_c n}\right)^2 \qquad (12b)$$

Self-sustained operational mode of MHD generator with non-equilibrium conductivity is realized then $0<q_i<q_{cr}$.

Developed model allows us to formulate requirements for parameters of ionizer and MHD generator at which MHD generator with nonequilibrium conductivity will operate in self-sustained mode. Moreover we can suppose algorithms for optimal choosing of the MHD parameters by using the discussed results. The next simple analysis demonstrates the possibilities for optimal choice of ionizer and magnetic system parameters.

MHD generator with non-equilibrium conductivity is a part of complex gas-dynamic system, so the electric energy production is not the only its function. MHD generator, located in scramjet, must effectively regulate characteristics of scramjet. According to next chapter, to noticeably improve scramjet performance it is necessary to ensure MHD interaction parameter $S_v \geq 0.1$, where $S_v = \sigma B^2 L / \rho v$, L is the length of MHD generator. Decrease the power density input to ionization causes the flow conductivity to be decreased. Thus to ensure required MHD interaction parameter while decreasing q_i it is necessary to increase

magnetic induction value. The decreasing curve in Fig.8 corresponds to constant value of MHD interaction parameter S_v=0.1. The increasing curve in Fig.8 corresponds to critical regime of MHD generator for which $q_g=q_i$. Parameters B and q_i which are located in shaded area correspond to self-sustained operational mode of MHD generator with non-equilibrium conductivity with MHD interaction parameter S_v>0.1. It follows from Fig.8 that there is optimal value of energy input to ionization, which ensures required regime of MHD generator in scramjet at minimal magnitude of magnetic induction.

Table 2

Optimal values of the power spent on flow ionization q_{opt} and the magnetic induction B_{opt} for scramjet with various values of the total turning angle θ_N for various values of flight Mach number M_0 at free stream dynamic pressure 40kPa, $S^*=0.1$, $L=1m$.

θ_N, degree	M_0	Position of MHD generator in scramjet according to the Fig.1					
		1		2		3	
		q_{opt}, W/cm^3	B_{min}, T	q_{opt}, W/cm^3	B_{min}, T	q_{opt}, W/cm^3	B_{min}, T
10	6	5.66	1.1	8.61	1.5	16.2	2.7
	8	9.04	0.75	15.3	1.1	29.7	2.0
	10	12.1	0.55	24.3	0.94	47.5	1.7
	12	16.4	0.45	35.2	0.80	58.0	1.2
15	6	6.35	1.2	11.2	1.9	14.3	2.7
	8	9.94	0.83	20.5	1.5	26.8	2.1
	10	14.3	0.63	34.9	1.3	44.4	1.7
	12	21.0	0.54	53.8	1.1	54.4	1.3
20	6	7.35	1.3	14.4	2.4	12.0	2.5
	8	12.0	0.96	27.7	2.0	23.0	2.2
	10	17.0	0.73	45.5	1.6	37.9	1.8
	12	23.1	0.59	67.2	1.4	44.5	1.3

Optimal values of power density spent on flow ionization and corresponding minimum magnitudes of magnetic induction are presented in the Table2 for various flight Mach numbers. Calculations were made for different inlets with the total turning angle varying from 10 to 20 degree. One can see that minimal magnetic induction decreases while increasing the flight Mach number. Magnetic induction in internal part of inlet needs to be greater than in external one. The total turning angle increase causes both the minimal magnetic induction and the optimal power density spent on flow ionization (in external part of inlet) to be increased. The q_{opt} value in internal part of inlet is greater than in external one. The values of e-beam current density required to realize the power densities can be estimated from the Fig.2. It is evidently that magnitudes of B_{min} presented in the Table 2 are technically achieved. If the optimal power spent on flow ionization presented in the Table 2 will be hard to achieve, the alternative regime with $q_i<q_{opt}$, as it follows from the Fig.8, can be realized at $B>B_{min}$.

To analyze potentiality of MHD control for improving characteristics of complex gas-dynamic system it is necessary to develop mathematical model of MHD systems. In this chapter we develop quasi-1D model of MHD generator with nonequilibrium conductivity.

Set of equations for stationary MHD flow in quasi-1D approach, according to [7] has a form:

$$\begin{aligned} &\rho vA=\text{const} \\ &\rho v\frac{dv}{dx}+\frac{dp}{dx}=F_x\equiv(\vec{j}\times\vec{B})_x \\ &\rho v\frac{d\left(h+\frac{v^2}{2}\right)}{dx}=\vec{j}\cdot\vec{E} \\ &p=R\rho T, \end{aligned} \tag{13}$$

where ρ is the flow density, v is the flow velocity, p is the static pressure, h is the enthalpy, A is the MHD channel cross-sectional area, x is the longitudinal coordinate, B is the magnetic field, E is the electric field, j is the current density, F is the Lorentz force We assume that $\vec{B}=\left(0,B_y,0\right)$, $\vec{E}=\left(E_x,0,E_z\right)$ and $\vec{v}=\left(v_x,0,0\right)$. The generalized Ohm's law determines relations between electromagnetic components:

$$\vec{j}+\mu\left(\vec{j}\times\vec{B}\right)=\sigma\left(\vec{E}+\vec{v}\times\vec{B}\right) \tag{14}$$

where μ is the electron mobility. In considered configuration of magnetic field the current density is determined from equation (14) by the ratio: $\vec{j}=\left(\frac{\sigma\left(E_x+\beta E_z+\beta B_y v_x\right)}{1+\beta^2},0,-\frac{\sigma\left(\beta E_x-E_z-B_y v_x\right)}{1+\beta^2}\right)$, where β is the Hall parameter $\beta=\mu\left|\vec{B}\right|$. We will consider two configurations for MHD generator. The first is ideally sectioned Faraday MHD generator, for which $\vec{j}=\left(0,0,j_z\right)$, $\vec{E}=\left(E_x,0,E_z\right)$. In this case we obtain the following expressions for the right part of equations (13):

$$\begin{aligned} &\left(\vec{j}\times\vec{B}\right)=\left(\vec{j}\times\vec{B}\right)_x=-(1-k)\sigma B^2 v \\ &\left(\vec{j}\cdot\vec{E}\right)=-k\left(1-k\right)\sigma B^2 v^2 \end{aligned}, \tag{15a}$$

where the load factor k is determined by the ratio $k=-E_z/(v_x\cdot B_y)$.

The second configuration is the Hall MHD generator, for which $\vec{E}=\left(E_x,0,0\right)$ and $\vec{j}=\left(j_x,0,j_z\right)$. In this case we obtain:

$$\begin{aligned} &\left(\vec{j}\times\vec{B}\right)_x=-\left(1+k\beta^2\right)\sigma B^2 v\Big/\left(1+\beta^2\right) \\ &\left(\vec{j}\cdot\vec{E}\right)=-k\left(1-k\right)\sigma B^2 v^2\beta^2\Big/\left(1+\beta^2\right) \end{aligned}, \tag{15b}$$

where the load factor k is determined by the ratio $k=-E_x/(\beta v_x B_y)$.

In the Hall MHD generator Lorentz force has not only x component but also z component and ratio of the components is:

$$\left|F_z/F_x\right|=\beta\left(1-k\right)\Big/\left(1+k\beta^2\right) \tag{16}$$

Therefore 1D approach for Hall MHD generator is quite correct only when $\left|F_z/F_x\right|\ll 1$.

In papers [8, 9] analytical solution for set of equations (1) for Faraday MHD generator was obtained in the form convenient for analysis of complex gas-dynamic systems including MHD systems. In [10] results of [8, 9] were extended on the case of Hall MHD generator. To develop mathematical model of MHD generator with nonequilibrium conductivity we use results from papers [8-10] taking into account model of nonequilibrium plasma developed above.

According to [10] relations of flow parameters at MHD generator exit (subindex 2) to the flow parameters at MHD generator entrance (subindex 1) can be written in the form:

$$\frac{T_2}{T_1} = G(\psi,\xi,M_1,\eta)\,,\ \frac{\rho_2}{\rho_1} = \left(\frac{T_2}{T_1}\right)^D,$$

$$\frac{p_2}{p_1} = \left(\frac{T_2}{T_1}\right)^{D+1},\ \frac{v_2}{v_1} = \sqrt{Z(\psi,\xi,M_1,\eta)}\,, \tag{17}$$

$$G(\psi,\xi,M_1,\eta) = 1+\psi\left(1+\xi\right)\omega\left(M_1\right)\eta$$

$$Z(\psi,\xi,M_1,\eta) = 1-\left(1+\psi\left(1+\xi\right)\right)\frac{\omega\left(M_1\right)\eta}{\omega\left(M_1\right)-1}$$

$$D = \frac{\gamma}{\gamma-1}\frac{\xi}{\xi+1}-1$$

where ξ is factor which is determined by the flow regime, η is the enthalpy extraction ratio, $\omega\left(M_1\right) = \left(\frac{\gamma-1}{2}M_1^2+1\right)$, M_1 is the Mach number at the MHD generator entrance, γ is the specific heat ratio, ψ is factor which characterizes the MHD generator type.

$$\psi = \begin{cases} \dfrac{1}{k}-1, & \text{for Faraday MHD generator} \\ \dfrac{1+\beta^2k^2}{\beta^2k(1-k)}, & \text{for Hall MHD generator} \end{cases} \tag{18}$$

Table 3
Values of ξ parameter for particular regimes of MHD flow

Flow regime	Type of MHD generator	
	Faraday	Hall
ρ-const	γ-1	γ-1
p-const	0	0
T-const	-1	-1
M-const	$-1-\dfrac{k}{(1-k)\omega}$	$-1-\dfrac{\beta^2k(1-k)}{(1+\beta^2k^2)\omega}$
v-const	$-\dfrac{1}{1-k}$	$-\dfrac{1+\beta^2k}{1+\beta^2k^2}$

Values of parameter ξ for some particular flow regimes are presented in the Table 3. Value ξ=0 corresponds to flow with constant static pressure along the channel length. When

$\xi>0$, static pressure increases along the channel length. Cross-sectional area of MHD channel A as a function of coordinate x can be determined from condition ρvA=const. Function of A from the enthalpy extraction ratio at given value of factor ξ can be easily obtained by using formulae (17): $A = A_1 / \left[G(\psi,\xi,M_1,\eta)^D \sqrt{Z(\psi,\xi,M_1,\eta)} \right]$. According to [10], the case of constant cross-sectional area of the MHD generator A=const is described well when $\xi = \tilde{\xi}(\psi)$. The $\tilde{\xi}(\psi)$ function is determined by the expression: $\tilde{\xi}(\psi) \equiv \gamma - 1 + \frac{\gamma + 1/\psi}{M_1^2 - 1}$. This ratio is obtained from condition $dA/d\eta = 0$.

To obtain dependence of the enthalpy extraction ratio upon the length of MHD generator for a given value of ξ parameter it is necessary to use the next relation from paper [8]:

$$\frac{dx}{dT} = \frac{dp}{dT} \frac{1}{\xi(1-k)^2 \sigma B^2 v} \tag{19}$$

Nonequilibrium conductivity, according to (7-10), depends upon flow parameters and power density spent on flow ionization in the form:

$$\sigma(q_i,\rho) = \sigma_0 \left[\frac{q_i}{q_0} \cdot \left(\frac{\rho_0}{\rho} \right)^2 \right]^b \tag{20}$$

By substituting (17,20) in (19) we obtain the next expression for MHD interaction parameter S_v as a function of the enthalpy extraction ratio η.

$$S_v = \frac{\omega(M_1)}{2k(1-k)\chi \cdot (\omega(M_1)-1)} \int_0^\eta \frac{G(k,\xi,M_1,\eta')^{(1+2b)D}}{\sqrt{Z(k,\xi,M_1,\eta')}} d\eta' \tag{21a}$$

$$\chi = \begin{cases} 1 & \text{for Faraday MHD generator} \\ \beta^2 / (1+\beta^2) & \text{for Hall MHD generator} \end{cases}$$

where $S_v = \sigma_1 B^2 L / \rho_1 v_1$. It is supposed that power density spent on flow ionization is constant in channel of MHD generator (q_i=q_1), $\sigma_1 = \sigma(q_1,\rho_1)$. Another physically reasonable situation can be determined by a constant value of e-beam current density along the channel length. In this case the power density spent on ionization, according to (6), is proportional to gas density $q_i \sim \rho$. Relation between S_v and η in this approach will takes up the form:

$$S_v = \frac{\omega(M_1)}{2k(1-k)\chi \cdot (\omega(M_1)-1)} \int_0^\eta \frac{G(k,\xi,M_1,\eta')^{(1+b)D}}{\sqrt{Z(k,\xi,M_1,\eta')}} d\eta' \tag{21b}$$

Formulae (21) determines MHD interaction parameter as a function of enthalpy extraction ratio $S_v(\eta)$ in approaches with a constant power density spent on ionization (21a) and with a constant e-beam current density (21b). By inverting the relations we obtain dependence of $\eta(S_v)$.

So, set of formulae (17,18,21) allows us to determine flow parameters along the length of MHD generator with non-equilibrium conductivity. In common case, according the formulae (7-11), the flow parameters change causes the critical parameters to be modified. In order to take into account these non-local effects on the limits of the self-sustained operational mode for MHD generator with nonequilibrium conductivity we introduce the next

integral quantities: W_{ion} is the power put to flow ionization in MHD generator channel, W_g is the power produced by the MHD generator. The power W_g is determined by the ratio $W_g = -\int_0^L (\vec{j}\cdot\vec{E})A(x)\,dx$, where L is the MHD generator length. The power W_{ion} is determined by the ratio $W_{ion} \equiv \int_0^L q_i A(x)dx$. Also we introduce factor r as the ratio of power input to ionization and power produced by MHD generator $r=W_{ion}/W_g$. It is obvious that self-sustained operational mode is realized when $0 \le r \le 1$.

The power W_g can be easily calculated in terms of the enthalpy extraction ratio η: $W_g = \eta \cdot W_0$, where $W_0 = A_1\rho_1 v_1 c_p T_1 \omega(M_1)$. To calculate W_{ion} we take into account that $A(x)=A_1\rho_1 v_1/\rho(x)v(x)$. Change of variables in integrating over x by using (17,19) let us obtain next formula for factor r:

$$r(\eta) = \frac{1}{\eta}\cdot\int_0^{\eta} \frac{d\eta'}{k(1-k)\chi\sigma B^2 v^2/q_i} \tag{22}$$

Let us assume that quantity q_{ion} is constant in the whole of MHD generator volume. By substituting (17, 20) in (22) we obtain:

$$r(\eta) = \left(\frac{q_{ion}}{q_{cr}}\right)^{1-b}\cdot\frac{1}{\eta}\int_0^{\eta}\frac{G(\psi,\xi,M_1,\eta')^{2bD}}{Z(k,\psi,M_1,\eta')}d\eta' \tag{23a}$$

In the case with a constant e-beam current density we obtain:

$$r(\eta) = \left(\frac{q_{ion}}{q_{cr}}\right)^{1-b}\cdot\frac{1}{\eta}\int_0^{\eta}\frac{G(\psi,\xi,M_1,\eta')^{(1+b)D}}{Z(k,\psi,M_1,\eta')}d\eta' \tag{23b}$$

Here the local critical power density q_{cr} is determined by the ratio:

$$q_{cr}^{1-b} = q_0^{-b}k(1-k)\chi\sigma_0(\rho_0/\rho_1)^{2b}B^2v_1^2 \tag{24}$$

When we use the second approach in determining of nonequilibrium conductivity the local critical power will be calculated under the formula (12b). Formulae (23) determine requirements to ionizer and MHD generator to maintain self-sustained operational mode.

Fig 9 shows function $r(\eta)$ for Faraday and Hall MHD generators at various values of Mach number M_1 and various values of a load factor k. In all the cases MHD flow is characterized by the value $\xi = \tilde{\xi}(\psi)$. One can see that function $r(\eta)$ is monotone increasing function. Value $\eta=\eta^*$ defined from relation $r(\eta^*)=1$ determines upper limit of the enthalpy extraction ratio at which self-sustained operational mode of MHD generator with nonequilibrium conductivity exists. One can see that values η^* for Faraday MHD generator is greater than for Hall MHD generator at the same conditions. It follows from Fig. 9 that range of existence of the self-sustained operational mode is extending both for Faraday and Hall MHD generators while increasing Mach number. Increase of load factor leads to extension of the range of self-sustained operational mode for Faraday MHD generator. For Hall MHD generator the same effect is achieved by decreasing the load factor.

Fig.10 demonstrates relative power characteristics both for Faraday and Hall MHD generators. Here and hereinafter to clarity we use the designation η_g instead of η to underline that $\eta_g=W_g/W_0$ is relative power produced by MHD generator. The factor $\eta_{ion}=W_{ion}/W_0$ is the relative power spent on flow ionization. The difference $\eta_g-\eta_{ion}=(W_g-W_{ion})/W_0$ determines the

so-called relative power excess or the real power produced by MHD generator with nonequilibrium conductivity. One can see that at some magnitude of MHD interaction parameter S_v the η_g and η_{ion} values become equal. So self-sustained operational mode for MHD generator with nonequilibrium conductivity is limited not only by parameters of ionizer and magnetic system, but also by the length of the MHD generator. Points in the Fig.10 mark the limiting values of MHD interaction parameter. As it follows from Fig.10 the limiting MHD interaction parameter for Hall MHD generator is less than for Faraday one.

Fig.11 shows relative power excess produced by Faraday MHD generator in the regimes with $\xi = \tilde{\xi}(\psi)$ (a) and $\xi=0$ (b). One can see that regime $\xi=0$ is more preferable regime for power production. While increasing the Mach number at MHD generator entrance the power excess increases too in both regimes. As it follows from Fig.11a the ionizer with a constant power density spent on ionization provide more power excess than ionizer with a constant e-beam current density in MHD generator with $\xi = \tilde{\xi}(\psi)$. For MHD generator with $\xi=0$ the tendency is contrary. In comparing Fig.11a and Fig.12 one can conclude that characteristics of ionizer and magnetic system, which according to (6,12b,24) are accumulated in the ratio q_i/q_{cr}, are essentially influence on the power excess produced by MHD generator with nonequilibrium conductivity.

Thus in this chapter the model of nonequilibrium plasma sustained by e-beam is developed. Simple relations to calculations of electron concentration are obtained. Quasi-1D model of MHD generator with nonequilibrium conductivity is developed. Brief analysis of the MHD generator is made. The main purpose of MHD generator investigating in the project is control of flow. Probably maximal power production is not necessity for the purpose. To formulate requirements to parameters of the MHD generator providing optimal control of gas-dynamic system it is necessary to develop mathematical model of the system. This will be done in the next chapter.

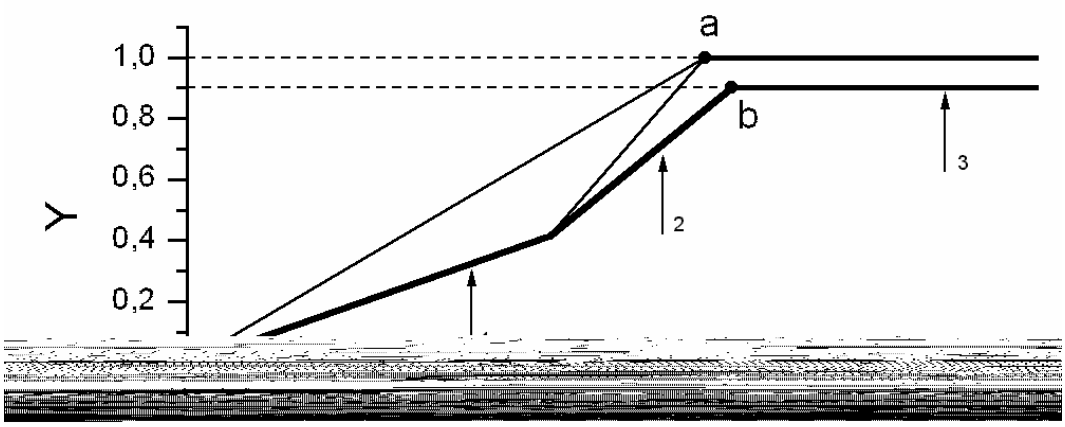

Fig.1. Geometry of scramjet which is characterized by the total turning angle θ_N=15° and Mach designed number M_d=10. Characteristic cross-sections used in calculations are denoted on the figure.

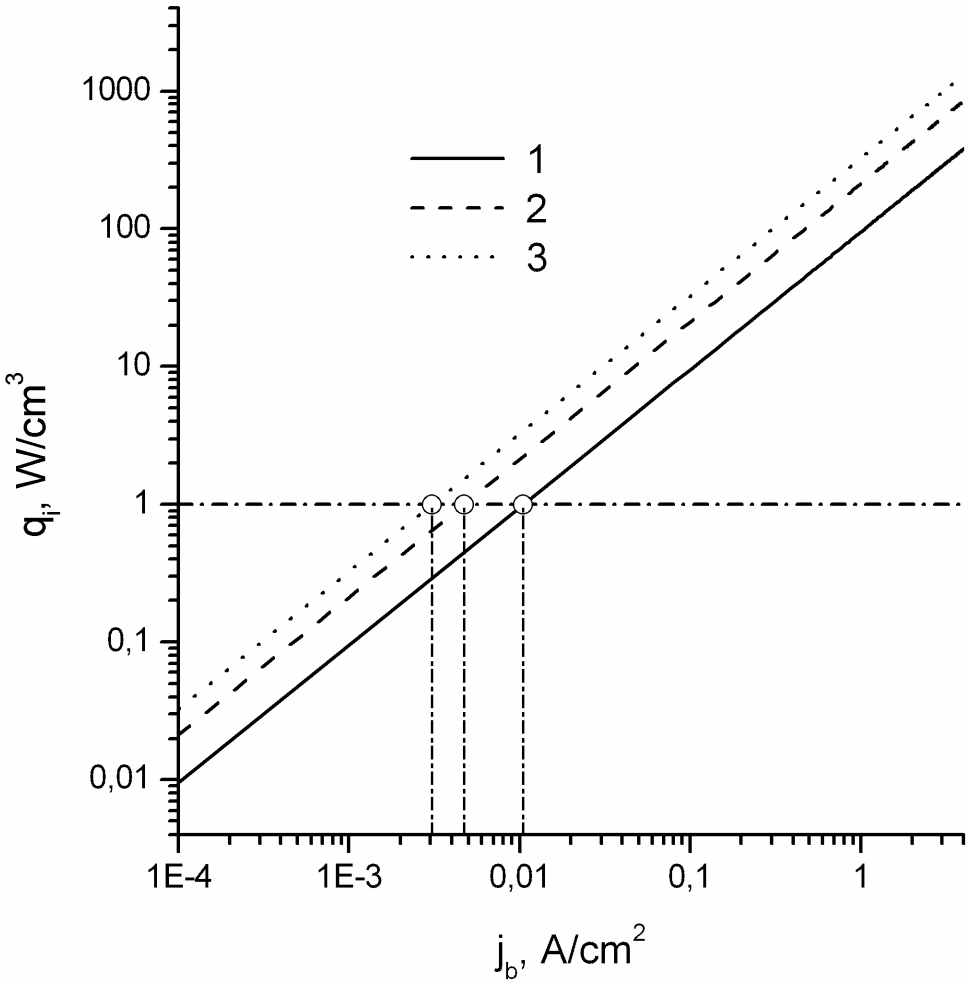

Fig.2. Electron beam power loss in various cross-sections of scramjet as a function of e-beam current density, E_b=100 keV. Numbers, which denote the curves, correspond to location of the cross-sections according to Fig.1. Flight Mach number M_∞=8, free-stream dynamic pressure is equal to 40 kPa.

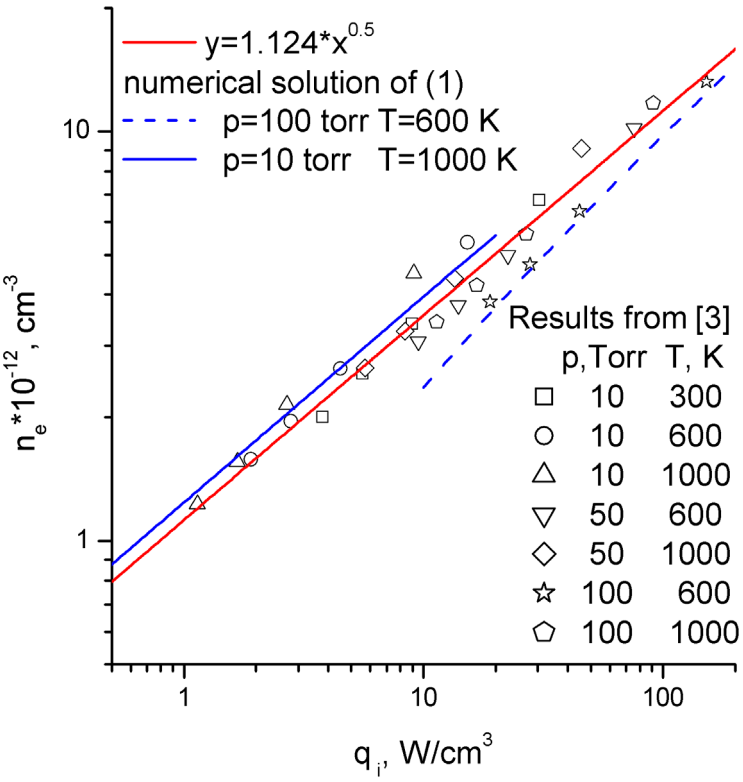

Fig.3. Electron concentration in air as a function of power loss by e-beam in unit of volume.

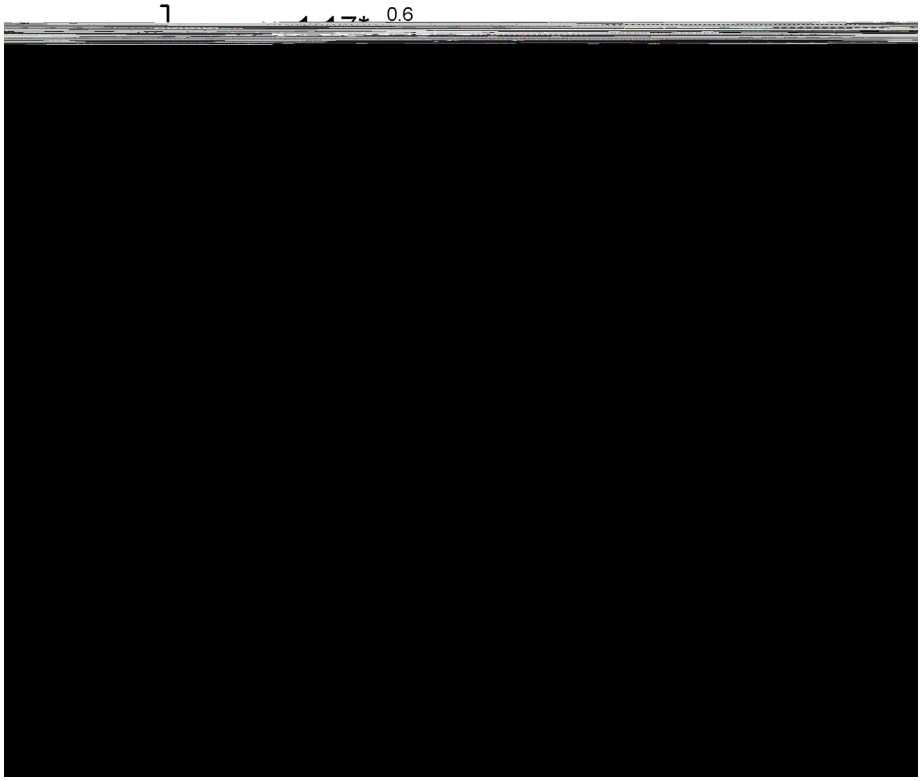

Fig.4. Ionization fraction in air as a function of power loss by e-beam in unit of volume.

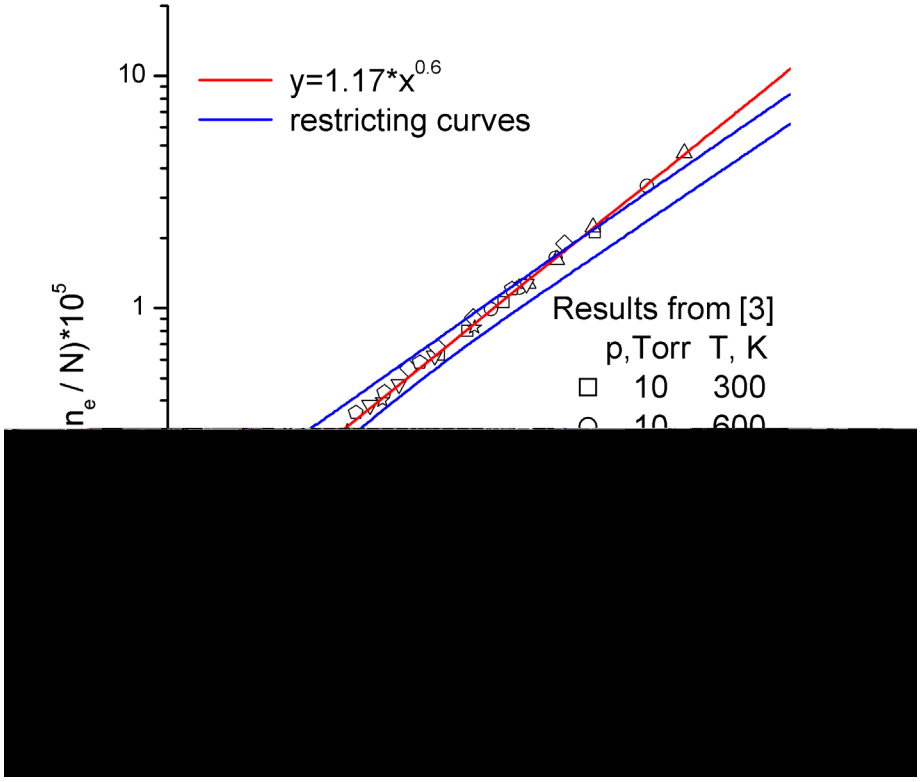

Fig.5 Ionization fraction in air plasma as a function of power loss by e-beam in unit of volume.

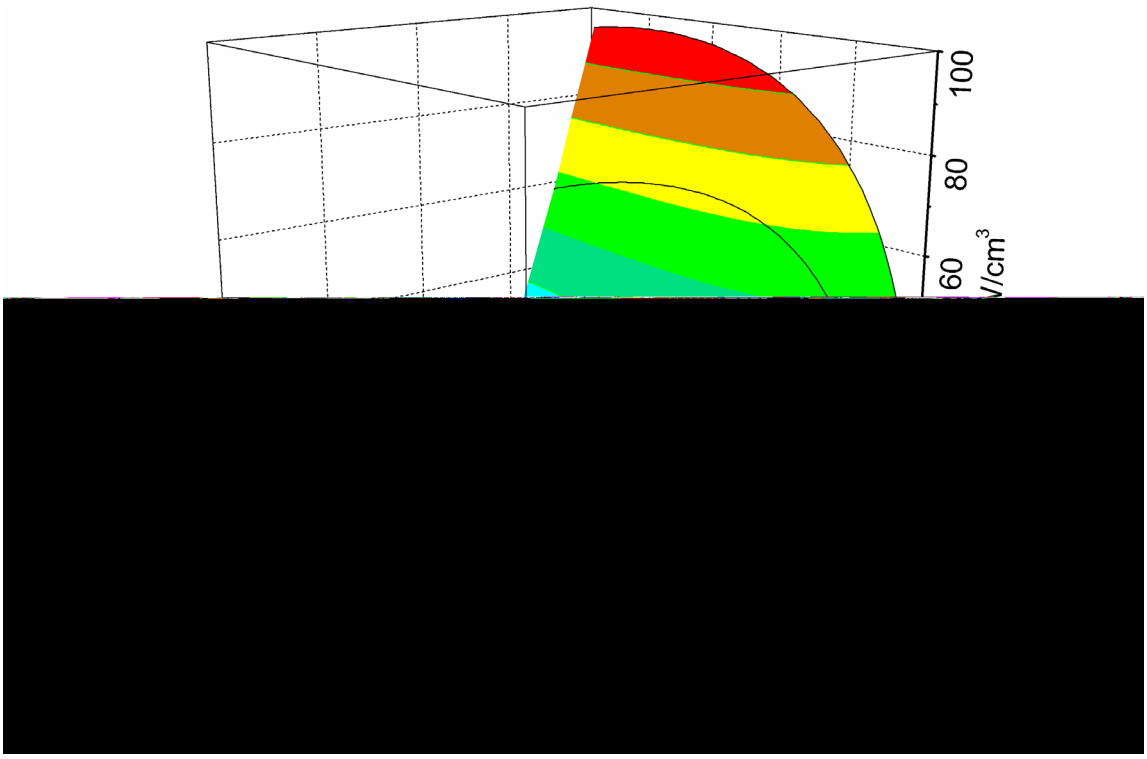

Fig.6. Power density produced by MHD generator except for power density input to ionization $(q_g\text{-}q_i)$ as a function of q_i and B. MHD generator is located in cross-section 2 (Fig.1), M_∞=6.

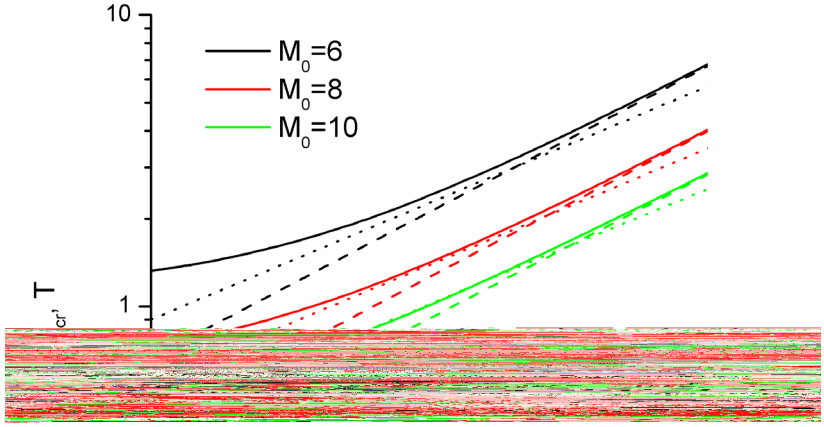

Fig.7. Critical values of magnetic induction calculated in different approaches for various values of flight Mach numbers. MHD generator is located in cross-section 2 of scramjet (Fig.1). Free stream dynamic pressure is equal to 40 kPa.

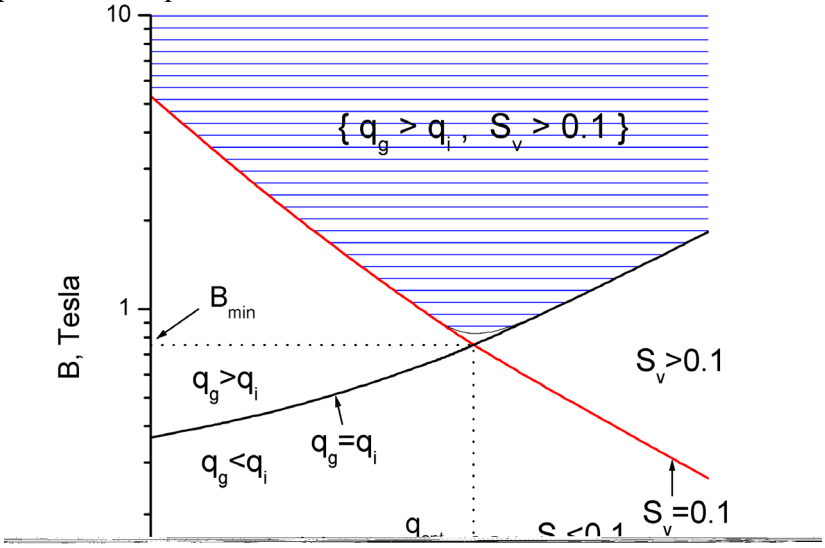

Fig.8. Range of values of magnetic induction B and power spent on flow ionization q_i, which ensure the self-sustained operational mode of MHD generator with non-equilibrium conductivity with MHD interaction parameter S_v>0.1. MHD generator is located in cross-section 1, M_∞=6.

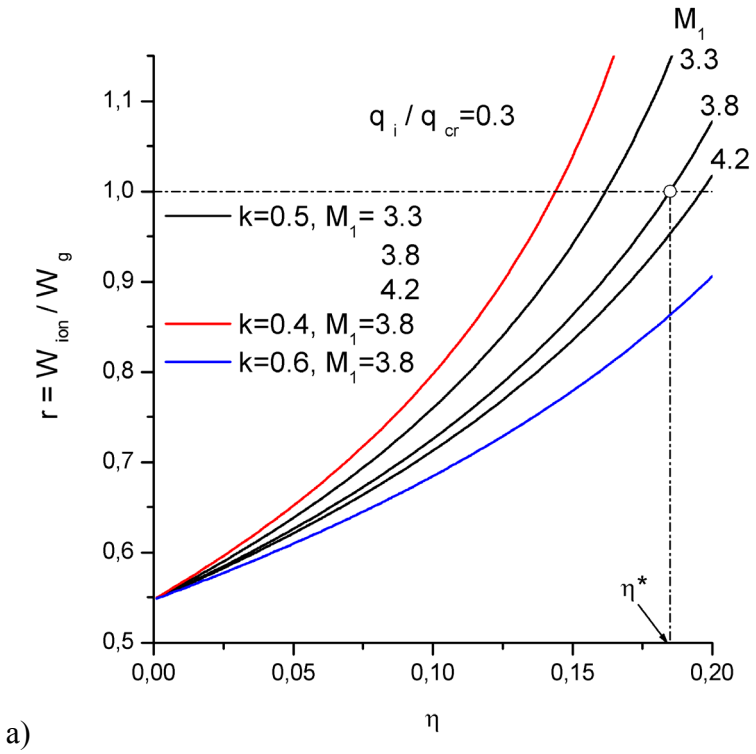

a)

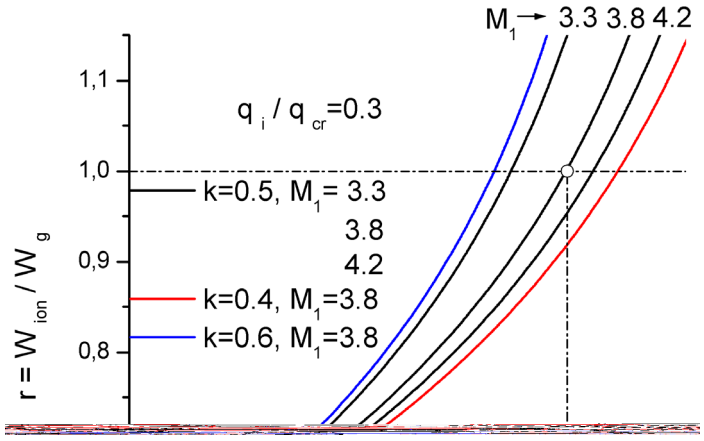

b)

Fig.9 Relative value of power put to flow ionization in channel of MHD generator as a function of the enthalpy extraction ratio for various values of Mach number and load factor. (q_i – constant)
a) Faraday MHD generator; b) Hall MHD generator with β=2

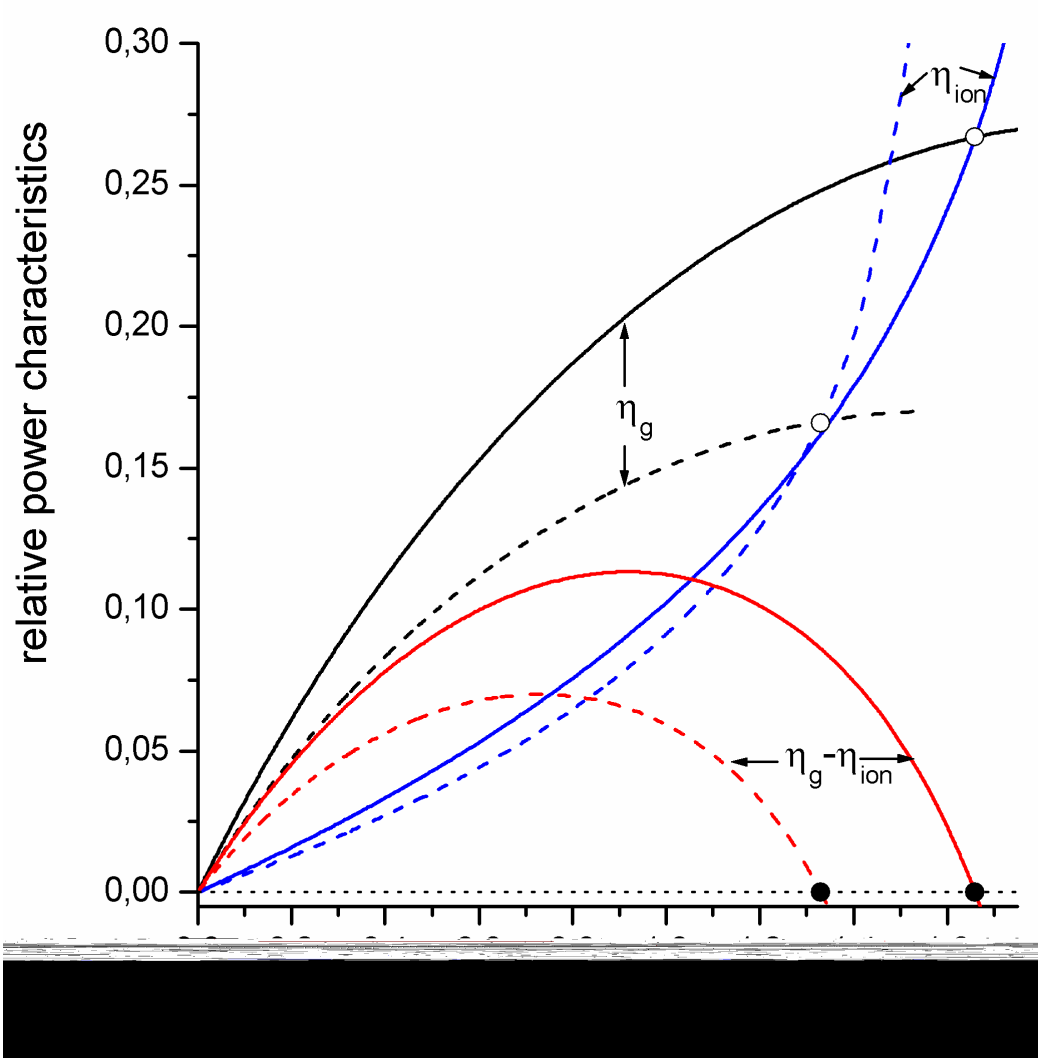

Fig.10 Relative power characteristics of MHD generator with nonequilibrium conductivity as a function of MHD interaction parameter. Solid curves for Faraday MHD generator and dashed curves for Hall MHD generator with β=2. M_1=3.3, (q_i – constant) q_i/q_{cr}=0.05, ξ=0.5, k=0.5.

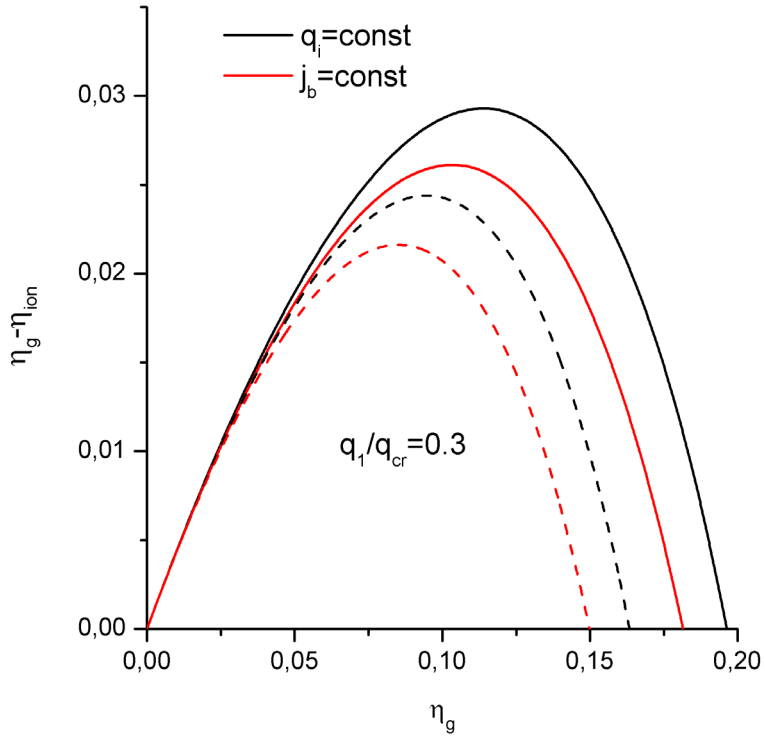

a)

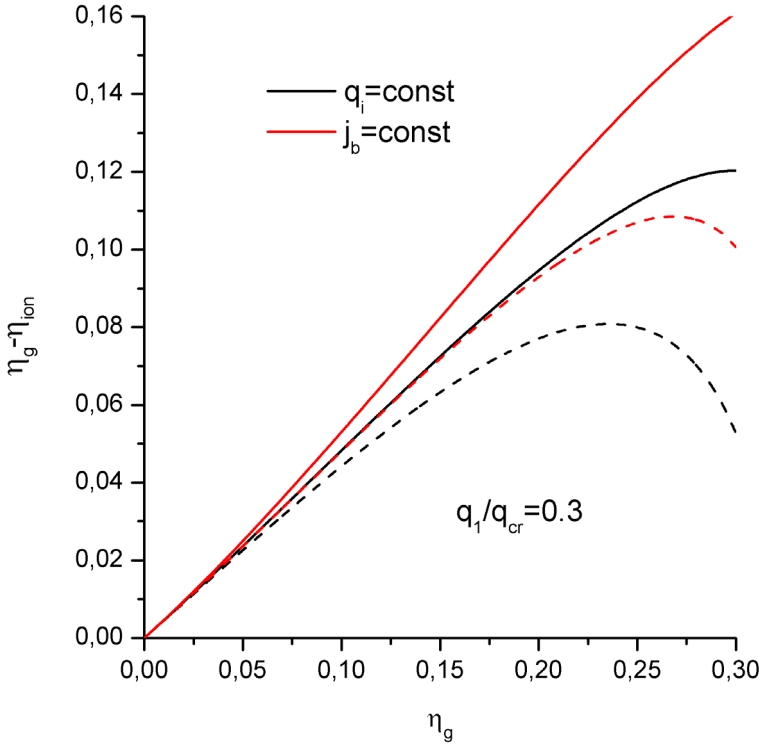

b)

Fig.11 Relative power excess produced by Faraday MHD generator with nonequilibrium conductivity: k=0.5, M_1=4.2 for solid lines M_1=3.3 for dashed lines; black lines correspond to constant power density spent on ionization, red lines correspond to constant e-beam current density. a) $\xi = \tilde{\xi}(\psi)$, b) $\xi=0$

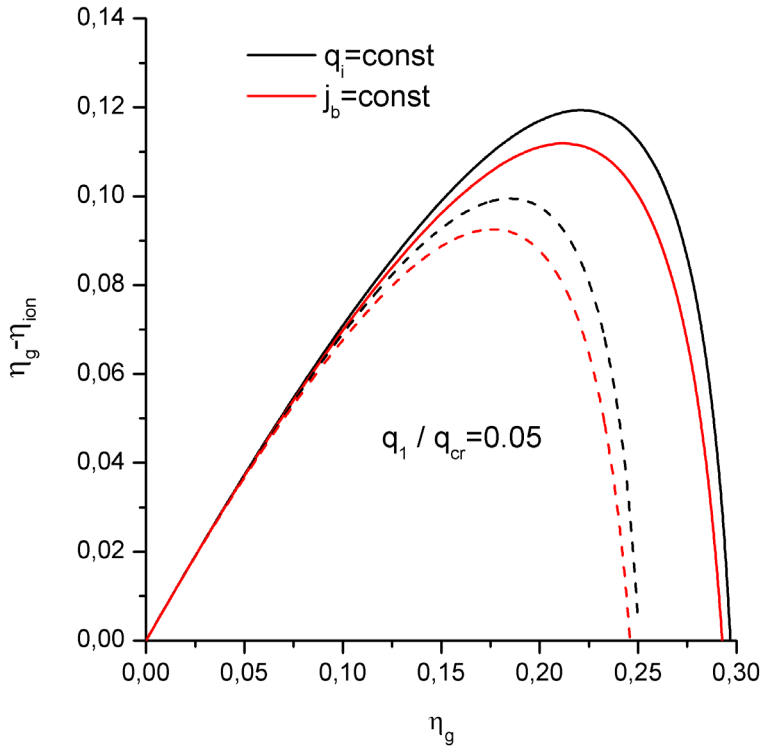

Fig.12 Relative power excess produced by Faraday MHD generator with nonequilibrium conductivity: k=0.5, $\xi = \tilde{\xi}(\psi)$; solid lines M_1=4.2, dashed lines M_1=3.3; black lines correspond to constant power density spent on ionization, red lines correspond to constant e-beam current density.

3. QUASI-1-D MODEL OF SCRAMJET WITH MHD CONTROL

This chapter is devoted to development of quasi-1-D mathematical model of combined gas-dynamical system, which includes MHD generator with non-equilibrium conductivity and to determination of conditions at which MHD interaction has essential influence on performance of the gas-dynamical system. As the combined gas-dynamical system let's analyze the scheme of scramjet with MHD control under "AJAX" concept [11]. Simplified scheme of the scramjet is presented in the Fig.13. MHD generators, disposed upstream the combustion chamber, transform part of flow enthalpy to electric power. The electric power produced by MHD generators is transferred to MHD accelerator disposed downstream the combustion chamber. Part of the electric power need to be used to provide necessary flow conductivity in MHD channel. Part of produced electric power can be transferred to onboard systems. Influence of external MHD generator on flow field in scramjet inlet will be investigated in the next chapter.

In this chapter only internal MHD systems will be considered. Scheme of scramjet and some peculiarities of quasi 1D model developed in the chapter are shown in the Fig.14. We analyze scheme in which whole of power excess produced by MHD generator with nonequilibrium conductivity is transferred to MHD accelerator. In the case when the MHD generator will be used as a power source but not a means of scramjet control (not analyzed in the project) it is necessary to estimate influence of power extraction (not recovered in MHD accelerator in this case) on the scramjet specific impulse. Flow-field upstream the MHD generator entrance is calculated in two-dimensional Euler approach. At cross-section 1 (Fig.14) the flow parameters are averaged. Downstream the cross-section 1 the 1D approach is used. To determine characteristics of nonequilibrium plasma in MHD channel we use results obtained in the previous chapter. We are taking into account that part r of the energy produced by MHD generator $W_{ion} = rW_g$ is transferred to ionizer. The rest of the energy, namely $(1-r)W_g$, is transferred to MHD accelerator. Combustion chamber is considered in two regimes with a constant pressure along the channel and with a constant gas density along the channel. A mass flow rate of fuel is usually much less than air mass flow rate $\dot{m}$, thus we will regard a fuel supply into the combustion chamber as a heat release without injection of mass. Flow in nozzle is considered as isentropic. Pressure at nozzle outlet is supposed to be equal the static pressure in incident flow.

We will use subscripts to note parameters of a flow in corresponding cross-sections of the engine channel. Let's use following numbering: 0 - incident flow; 1 - entrance of MHD generator; 2 - entrance of the combustion chamber; 3 - entrance of MHD accelerator; 4 - entrance of nozzle; 5 - exit of nozzle. For obviousness these designations are indicated in the Fig. 14. Now we introduce mathematical models for subsystems of the engine.

0-1. Inlet

The inlet implements a multi-shock gas-dynamical compression of an incident flow. The following characteristics are used: N - number of shocks in an external part, θ_N - a total turning angle of a flow in the inlet, σ_{in} - a total pressure recovery coefficient. Characteristics of inlet were calculated in a wide range of inlet configuration for various values of flight Mach number. Typical flow field in inlet with N=2 in the case when flight Mach number M_0 is equal to design Mach number M_d is shown in the Fig.15. Pressure distribution across the

channel for various flight Mach numbers are shown in the Fig.16. Dashed lines in the figure are averaged pressures for corresponding conditions.

If a temperature at an exit of the inlet (entrance of MHD generator) is assigned a value T_1, a pressure and velocity at the exit are determined by the following ratios:

$$\begin{aligned} &\frac{p_1}{p_0} = \sigma_{in}\left(\frac{T_1}{T_0}\right)^{\frac{\gamma}{\gamma-1}} \\ &\frac{v_0^2}{2} + c_p T_0 = \frac{v_1^2}{2} + c_p T_1 \end{aligned}, \qquad (25)$$

where c_p is specific heat of air. Total pressure recovery coefficient σ_{in} is calculated from upper relation (25) in terms of calculated numerically ratios p_1/p_0 and T_1/T_0, for any given inlet.

Fig.17 shows dependencies both of relative pressure increase p_1/p_0 and relative temperature increase T_1/T_0 in the inlet with total turning angle θ_N=15° and Mach designed number M_d=10 upon relative values of the inlet throat F_{th} for various values of flight Mach number.

1-2. MHD generator with nonequilibrium conductivity

The MHD generator is described in the approach developed in previous chapter. It is characterized by parameters ξ_1, k_1, enthalpy extraction ratio η and relative value of power spent on flow ionization $r=W_{ion}/W_g$. The change of flow parameters in a channel of MHD generator is determined as follows:

$$\begin{aligned} &\frac{T_2}{T_1} = 1 + \psi_1\left(1+\xi_1\right)\omega\left(M_1\right)\eta \\ &\frac{p_2}{p_1} = \left(\frac{T_2}{T_1}\right)^{D_1+1} \\ &\frac{v_2}{v_1} = \sqrt{1-\left(1+\psi_1\left(1+\xi_1\right)\right)\frac{\omega\left(M_1\right)\eta}{\omega\left(M_1\right)-1}} \end{aligned} \qquad (26)$$

where $D_1 = \frac{\gamma}{\gamma-1}\frac{\xi_1}{\xi_1+1} - 1$, Mach number at MHD generator entrance M_1 is determined in terms of M_0 and T_1/T_0 by the obvious ratio: $M_1 = \sqrt{\frac{M_0^2 + 2/(\gamma-1)}{T_1/T_0} - \frac{2}{\gamma-1}}$, factor ψ is determined as in (18) but instead of k the load factor k_1 is substituted.

The electrical power W_g, produced by MHD generator is determined by the following ratio: $W_g = \dot{m} c_p T_0 \cdot \omega(M_0) \cdot \eta$. Factor $r=W_{ion}/W_g$ which defines the relative power spent on flow ionization is determined by the formulae (23). The power spent on flow ionization, ultimately, as a result of recombination processes, passes into a heat. We suppose approximately that this additional heat release is implemented in the combustion chamber.

2-3. Combustion chamber

Set of equations for 1D model of combustion chamber in approach with a constant specific heat is presented here:

$$\begin{aligned} &\rho v A = \dot{m} = const \\ &\rho v \frac{dv}{dx} + \frac{dp}{dx} = 0 \\ &\rho v \frac{d}{dx}\left(c_p T + \frac{v^2}{2} \right) = q(x) + q_r \\ &p = R\rho T \end{aligned} \tag{27}$$

where $q(x)$ is power density released in combustion chamber in result of fuel combustion, q_r is density of heat release in result of plasma recombination processes. Total heat addition in combustion chamber $Q=Q_f+Q_r$, where $Q_f = \int_0^L q(x) A(x) dx$, $Q_r = \int_0^L q_r \cdot A(x) dx \equiv W_{ion}$.

Let's consider the combustion chamber working in a mode with a constant pressure and in a mode with a constant density. It is evidently from the set (27) that flow parameters modification in combustion chamber with a constant pressure are determined by the ratios:

$$\begin{aligned} &T_3 = T_2 + \Delta T + \frac{W_{ion}}{\dot{m} c_p} \\ &p_3 = p_2,\ v_3 = v_2 \\ &\Delta T = \frac{H_u}{c_p(\alpha L_0 + 1)} \end{aligned} \tag{28a}$$

where Hu - a calorific value of fuel, L_0 - stochiometric factor, α is air-fuel ratio ($\alpha \geq 1$). Corresponding ratios for combustion chamber with a constant density have a form:

$$\begin{aligned} &T_3 = T_2 + \gamma \cdot \left(\Delta T + \frac{W_{ion}}{\dot{m} c_p} \right) \\ &p_3 = p_2 \cdot (T_3 / T_2) \\ &\frac{v_3^2}{2} = \frac{v_2^2}{2} - (1 - 1/\gamma) \cdot c_p \cdot (T_3 - T_2) \end{aligned} \tag{28b}$$

3-4. MHD accelerator

The MHD accelerator is characterized by parameters ξ_3, k_3. (For MHD accelerator the load factor k_3 is greater than unity $k_3>1$) It is supposed that part $(1-r)$ of power produced by MHD generator is transferred to MHD accelerator $W_a = (1-r) W_g$. Flow parameters in MHD accelerator are described according to theory developed in [8, 9]. The change of flow parameters in a channel of MHD accelerator is determined as follows:

$$\begin{aligned} &T_4 = T_3 + \frac{k_3 - 1}{k_3}(1 + \xi_3) \cdot T_0 \cdot \omega(M_0) \cdot \eta \cdot (1 - r) \\ &\frac{v_4^2}{2} = \frac{v_3^2}{2} + \frac{1 - \xi_3 \cdot (k_3 - 1)}{k_3} c_p T_0 \cdot \omega(M_0) \cdot \eta \cdot (1 - r) \\ &\frac{p_4}{p_3} = \left(\frac{T_4}{T_3} \right)^{D_3 + 1} \end{aligned} \tag{29}$$

where $D_3 = \frac{\gamma}{\gamma - 1}\frac{\xi_3}{\xi_3 + 1} - 1$.

4-5. Nozzle

We suppose that nozzle flow is isentropic. Thus the relationship between a relative change of a flow pressure and a relative change of a flow temperature in the nozzle is as follows:

$$\begin{aligned} \frac{p_5}{p_4} &= \left(\frac{T_5}{T_4}\right)^{\frac{\gamma}{\gamma-1}} \\ \frac{v_5^2}{2} &= \frac{v_4^2}{2} + c_p \cdot (T_4 - T_5) \end{aligned} \tag{30}$$

We consider nozzle operating at design conditions, so the set of equations (25,26,28-30) can be closed in supposing the pressure at an exit of the nozzle is equal to pressure in a surrounding medium $p_5=p_0$. In this situation we use evident relation:

$$\frac{p_5}{p_0} = \frac{p_5}{p_4}\cdot\frac{p_4}{p_3}\cdot\frac{p_3}{p_2}\cdot\frac{p_2}{p_1}\cdot\frac{p_1}{p_0} = 1$$

In view of this ratio, we can obtain formula for calculation of a flow temperature at the exit of the nozzle from the set of equations (25,26,28-30). In the case when combustion chamber working in a mode with a constant pressure we obtain:

$$T_5 = \frac{T_4}{\sigma_{in}^{(1-1/\gamma)}\left[\frac{T_1}{T_0}\left(\frac{T_2}{T_1}\right)^{\frac{\xi_1}{\xi_1+1}}\left(\frac{T_4}{T_3}\right)^{\frac{\xi_3}{\xi_3+1}}\right]} \tag{31a}$$

In the case when combustion chamber working in a mode with a constant density we obtain:

$$T_5 = \frac{T_4}{\frac{T_1}{T_0}\cdot\left(\frac{T_2}{T_1}\right)^{\frac{\xi_1}{\xi_1+1}}\left(\sigma_{in}\cdot\frac{T_3}{T_2}\right)^{(1-1/\gamma)}\left(\frac{T_4}{T_3}\right)^{\frac{\xi_3}{\xi_3+1}}} \tag{31b}$$

The exhaust velocity of gas from the nozzle is determined through temperature T_5 with use of an energy conservation law by the following ratio:

$$v_5 = \sqrt{v_0^2 + 2c_p(T_0 + \Delta T - T_5)} \tag{32}$$

The obtained ratios allow calculating specific impulse of scramjet with MHD control I_{sp}. An explicit formula for the specific impulse of air-breathing propulsion systems when a mass flow rate of a fuel is neglected in a comparison with a mass flow rate of an air, according to [11] is as follows:

$$I_{sp} = \frac{\alpha L_0}{g}(\varphi_N v_5 - v_0) \tag{33}$$

where φ_N is the nozzle non-ideality factor (in calculations we suppose that φ_N=1).

The set of the formulas (25,26,28-33) allows one calculating specific impulse of the scramjet with MHD control at given parameters of the inlet, MHD systems and the

combustion chamber. To determine the range of parameters at which MHD interaction improves scramjet performance we use an obvious functional ratio $\left(\partial I_{sp}/\partial\eta\right)\Big|_{\eta\to 0} > 0$.

Having done necessary transformations we obtain requirements for ξ_1 parameter. In the case of combustion chamber working in a mode with a constant pressure, MHD interaction increases specific impulse of scramjet if the next inequality is true:

$$\xi_1 > \frac{T_1}{\Delta T}\cdot\left[1+\frac{\delta}{\psi_1}\right],\ \delta=\left(1-\frac{1}{k_3}\left(1-r(0)\right)\right) \tag{34a}$$

It is evidently that $r(0)$ can be determined as the ratio of power densities $r(0)=q_i/q_g$. As $0\le r(0)\le 1$ and $k_3\ge 1$ the factor δ has a value in the range $0\le\delta\le 1$. Inequality (34a) combines some parameters of scramjet, MHD systems and ionizer. Cursory analysis of the inequality let us to do the inference that internal MHD generator allows one to increase the scramjet specific impulse only when we use MHD generator in regime with pressure increasing along the channel length. Indeed for MHD generator $\psi_1>0$ and $0\le\delta\le 1$, so the right part of (34a) is positive. According to [8], condition $\xi_1>0$ corresponds to MHD flow with $dp/dx>0$. If we consider MHD generator with constant cross-sectional area the inequality (34a) takes on the next form:

$$\gamma-1+\frac{\gamma+1/\psi_1}{M_1^2-1} > \frac{T_1}{\Delta T}\cdot\left[1+\frac{\delta}{\psi_1}\right] \tag{34b}$$

This inequality prescribes the range of variation of MPCE subsystems parameters at which using of MHD generator with a constant cross-sectional area allows one to increase scramjet specific impulse.

According to Fig.16 and 17 the temperature T_1 depends on the flight Mach number M_0. The value M_1 in (34b) according to (26) depends on the flight Mach number too. Thus in result of analysis of the inequality (34b) we obtain limitations on flight Mach number at which MHD interaction causes the MPCE specific impulse to be increased. Fig.18 shows dependencies of maximal flight Mach number upon factor δ for various values of ψ factor. MHD interaction increase specific impulse of scramjet in the case when flight Mach number $M_\infty < M_{max}$. As it follows from (34a) factor δ mainly characterize relative power spent on flow ionization. In situation when power spent on ionization is equal to zero (initially ionized flow) $\delta=0$. Factor $\delta=1$ describes situation for which whole of power produced by MHD generator is spent on flow ionization. It is evidently that while increasing the factor δ the M_{max} is decreasing. Decrease of the total turning angle θ_N causes the maximal Mach number M_{max} to be increased. At small value of δ, minimization of ψ factor provides expansion of range of Mach number at which MHD interaction improves scramjet performance. Contrary at $\delta\approx 1$ increase of ψ factor causes the M_{max} to be increased.

In the case of combustion chamber working in a mode with a constant density, MHD interaction increases specific impulse of scramjet if the next inequality is true:

$$\xi_1 > (\gamma-1)+\frac{T_1}{\Delta T}\cdot\left[1+\frac{\delta}{\psi_1}\right] \tag{35a}$$

If we consider MHD generator with constant cross-sectional area the inequality (35a) takes on the next form:

$$\frac{\gamma+1/\psi_1}{M_1^2-1} > \frac{T_1}{\Delta T}\cdot\left[1+\frac{\delta}{\psi_1}\right] \qquad (35b)$$

One can see that inequality (35a) prescribes more intensive increase of pressure in MHD generator channel than inequality (34a) to improve scramjet performance. Fig.19 demonstrates comparison of Maximal Mach numbers for scramjet with θ_N=10° for two regimes of combustion chamber. MHD generator with constant cross-sectional area is considered. One can see that MHD control can be used in wider ranges of flight Mach numbers for scramjet with combustion chamber working in a mode with a constant pressure. In analysis of scramjet the combustion chamber working in a mode with a constant pressure is traditionally considered. So hereinafter we will consider the same regime in investigating the scramjet with MHD control.

To choose preferential regime of flow in MHD generator we compare specific impulses of scramjet with MHD control for various values of ξ_1 factor. Relative values of specific impulse for scramjet with MHD control (namely specific impulse of "MHD scramjet" divided by specific impulse of classical scramjet) as a function of the enthalpy extraction ratio are shown in the Fig.20a. One can see that increase of factor ξ_1 causes the scramjet specific impulse to be increased. Fig.20b demonstrates dependency of relative power spent on ionization $r=W_{ion}/W_g$ as a function the enthalpy extraction ratio. While increasing the ξ_1 the factor r rise take place. The flow regime characterized by minimal ξ_1 is preferable if MHD generator with nonequilibrium conductivity is considered as a power source. Requirements for ξ_1 parameter in the case when MHD generator is used for scramjet control are opposite. In this research we consider possibilities of nonequilibrium MHD generator for flow control and so maximal realizable factor ξ_1 is required. Factors $\xi_1 > \tilde{\xi}(\psi_1)$ correspond to convergent channel and undesirable to avoid additional shock waves. So hereinafter we will consider MHD flows characterized by factor $\xi_1 = \tilde{\xi}(\psi_1)$, which approximately describes MHD generator with constant cross-sectional area.

In the calculations the factor ξ_3 was assumed to be zero. Numerical calculations of specific impulse for various values of factor ξ_3 have shown that flow regime in channel of MHD accelerator practically doesn't influence on the specific impulses value. So hereinafter we suppose ξ_3=0.

Various regimes of power spending on ionization of flow are compared in the Fig.21. One can see that ionization regime with a constant power density spent on ionization gives us opportunity to reach greater values of specific impulse and power excess than the regime with a constant e-beam current density. This tendency is correct both for Faraday and Hall MHD generators. So hereinafter we will consider the regime with a constant power density spent on ionization.

Fig.22 demonstrates dependencies of relative specific impulse as a function of the load factor for various flight Mach numbers and various values of enthalpy extraction ratio. One can see that positive influence of MHD interaction on specific impulse increase while decreasing the flight Mach number.

Fig.23 demonstrates dependencies of MPCE specific impulse upon the MHD interaction parameter for various relative values of inlet throat. Results are presented for limiting case for which q_i/q_{cr} =0. One can see, the more is the inlet throat F_{th} the greater is the positive influence of MHD interaction on specific impulse of scramjet both for Faraday and Hall MHD generators. Influence of MHD generator type on specific impulse of scramjet is

compared in the Fig.24a. For small value of S_v the Hall MHD generator provides more noticeable increase of scramjet specific impulse than Faraday one. For S_v>0.7 the Faraday MHD generator gives greater increment of scramjet specific impulse than Hall one. Fig.24b shows dependencies of the enthalpy extraction ratio for various relative values of inlet throat. One can see, the more is the inlet throat F_{th} the greater is the value η_g. Faraday MHD generator produces more electric power than Hall one in all the cases.

Fig.25a demonstrates how relative specific impulse of scramjet with MHD control depends upon MHD interaction parameter for various relative power density spent on ionization q_i/q_{cr}. One can see that increase of q_i/q_{cr} value causes the scramjet specific impulse to be decreased both for Faraday and Hall MHD generators. In the case of q_i/q_{cr} >0 there are optimal MHD interaction parameters at which relative specific impulse has a maximum. The maximal impulse and optimal MHD interaction parameter decrease while increasing the ratio q_i/q_{cr}. The same behavior is observed for power excess presented in the Fig.25b.

Dependencies of relative specific impulse upon MHD interaction parameters for scramjet with two different total turning angles in inlet are shown in the Fig.26. One can see that positive effect of MHD control in scramjet increase while decreasing the total turning angle. This tendency is observed for various values of the load factor both for Faraday MHD generator (Fig.26a) and Hall MHD generator (Fig.26b). The same behavior is observed for power excess presented in the Fig.27. Besides that, one can see that at small MHD interaction parameter maximal power generation is achieved at the load factor k_1=0.5. For Faraday MHD generator (Fig.27a) optimal load factor becomes greater than 0.5 while increasing S_v parameter. For Hall MHD generator (Fig.27b) opposite tendency is observed, namely the optimal load factor becomes less than 0.5 while increasing S_v.

Figs.28 demonstrate how specific impulse and power characteristics of scramjet with Hall MHD generator depend on the Hall parameter. As it follows from the Fig28a the scramjet specific impulse, at small values of S_v parameter monotonically decreases while increasing the Hall parameter. At S_v parameter near to unity the dependence becomes non-monotonic. The relative power excess (Fig.28b) monotonically increases while increasing the Hall parameter. One can see that both specific impulse and power excess for scramjet with Hall MHD generator are trending toward corresponding dependencies for scramjet with Faraday MHD generator while increasing the Hall parameter.

Figs.29 demonstrate influence of MHD accelerator load factor on the relative specific impulse of scramjet with MHD control. One can see that decrease of the load factor of MHD accelerator k_3 causes the scramjet specific impulse to be increased both for scramjet with Faraday and Hall MHD generators. This behavior is observed for various values of load factor of MHD generator k_1, but for k_1=0.5 the influence of k3 on specific impulse is more significant. It is evidently that maximal specific impulse can be obtained at k_3=1, but it is unachievable limit, because the power density input in MHD accelerator q_a is proportional to $k_3(1-k_3)$. Thus, when $k_3 \to 1$ the volume and hence the length of MHD accelerator $L_a \to \infty$. In reality it is inexpedient to take up the k_3 factor less than 1.1.

Fig.30 demonstrates contours of relative specific impulse for scramjet with MHD control for various values of q_i/q_{cr} ratio in coordinates: the load factor k_1 and the MHD interaction parameter S_v. Left contours in the Fig.30 correspond to Faraday MHD generator and right contours correspond to Hall MHD generator with β=2. Values of q_i/q_{cr} ratio are shown near the corresponding figures. One can see that contours for Hall MHD generator are quite similar to mirroring of Faraday MHD generator contours. When q_i/q_{cr} =0, maximal specific impulse is achieved at intermediate values of load factor k_1 and maximal values of

MHD interaction parameters. For Faraday MHD generator increase of q_i/q_{cr} ratio leads to decrease of optimal values both for k_1 factor and MHD interaction parameter. So we can conclude that ratio q_i/q_{cr} is important parameter that influence on optimal value both for load factor and MHD interaction parameter. According to previous chapter this ratio is determined by parameters of ionizer, magnetic system and flow parameters. To formulate requirements to these subsystems we have calculated characteristics of scramjet using dimensional parameters.

Fig.31 shows contours for relative specific impulse and power excess produced by MHD generator in scramjet with MHD control in the axes: magnetic induction and power density spent on ionization. These results are obtained for free stream dynamic pressure 40 kPa. These dependencies correlate with the qualitative results presented in the Fig.8. Namely there are optimal values of power density q_i at which required both specific impulse and power excess can be achieved at minimal value of magnetic induction.

As it follows from the Fig.32-33 optimal value of the load factor for specific impulse differ from one for power excess. Maximal power excess is achieved at k_1 near 0.5 both for case with given power density spent on ionization (Fig.32) and case with given magnetic induction (Fig.33). As for specific impulse its maximal values can be achieved at the load factors, which are essentially less than 0.5.

Obtained results show that MHD generator with nonequilibrium conductivity can be used on hypersonic aircraft both for electric power production and for scramjet specific impulse increasing. Requirements for parameters of the MHD generator depend on its functionality.

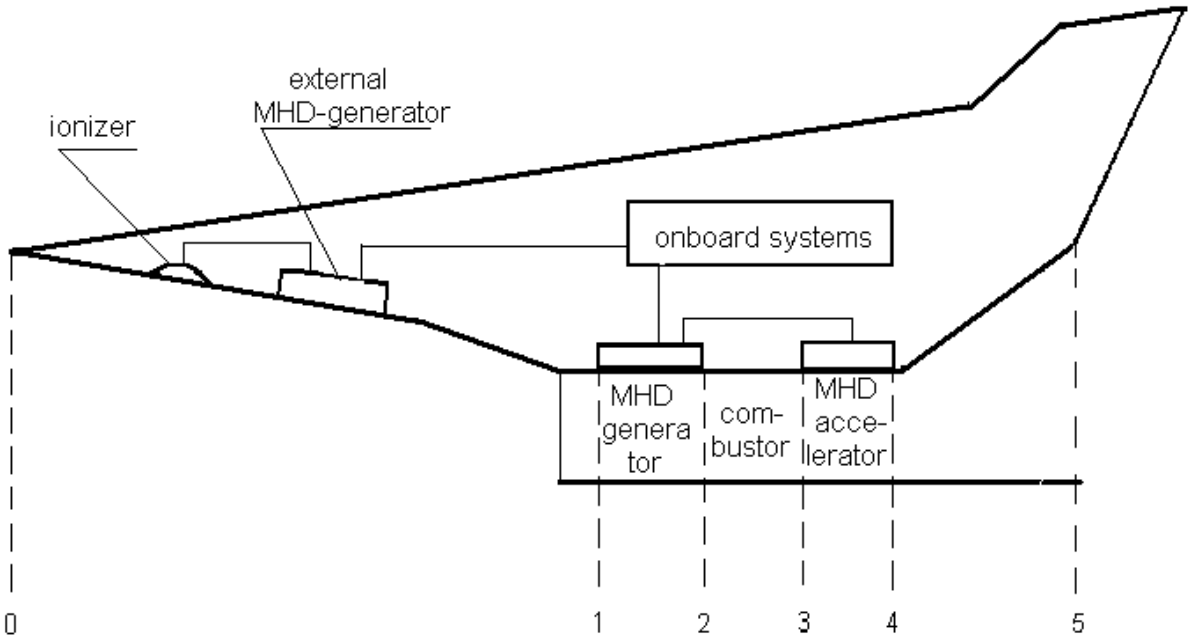

Fig.13 Simplified scheme of scramjet with MHD control under “AJAX” concept, according to [11]

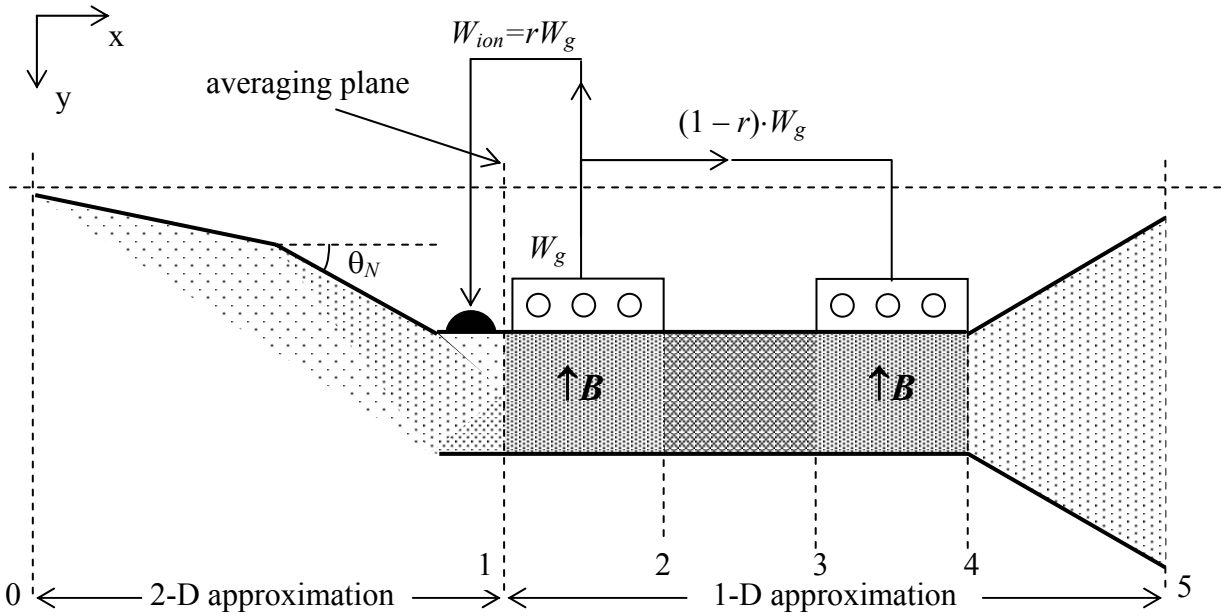

Fig.14 Simplified scheme of scramjet with MHD control in quasi-1-D model
0-1 – inlet; 1-2 MHD generator; 2-3 – combustion chamber; 3-4 – MHD accelerator; 4-5 – nozzle

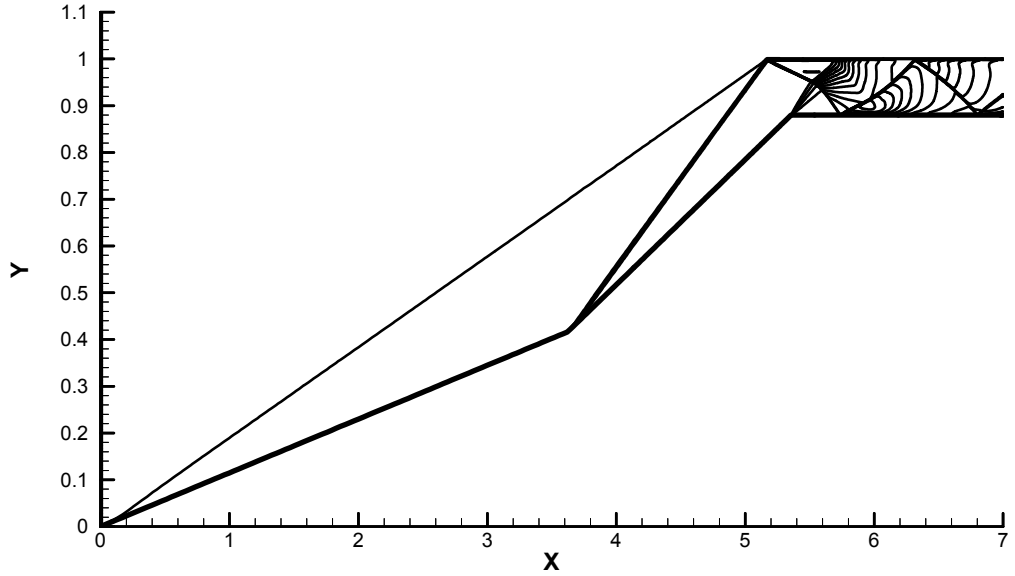

Fig.15. Density contours in scramjet inlet. M_d=10, θ_N=15°, F_{th}=0.12, M_0=10

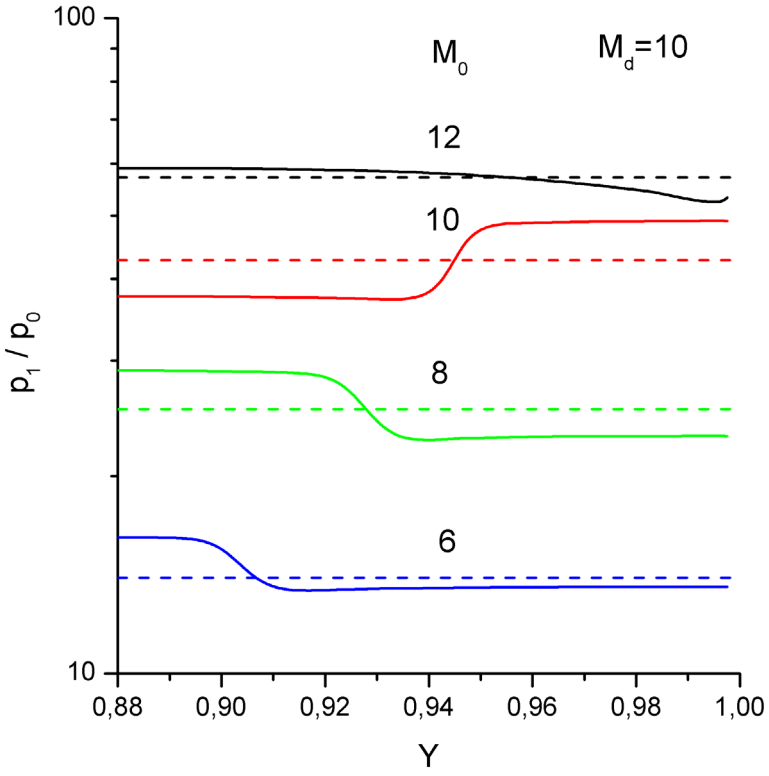

a)

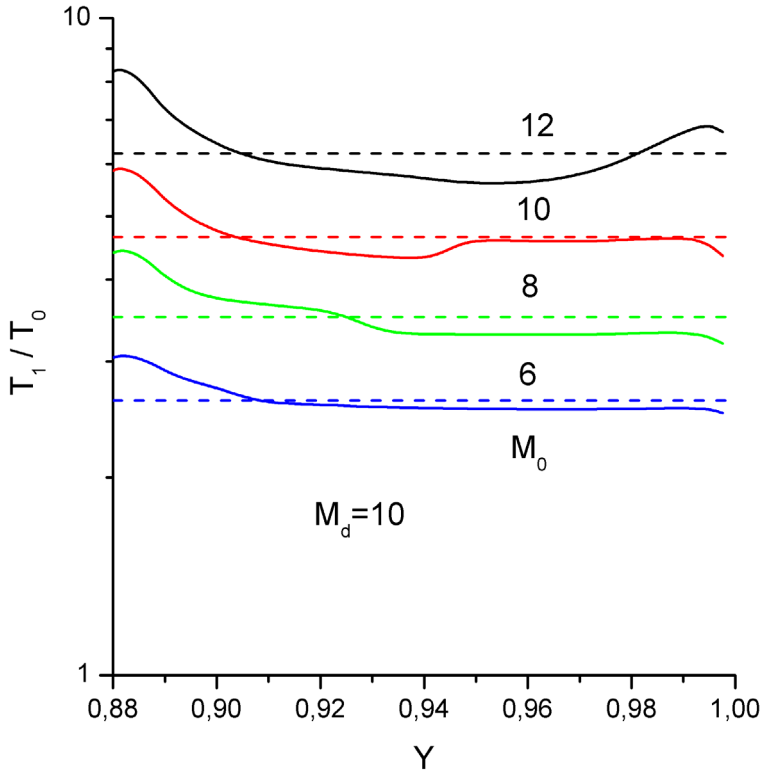

b)

Fig.16. Relative pressure (a) and temperature (b) distributions in scramjet inlet at cross-section (1) for various flight Mach numbers (shown near the curves) obtained in 2D calculations (solid lines) and used in 1D model (dashed lines). M_d=10, θ_N=15°, F_{th}=0.12.

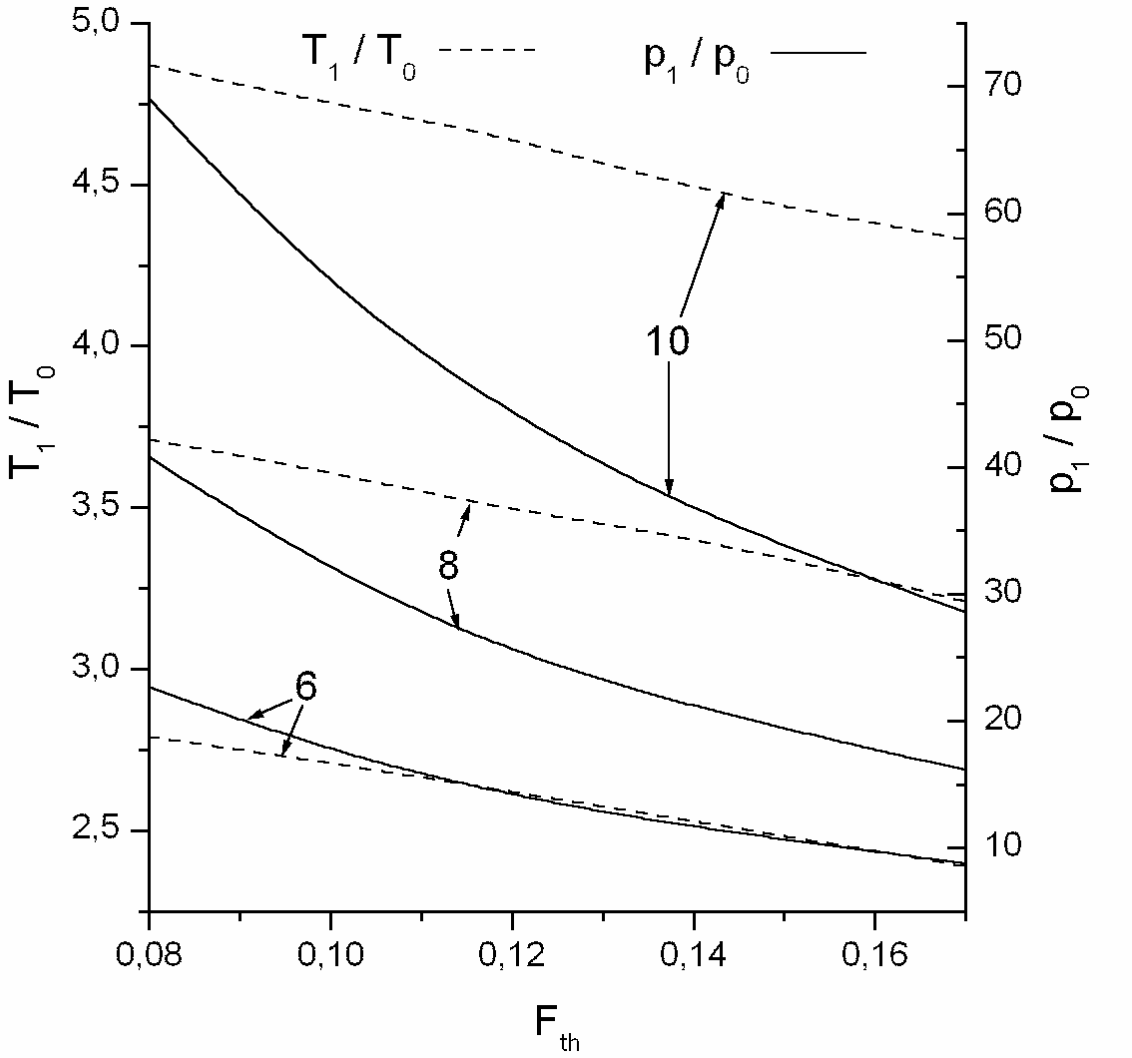

Fig.17 Relative temperature and pressure increase in inlet with total turning angle θ_N=15° and Mach design number M_d=10 as a function of relative value of the inlet throat F_{th}. Flight Mach number values are shown in the figure.

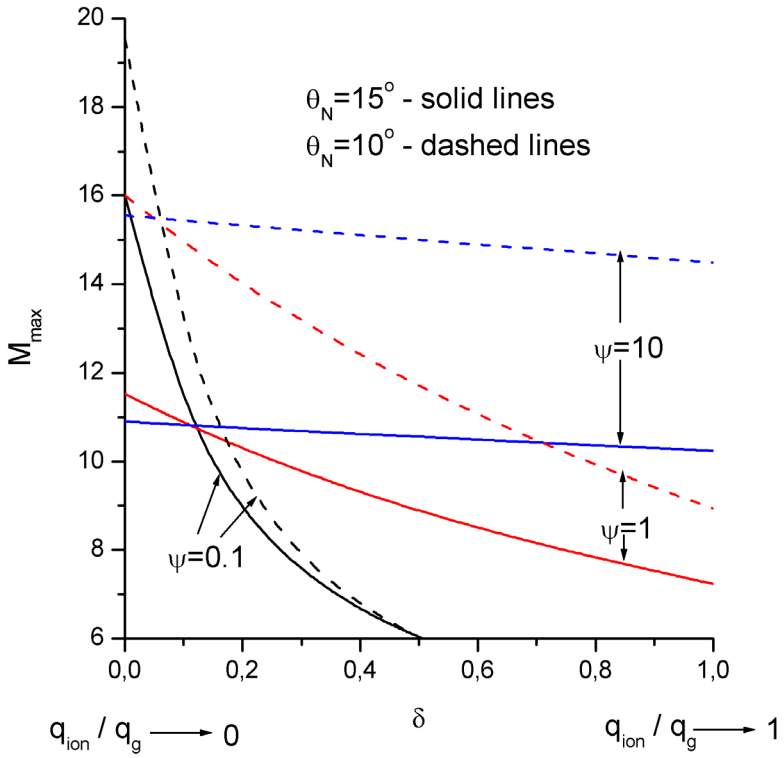

Fig.18 Maximal value of flight Mach number at which MHD interaction increase scramjet specific impulse vs. δ parameter for various values of ψ and θ_N.

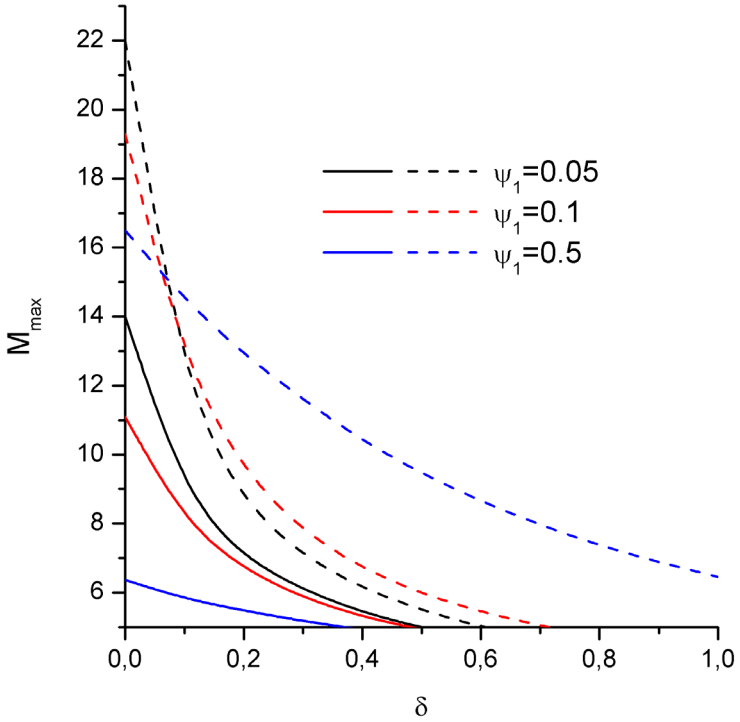

Fig.19 Maximal value of flight Mach number at which MHD interaction increase scramjet specific impulse vs. δ parameter for various ψ. For combustion chamber working in a mode with a constant density (solid lines) and with a constant pressure (dashed lines).

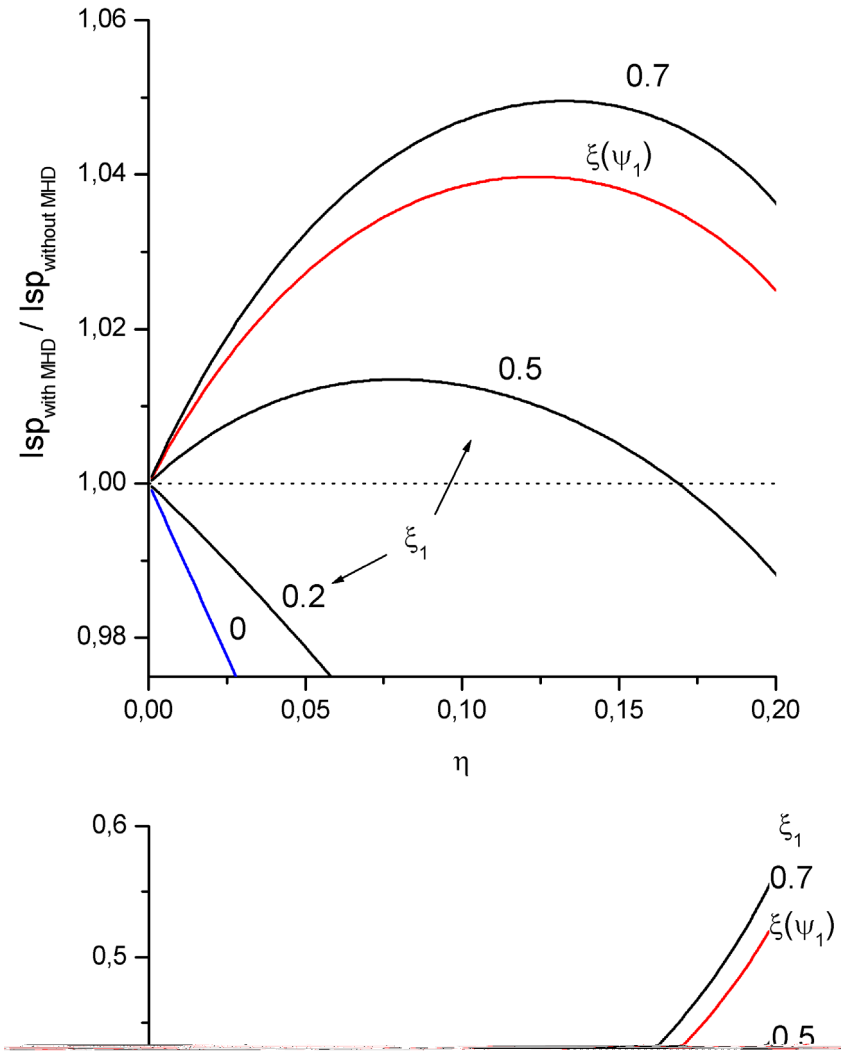

a)

b)

Fig.20 Relative specific impulse (a) and relative power spent on ionization (b) for MHD generator with various parameters ξ_1. θ_N=15°, M_d=10, F_{th}=0.12, M_0=6, q_i/q_{cr}=0.05, power density is constant in MHD generator volume.

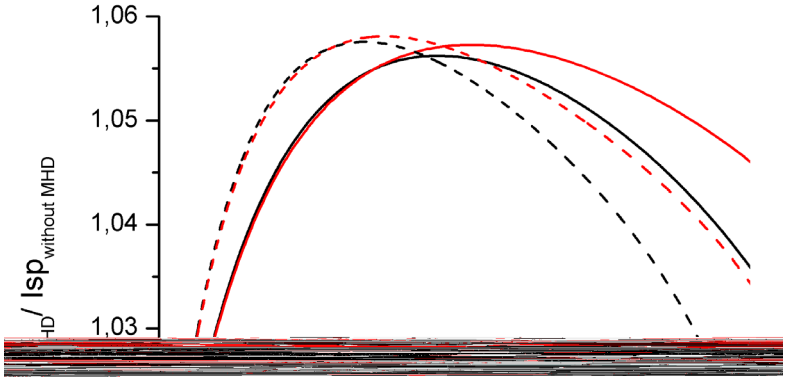

a)

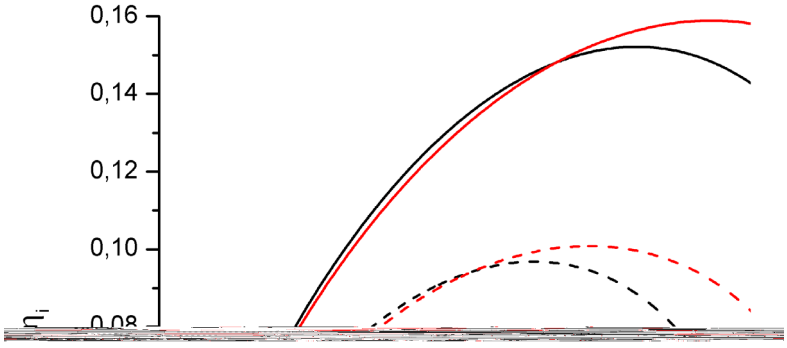

b)

Fig.21 Relative specific impulse (a) and relative power excess (b) vs. MHD interaction parameter for scramjet with Faraday (solid lines) and Hall (dashed lines) MHD generators. Red lines correspond to constant power density spent on ionization; black lines correspond to constant density of e-beam current. θ_N=15°, M_d=10, F_{th}=0.12, M_0=6, q_i/q_{cr}=0.01, k_I=0.5

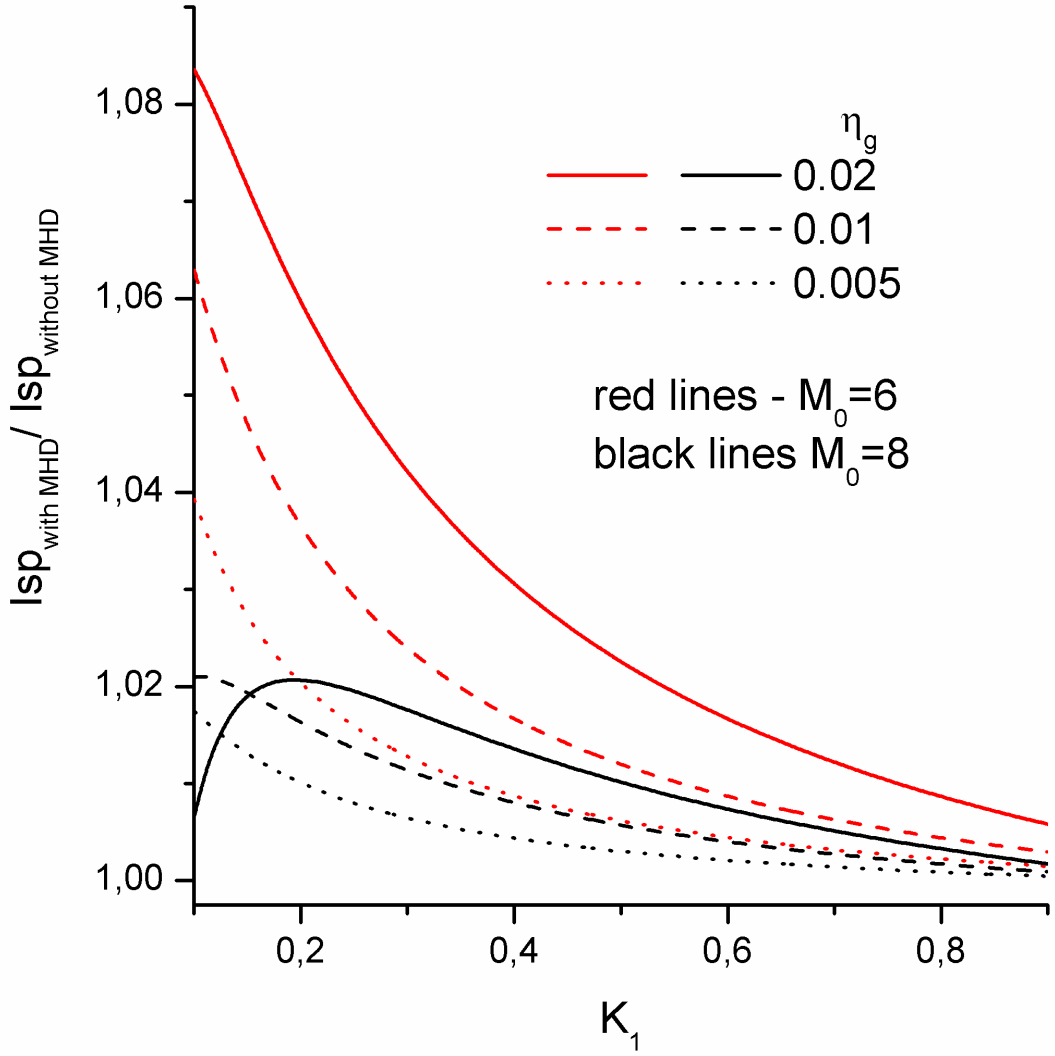

Fig.22 Relative specific impulse vs load factor for scramjet with Faraday MHD generator for various values of enthalpy extraction ratio. θ_N=15°, M_d=10, F_{th}=0.17, M_0=6, q_i/q_{cr}=0.01, k_3=1.1

a)

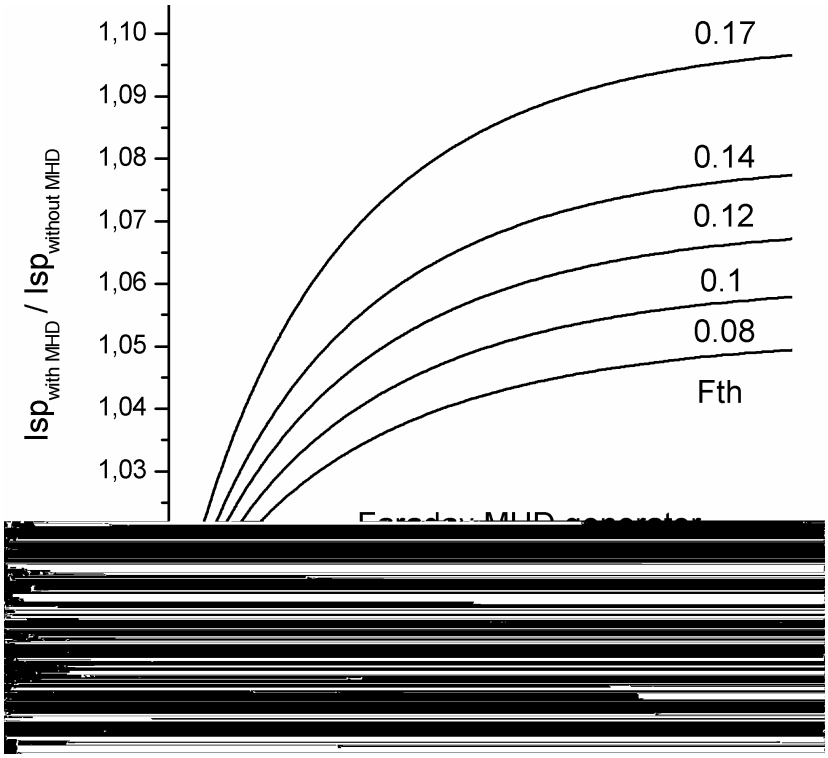

b)

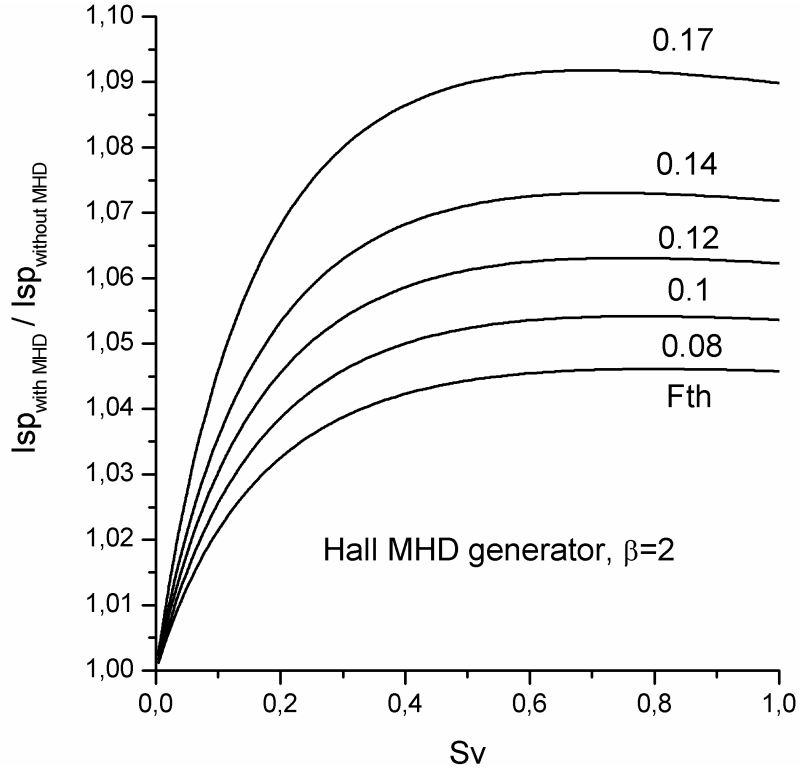

Fig.23 Relative specific impulse vs MHD interaction parameter for various relative values of inlet throat F_{th} for scramjet with: (a) Faraday MHD generator, (b) Hall MHD generator. θ_N=15°, M_d=10, M_0=6, q_i/q_{cr}=0, k_1=0.5, k_3=1.2.

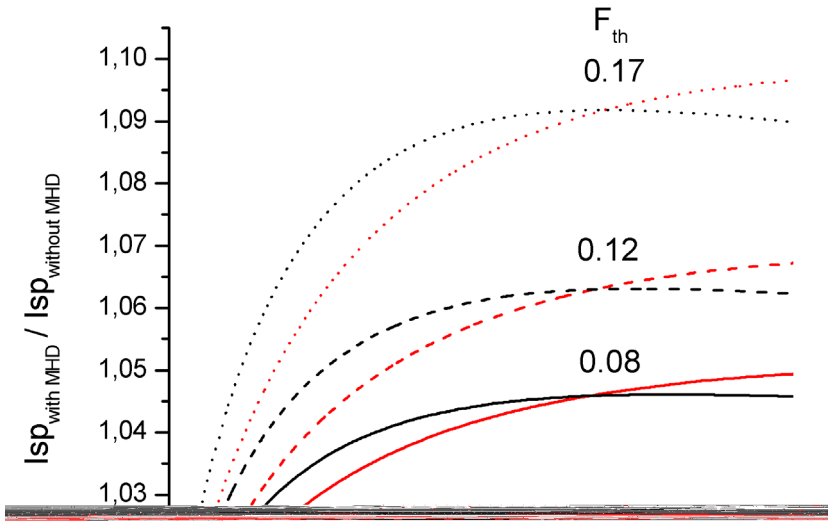

a)

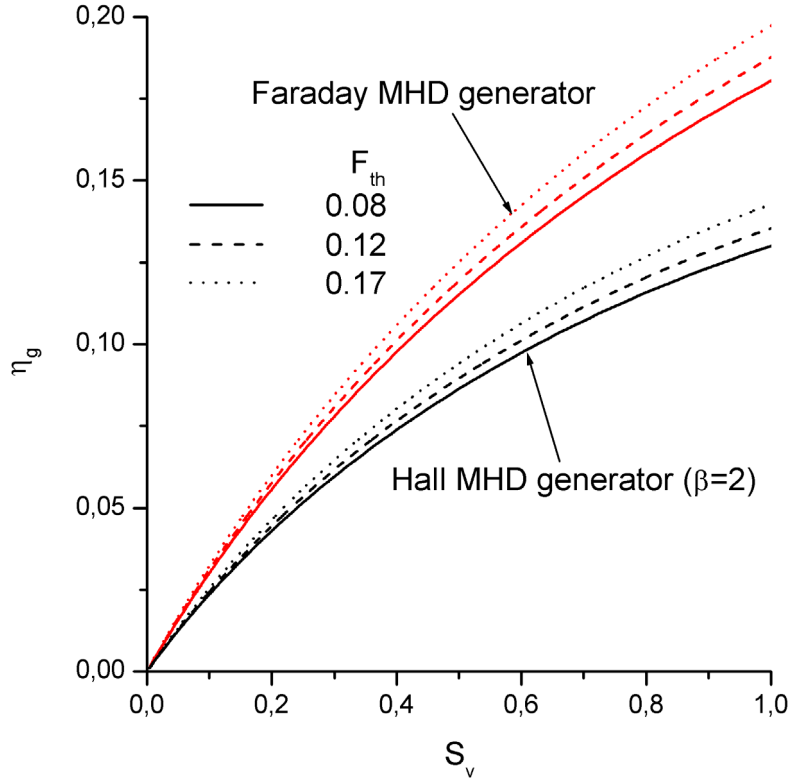

b)

Fig.24 Relative specific impulse (a) and power produced by MHD generator in scramjet vs MHD interaction parameter for various relative values of inlet throat F_{th}. θ_N=15°, M_d=10, M_0=6, q_i/q_{cr}=0, k_1=0.5, k_3=1.2.

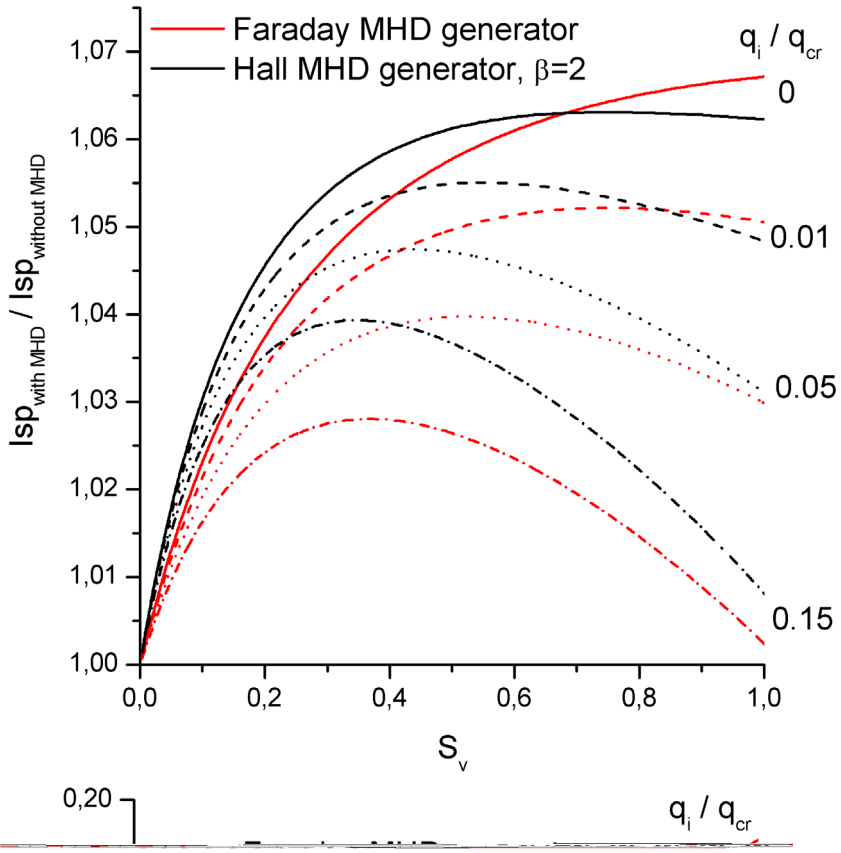

a)

b)

Fig.25 Relative specific impulse (a) and power excess (b) in scramjet with MHD control as a function of MHD interaction parameter for various relative values of q_i/q_{cr}. θ_N=15°, F_{th}=0.12, M_d=10, M_0=6, k_1=0.5, k_3=1.2.

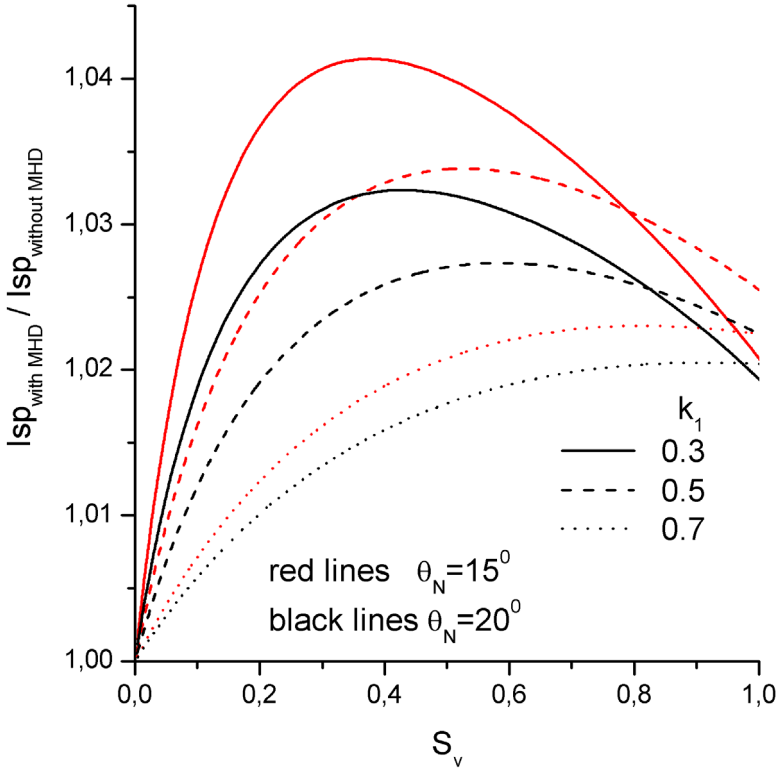

a)

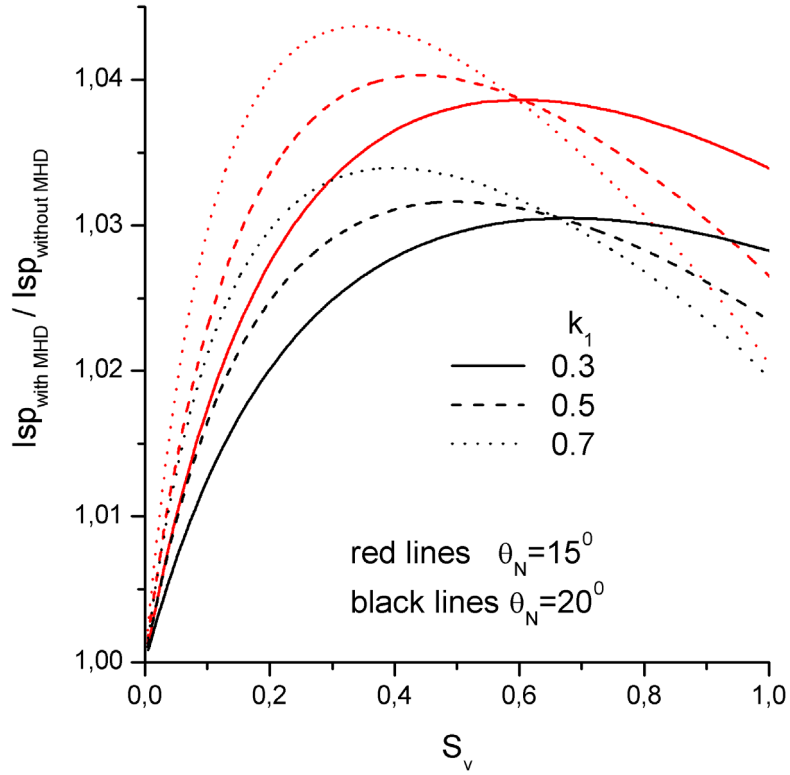

b)

Fig.26 Relative specific impulse for scramjet with MHD control vs MHD interaction parameter for various inlet configurations and various load factors. M_d=10 F_{th}=0.1, M_0=6, q_i/q_{cr}=0.05, k_3=1.2. (a) Faraday MHD generator, (b) Hall MHD generator with β=2

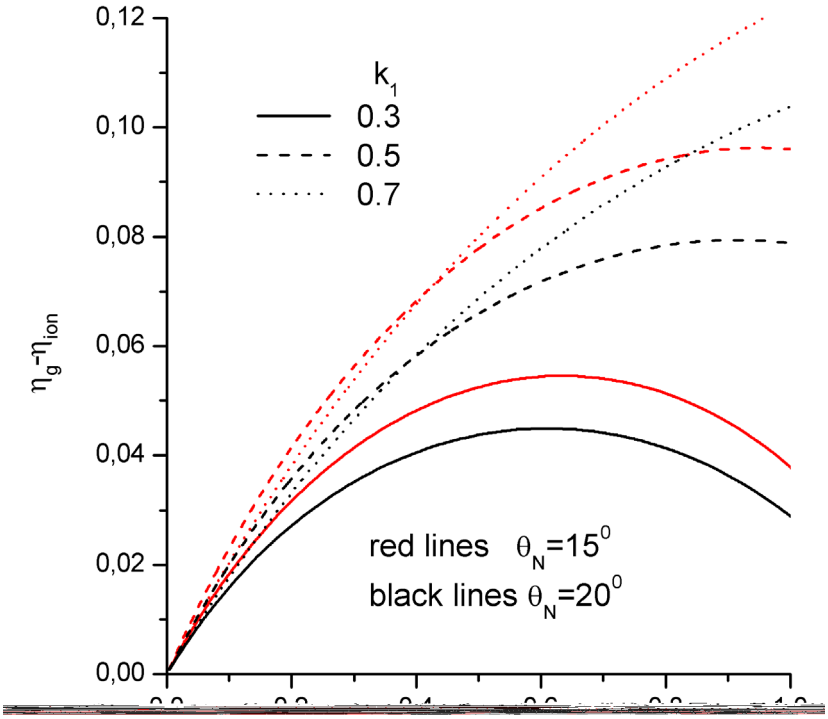

a)

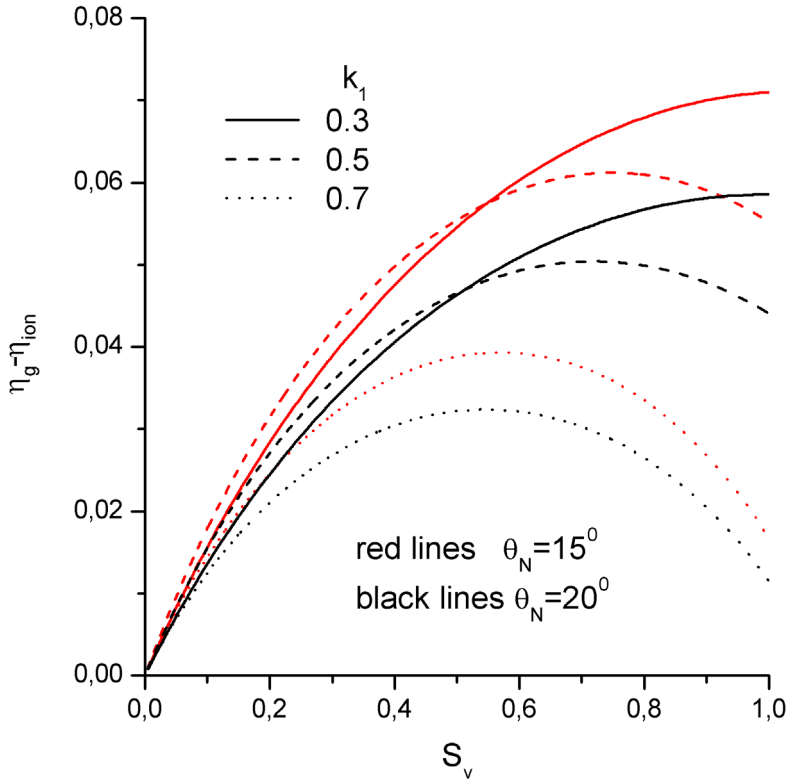

b)

Fig.27 Relative power excess produced by MHD generator in scramjet vs MHD interaction parameter for various inlet configurations and various load factors. M_d=10 F_{th}=0.1, M_0=6, q_i/q_{cr}=0.05, k_3=1.2. (a) Faraday MHD generator, (b) Hall MHD generator with β=2

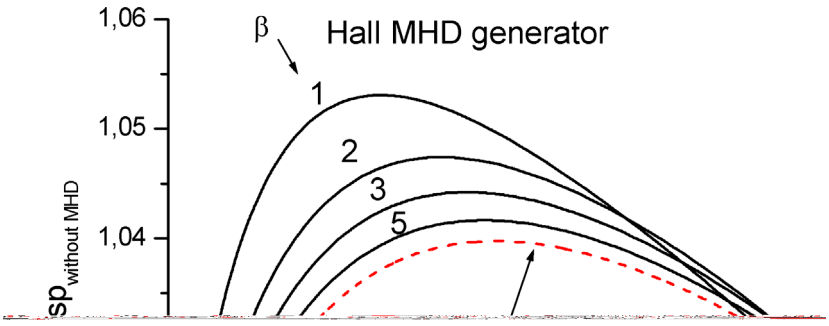

a)

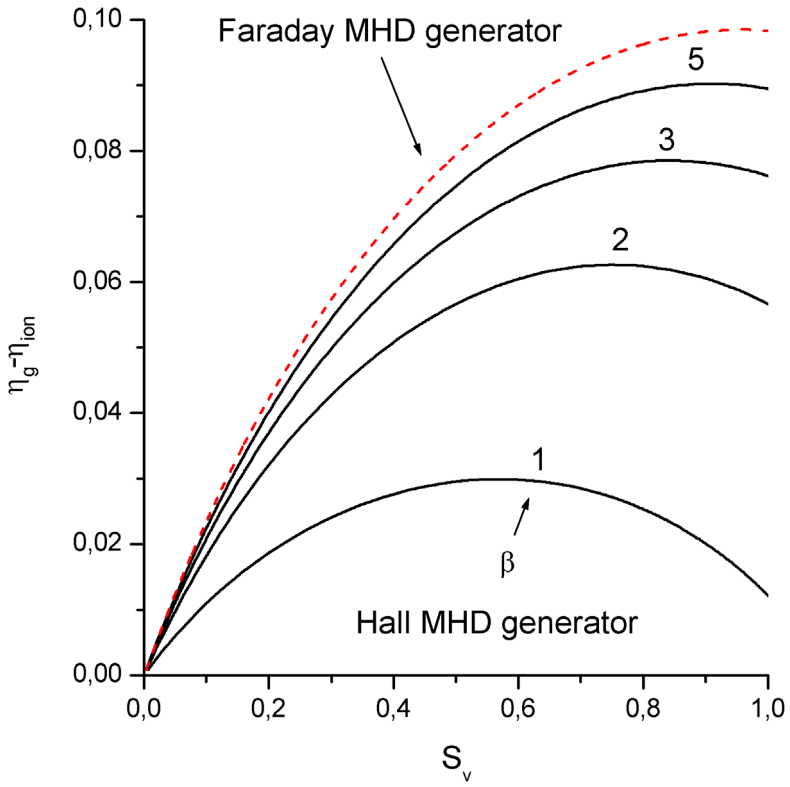

b)

Fig.28 Relative specific impulse (a) and power excess (b) vs MHD interaction parameter for scramjet with Hall MHD generator at various values of Hall parameter. M_d=10 F_{th}=0.12, M_0=6, q_i/q_{cr}=0.05, k_3=1.2. Red curves correspond to Faraday MHD generator.

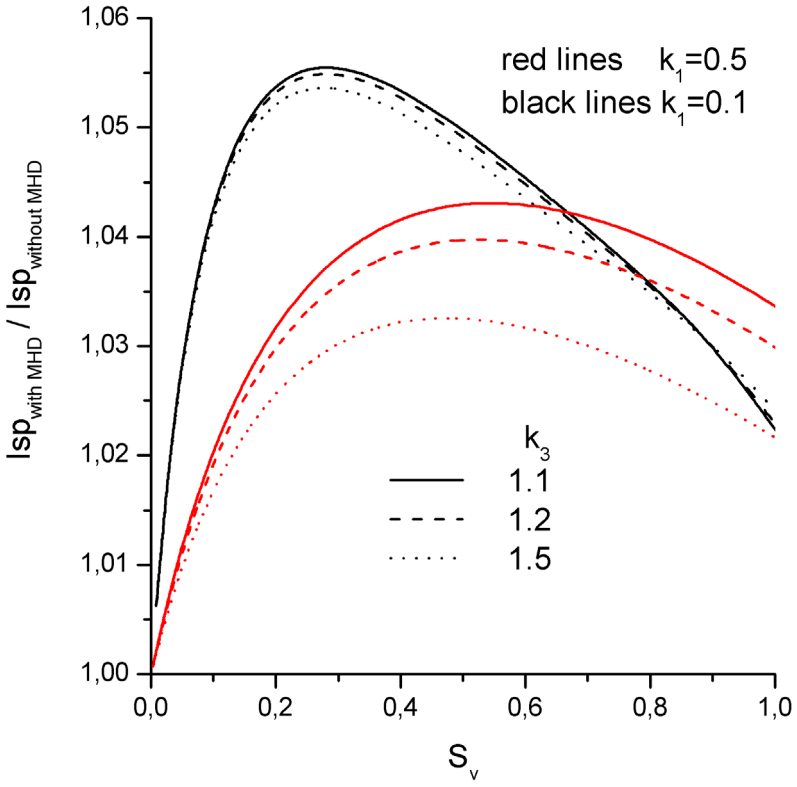

a)

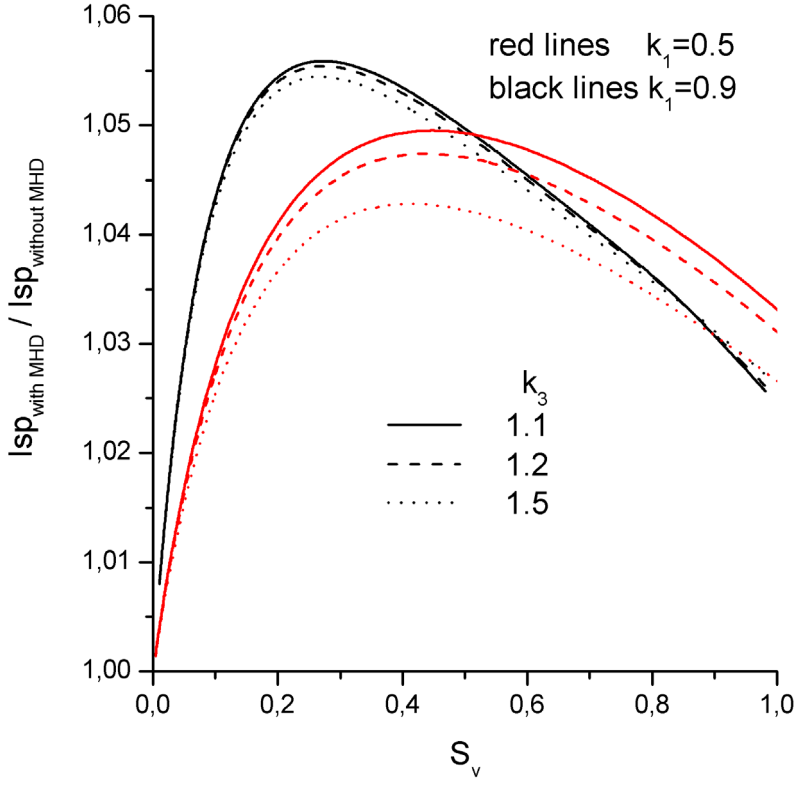

b)

Fig.29b Relative specific impulse of scramjet with MHD control as a function of MHD interaction parameter for various load factor of MHD accelerator k_3: a) Faraday MHD generator, b) Hall MHD generator with β=2. M_d=10 F_{th}=0.12, M_0=6, q_i/q_{cr}=0.05.

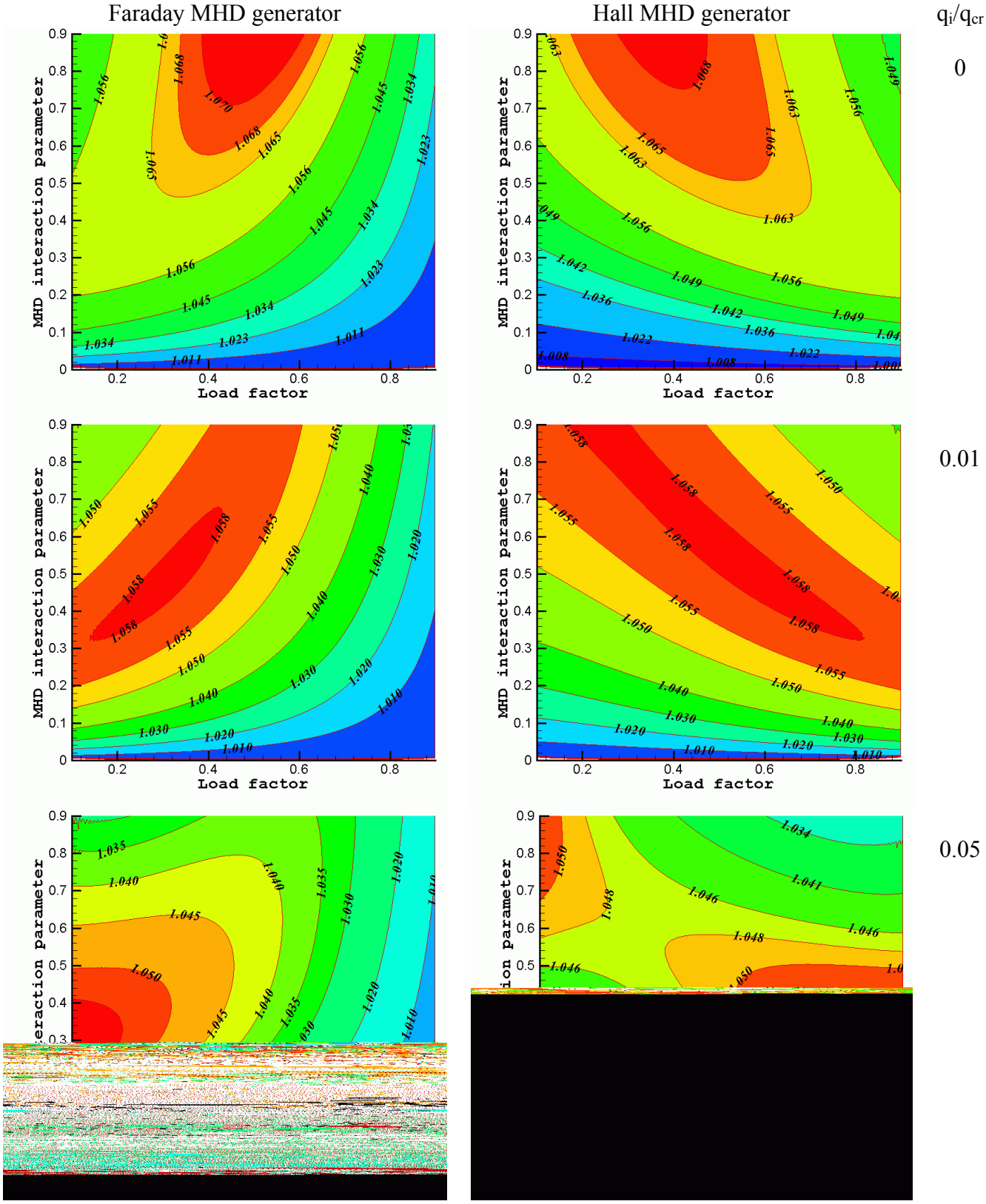

Fig.30 Contours of relative specific impulse for scramjet with MHD control. M_0=6, M_d=10, θ_N=15°, F_{th}=0.12, k_3=1.1, β=2

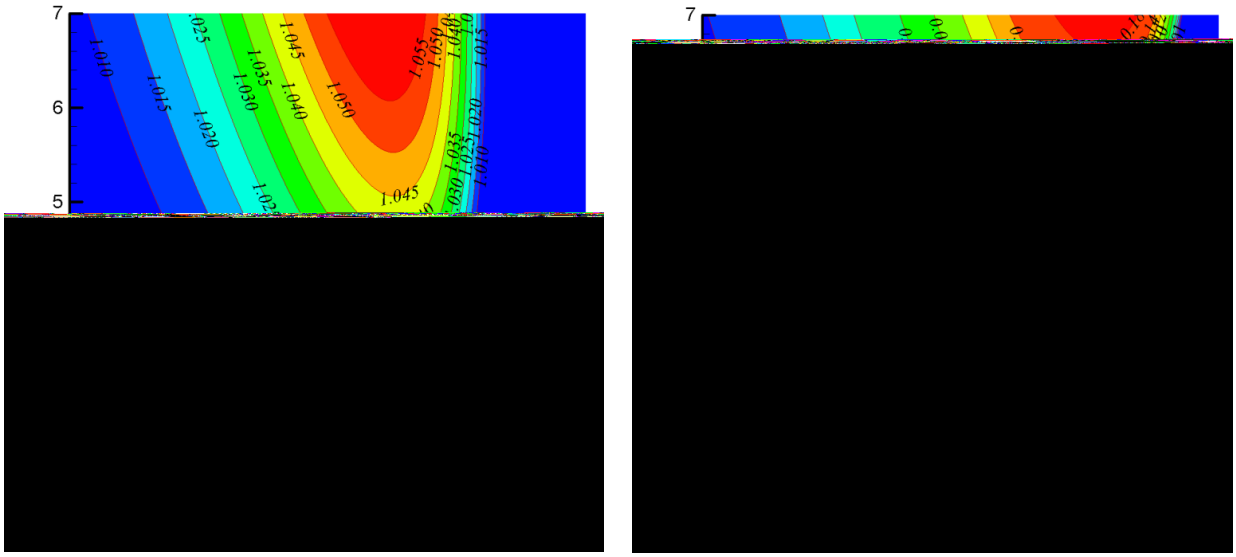

a) b)

Fig.31 Contours of relative specific impulse (a) and power excess (b) for scramjet with Faraday MHD generator. θ_N=15°, M_d=10, F_{th}=0.12. M_0=6, L=2m, k_1=0.5, k_3=1.1

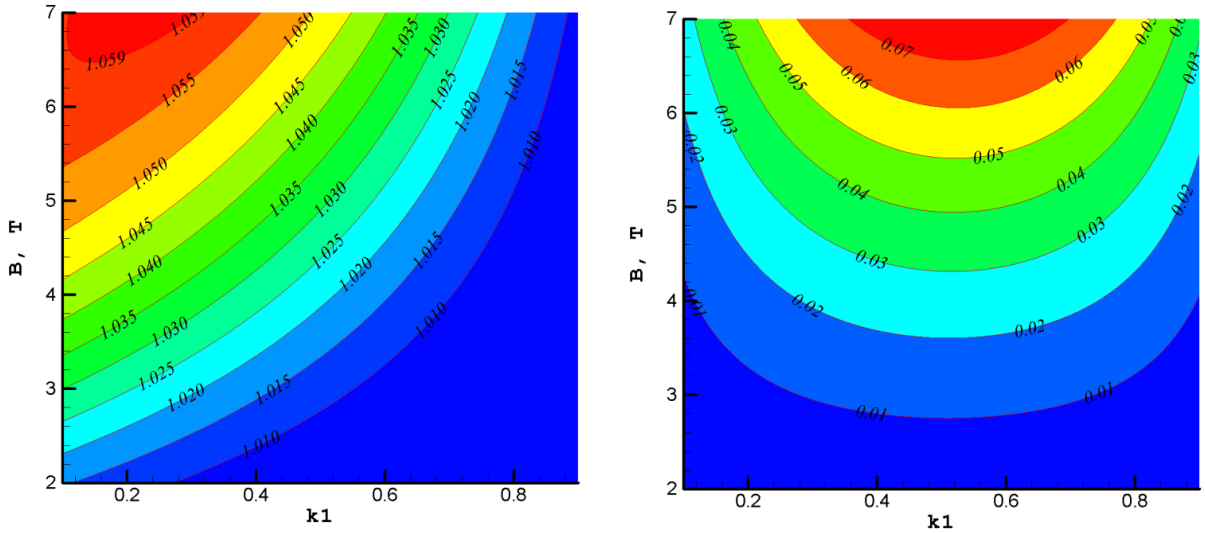

a) b)

Fig.32 Contours of relative specific impulse (a) and power excess (b) for scramjet with Faraday MHD generator. θ_N=15°, M_d=10, F_{th}=0.12. M_0=6, L=2m, q_i=1W/cm^3, k_3=1.1

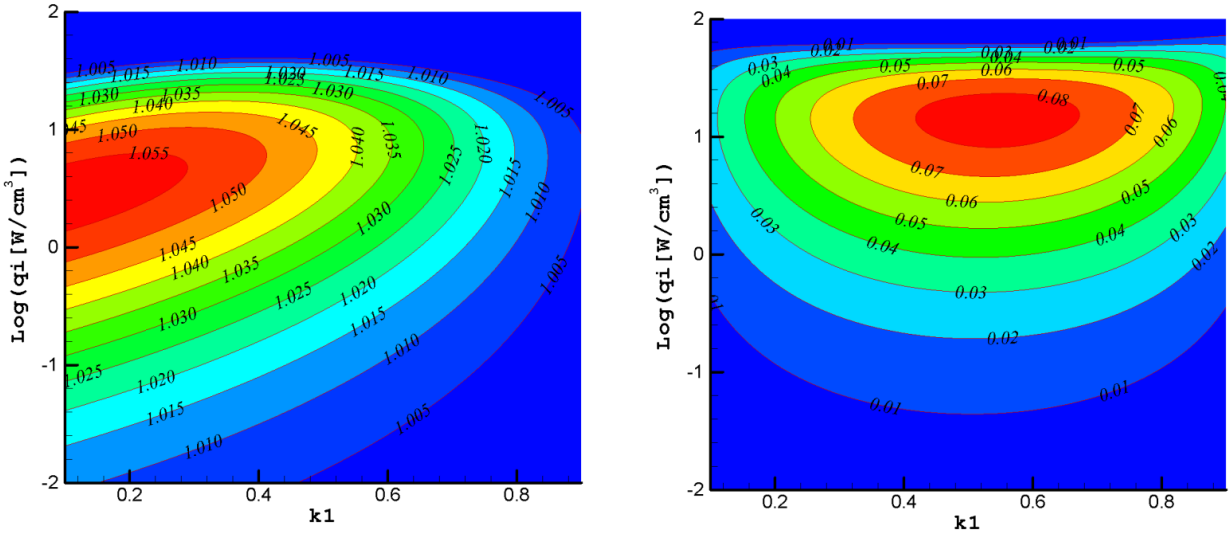

a) b)

Fig.33 Contours of relative specific impulse (a) and power excess (b) for scramjet with Faraday MHD generator. θ_N=15°, M_d=10, F_{th}=0.12. M_0=6, L=2m, B=5T, k_3=1.1

4. TWO-DIMENSIONAL MODEL FOR MHD CONTROLLED INLET OF SCRAMJET

This chapter is devoted to development of mathematical model of combined gas-dynamical system which includes MHD generator and ionizer in two-dimensional approach and numerical calculations of flow-fields in gas-dynamical channel in a wide spectrum of flow parameters, configuration of gas-dynamical system, power spent on flow ionization, shape and length of plasma formation. As the combined gas-dynamical system we consider scramjet, which includes MHD generator with non-equilibrium conductivity, located in inlet of the scramjet. It is supposed that MHD generator allows us to control flow-field and improve scramjet performance.

Typical geometry of scramjet inlet with design Mach number M_d=10, total turning angle θ_N=15° and relative value of inlet throat F_{th}=0.1 is shown in the Fig.34 ($F_{th}=1-Y_b/Y_a$). Arbitrary ionized region, where MHD interaction is effected, is shown in the Fig.34. We consider homogeneous magnetic field which has both x and y components ($\vec{B}=\{B_x,B_y,0\}$). Magnetic field will be characterized by two parameters: modulus of magnetic induction $B\equiv\left|\vec{B}\right|=\sqrt{B_x^2+B_y^2}$ and angle of magnetic field orientation α ($B_x=B\cdot\cos(\alpha)$, $B_y=B\cdot\sin(\alpha)$). It is supposed that electrodes of MHD generator are located in the plane of the figure at coordinates z=-∞ and z=∞. Conductivity of flow is created by using of e-beam ionizer. Flow conductivity depends upon the power density spent on flow ionization and flow parameters. To calculate flow conductivity we use formulas presented in the second chapter. Position and shape of ionized region are chosen arbitrarily to investigate how the geometrical characteristics of the ionized region influence on the inlet performance.

Flow-field in the MHD-controlled inlet of scramjet is calculated in two-dimensional Euler approach. Set of equations used in calculations is listed below:

$$\begin{aligned}
&\frac{\partial\rho v_x}{\partial x}+\frac{\partial\rho v_y}{\partial y}=0,\\
&\frac{\partial\left(\rho v_x^2+p\right)}{\partial x}+\frac{\partial\rho v_x v_y}{\partial y}=f_x,\\
&\frac{\partial\left(\rho v_y^2+p\right)}{\partial y}+\frac{\partial\rho v_x v_y}{\partial x}=f_y,\\
&\frac{\partial(e+p)v_x}{\partial x}+\frac{\partial(e+p)v_y}{\partial y}=q_g+q_r,\\
&e=\rho\left(c_vT+\left(v_x^2+v_y^2\right)/2\right),\quad p=R\rho T,
\end{aligned}\qquad (36)$$

where ρ is the flow density, v_x and v_y are the x and y components of flow velocity, p is the static pressure, T is the flow temperature, c_v is the specific heat, R is the absolute gas constant. Expressions for the right side of equations (36) have the following view: $\vec{f}=\{f_x,f_y,0\}$, $\vec{f}=\vec{j}\times\vec{B}$, $q_g=\vec{j}\cdot\vec{E}$, where j is the current density, E is the electric field. The generalized Ohm's law determines relations between electromagnetic components:

$$\vec{j}+\mu\left(\vec{j}\times\vec{B}\right)=\sigma\left(\vec{E}+\vec{v}\times\vec{B}\right)\quad (37)$$

where μ is the electron mobility, σ is the electrical conductivity. The quantity q_r included in a right side of (36) determines the power density put into a flow as a result of a recombination of charged particles.

Functions f_x, f_y, and q_g from the right part of (36) are determined from (37) as a functions of parameters B_x, B_y, v_x, v_y, E_x, E_y, E_z and σ. We consider ideally sectioned Faraday MHD generator for which current density has only z component ($\vec{j} = (0, 0, j_z)$). In this case MHD interaction can be characterized by dimensionless factor $k=-E_z/v_0B_0$ by the ratios:

$$f_x = -\left(\frac{v_x B_y}{v_0 B_0} - \frac{v_y B_x}{v_0 B_0} - k \right) \sigma v_0 B_0 B_y$$

$$f_y = \left(\frac{v_x B_y}{v_0 B_0} - \frac{v_y B_x}{v_0 B_0} - k \right) \sigma v_0 B_0 B_x \qquad (38)$$

$$q_g = -k \left(\frac{v_x B_y}{v_0 B_0} - \frac{v_y B_x}{v_0 B_0} - k \right) \sigma v_0 B_0^2$$

Computational procedures for solution the set of equations (36) are based on the explicit high-resolution shock-capturing Godunov-type scheme for space-marching calculations of stationary supersonic flows. Initial conditions are given by incoming flow. Normal velocity component on the wall is assumed to be zero.

Fig.35 demonstrates pressure contours in scramjet inlet without MHD interaction at design conditions. Fragment of computational grid from red rectangular area marked in the Fig.35a are shown in the Fig.35b. In this calculation the size of grid was 2529×200. Grid is adaptive in x direction. Fragments of computational grid in MHD controlled inlet are shown in the Fig.36. Fig.36a corresponds to inlet without MHD interaction. In this case the grid is uniform. Fig.36b corresponds to inlet with MHD generator located in the range $1 \le x \le 1.2$. In this case the grid becomes nonuniform. Step of the grid decreases in x direction in the MHD interaction area.

In calculations of MHD controlled inlet we will consider various simple geometries of ionized region, which are shown in the Fig.37. MHD generator with nonequilibrium conductivity is considered. Flow conductivity σ in ionized region is a function of flow parameters and power density spent on flow ionization q_i (the chapter 2). Gas-dynamic flow compression in scramjet inlet occurs in series of oblique shocks. So flow parameters in scramjet without MHD interaction (see Fig.35a) are inhomogeneous. Thus requirements to parameters of ionizer and magnetic system, which provide self-sustained operational mode for MHD generator with nonequilibrium conductivity will be a function of geometry of inlet and position of, ionized region. In the general case the condition for self-sustained operational mode for the MHD generator can be written in the form:

$$\iint_V q_i(x, y)\, dxdy \le \iint_V q_g(q_i, x, y)\, dxdy \qquad (39)$$

where V is a volume in which ionization of a flow and extraction of electric power by MHD generator take place, q_g is calculated according to (38). In calculations we suppose that q_i has a constant value in the region of ionization. Function q_g depends on the x and y coordinates because variables v_x, v_y and σ are functions of the coordinates. The magnitude of q_i at which in expression (39) is implemented a sign of equality, corresponds to critical operational mode of MHD generator with nonequilibrium conductivity. It is easy to see from (39) that the following equation determines critical power in nonlocal approach:

$$q_{cr} = \frac{1}{V} \iint_V q_g(q_{cr}, x, y) dxdy$$

MHD generator with nonequilibrium conductivity operates in self-sustained operational mode if $0<q_i \le q_{cr}$. When the volume V tends to zero volume, the value q_{cr}, determined from the ratio tends to value determined from (12b) or (24) in local approach. The calculations of dependencies of q_{cr} upon the longitudinal size of plasma formation were carried out for shape of ionized region presented in the Fig.37b. We have considered height of the region Y_2=1m. Position of the region is determined by condition: $y<Y_2$ and $x_1 \le x \le x_2$. Results presented in the Fig.38 correspond to ionized region with x_1=0. In calculations we vary length of the plasma formation (x_2), load factor k and angle of magnetic field orientation α. All critical powers q_{cr} are normalized on the critical powers obtained for x_2=0.5 m and $\alpha=90°$ for corresponding values of the load factor. Calculations have been done for scramjet configuration shown in the Fig.34. Fig.38a demonstrates that critical power decreases while increasing the plasma length practically in similar way for various load factors. Fig.38b demonstrates dependencies of the critical power upon the angle α for identical plasma regions with x_2=0.5 m. One can see that maximal critical power is achieved at $\alpha=90°$. The greater is the load factor the more sensitive is the critical power value to the angle of magnetic field orientation. So one can see that critical power essentially depends upon considered configuration. In studying the MHD controlled scramjet we verify condition (39) in all computations. Situations in which the condition is failed are not considered in the report.

The first step of our research is devoted to investigation of possibilities of MHD generator to move shock wave position. We consider flow with initial Mach number M_0=8 and free stream dynamic pressure 40 kPa flowing around the wedge with the angle 10°. Pressure colour map without MHD interaction is shown in the Fig.39a. We suppose that in configuring the magnetic field in such a way that the Lorentz force will be directed away from the wedge (or will be positive in our coordinate system (Fig.34)) the angle of oblique shock will be increased. To decrease the angle of oblique shock it is necessary to form the Lorentz force directed toward the wedge. It can be done only when $f_y<0$. We assume that $B_y>0$. For MHD generator $q_g<0$ and force $f_x<0$. Thus it is evidently from (38) that force $f_y<0$ only when $B_x<0$. So, it is necessary to have magnetic field with $\alpha>90°$ in order to decrease the angle of oblique shock.

Pressure colour map in the flow around the wedge with MHD control with magnetic field which is characterized by $\alpha=45°$ is shown in the Fig.39b. Range of MHD interaction is band located in $2 \le x \le 2.5$ (which is schematically shown in the Fig 37a). One can see that MHD interaction essentially increases the angle of the oblique shock. Fig.39c demonstrates pressure colours map for MHD control which is characterized by B=3T and $\alpha=90°$. Despite of the y-component of the Lorentz force is equal to zero in this case, the oblique shock deviation is greater than in the case presented in the Fig.39b. In the Fig. 40 the relative pressure contours (pressure normalized on pressure in free stream) in stream flowing around the wedge for two configuration of magnetic field are compared. One can see that in the case with $\alpha=90°$ the MHD interaction provides noticeable increase of static pressure. In the Fig. 41 the relative temperature (temperature normalized on temperature in free stream) contours in stream flowing around the wedge for two configuration of magnetic field are compared. One can see that in the case with $\alpha=45°$ the MHD interaction practically doesn't increase the temperature behind the shock. So we can conclude that increase of the angle of oblique shock in result of MHD influence on flow can be realized both with slight modification of pressure and temperature behind the shock ($\alpha=45°$) and with considerable increase of these parameters behind the shock ($\alpha=90°$). Thus if we are interested in increasing the pressure and

temperature behind the shock when oblique shock is deflected by magnetic field it is necessary to use magnetic field with $\alpha=90°$. Otherwise it is necessary to apply magnetic field with $\alpha<90°$.

Now we consider peculiarities of MHD interaction on stream flowing around the wedge when $\alpha>90°$. Pressure colour map in the flow around the wedge with MHD control with magnetic field which is characterized by $\alpha=135°$ is shown in the Fig.42. In this case the Lorentz force is negative and we expect that MHD interaction decrease the angle of oblique shock. In comparing the Fig.42 and Fig.39 one can conclude that oblique shock position in this case is practically similar to position of oblique shock without MHD interaction. It can be explained by pressure increase behind the shock. Fig.43 demonstrates that pressure increase behind the shock in this case is significant in comparison with $\alpha=45°$ MHD interaction (Fig.40a) and practically the same as in the case of MHD interaction with $\alpha=90°$ (Fig.40b). According to the Fig.44 the temperature increase behind the shock for $\alpha=135°$ is essentially less when one for $\alpha=90°$ (Fig.41b). Fig.45 demonstrates positions of oblique shocks in the case of MHD interaction with $\alpha=45°$ and $\alpha=135°$ and in the absence of MHD interaction. One can see that MHD interaction with $\alpha=45°$ increases angle of oblique shock and MHD interaction with $\alpha=135°$ very slightly decreases angle of oblique shock. Such effect is obtained for B=5T ($\alpha=135°$) and B=1T ($\alpha=45°$). So one can conclude that decreasing the angle of oblique shock by MHD control is more complicated problem than increasing one.

And now we consider possibilities of MHD control for modification of flow field in inlet at off-design conditions. Firstly situation for flight Mach number greater than design Mach number will be investigated. In papers [12,13] it was shown that MHD control in this case allows us to modify flow field in such a way that it becomes like a flow field in design conditions. Thus in this report we only briefly consider how various plasma configurations influence on the flow field at $M_0>M_d$.

The Fig.46 demonstrates possibilities of MHD interaction, which is located in the range $0\le x\le 0.5$, to modify flow field in scramjet inlet. Fig.46a shows Mach number contours in inlet at off-design conditions without MHD interaction at flight Mach number $M_0=12$. In this case, unlike to design conditions (see the Fig.35), the oblique shocks intersection occurs not in cowl lip. Increase of power density spent on ionization (Fig.46 b-d) causes the oblique shocks angles to be increased. When $q_i=0.022 W/cm^3$ oblique shocks are intersected in the cowl lip and flow field becomes quite similar to the one shown in the Fig.35. When q_i becomes greater than $0.022\ W/cm^3$ (Fig.46d) the flow field becomes similar to situation with the flight Mach number is less than design one.

In the Fig.47a MHD interaction is realized in the range $3\le x\le 3.5$. In this situation oblique shocks intersection occurs not exactly in cowl lip. But the point of shocks intersection is nearer to cowl lip than in the case without MHD interaction (Fig.46a). In the Figs.47b-c MHD interaction is realized in the range with $3\le x\le 4$ and $y\le 0.7$, which is schematically shown in the Fig 37b. When magnetic field is orthogonal to x-axis ($\alpha=90°$) the shocks intersection occurs not exactly in cowl lip (Fig.47b). But in changing the magnetic field orientation ($\alpha=45°$) point of oblique shocks intersection moves to cowl lip (Fig.47c).

Fig.47d corresponds to ionized range located in $0\le x\le 5$ and $y\le 0.2\cdot x$, which is schematically shown in the Fig 37d. One can see that in this case the flow field is quite similar to the flow field at design conditions. Fig.48 demonstrates density distributions in cross-section of MHD controlled inlet at x=7.1 for the configuration of ionized region. It

follows from the Fig.48 that density distribution tends to the distribution at design conditions while increasing the power density spent on flow ionization.

And now we will investigate possibilities of MHD generator to control flow in scramjet inlet when flight Mach number is less than design Mach number. Flow field in scramjet inlet in this situation is shown in the Fig.49. The serious disadvantages of the flight regime are decrease of flow compression and air capture in scramjet. The aim of our investigation is finding the regimes of MHD influence on flow, which allow us to increase both, flow compression and air mass flow rate in scramjet for such flight regimes. In analyzing we consider two characteristics of inlet: relative pressure increase (flow compression) p_1/p_0, where p_0 is the incoming flow static pressure and p_1 is the averaged static pressure at exit of inlet (in our computations $x=7.1$); and relative air mass flow $\varphi = \dot{m}/\dot{m}_0$ which corresponds to ratio of air mass flow in inlet $\dot{m}$ (which is computed at exit of inlet $\dot{m} = \int \rho v_x dy \cdot \Delta z$) to the free stream mass flow $\dot{m}_0$ which is restricted by the non-disturbed line of flow closed in the cowl lip and x axis. We consider only zero angle of attack, thus $\dot{m}_0 = \rho_0 v_0 Y_c \cdot \Delta z$, here Δz is characteristic width of inlet in z direction, Y_c is y coordinate of the cowl lip (in our consideration Y_c=1m (see Fig.49)).

Fig.50 demonstrates dependencies of relative mass flow and flow compression in MHD controlled inlet upon power density spent on flow ionization for various configurations of magnetic fields. Ionization range is a band which is located in $x_1 \le x \le x_1 + \Delta x$. For Fig.50a x_1=0 and for Fig.50b x_1=1, Δx=1m in all the cases. Green lines in the figure correspond to relative mass flow (solid lines) and relative pressure increase (dashed lines) in scramjet without MHD interaction. One can see that for x_1=1 and α=135° there is a range of q_i variation for which MHD interaction leads to insignificant increase of air mass flow. Relative pressure rises while increasing the q_i value when α=135°. If α<90°, the increase of power density spent on flow ionization causes both the relative pressure and relative air mass flow to be decreased. This effect correlates with results obtained in investigations of wedge in magnetic field and can be explained by Lorentz force direction.

Fig.51 demonstrates dependencies of relative air mass flow (a) and relative pressure increase (b) in MHD controlled inlet vs. power densities spent on flow ionization for various positions of ionized region. Orientation of magnetic field α=135°. One can see that maximal air mass flow can be achieved when x_1=3. In considered conditions MHD interaction monotonically increase the pressure in MHD controlled inlet. As for air mass flow there are some optimal q_i at which maximal air capture in the inlet can be realized. Additional increase of MHD interaction will provide negative influence on the air mass flow.

Fig.52 demonstrates Mach number contours in MHD controlled inlet at flight Mach number M_0=8 which is less than design Mach number M_d=10. Flow fields correspond to three various configurations of magnetic field with magnetic induction B=1T. Level of MHD interaction corresponding to these figures is not very strong. The angles of oblique shocks slightly increase for $\alpha \le 90°$. For α=135° shock wave positions is practically not changed.

Fig.53 demonstrates Mach number contours in MHD controlled inlet with magnetic induction B=3T at conditions which are same to the Fig.52. In this case the level of MHD interaction is strong enough and modification of flow field is more significant than in Fig.52.

In order to view relative influence of MHD control on the air mass flow and on the flow compression in inlet we will consider normalized ratios: the normalized relative air mass flow (φ/φ_0), where φ_0 is the relative air mass flow in scramjet without MHD control, and

normalized flow compression (π/π_0), where $\pi \equiv (p_1/p_0)$ is the flow compression in MHD controlled inlet and π_0 is the flow compression in the inlet without MHD control. Fig.54 demonstrates how the normalized relative ratios depend on the orientation angle of the magnetic induction α for various values of B. Flight Mach number $M_0=8$, $M_d=10$. Ionized region is a band located in $3 \le x \le 4$. One can see that both for mass flow and for flow compression there are optimal values of α angle, greater than 90°, at which these parameters achieve a maximum. Maximal air capture in inlet increase while increasing the magnetic induction from 1 to 3 Tesla.

Fig.55 shows dependencies of φ/φ_0 as a function of the load factor k for various orientations of magnetic field at value $B=3T$. Results of calculations correspond to flight Mach number M_0=8. Ionized region is a band located in $3 \le x \le 4$. It is easy to see that in the considered situation MHD control allows us to increase the air capture. There are some optimal values for load factor (depending on the angle α) at which maximal air mass flow in MHD controlled inlet can be achieved. Maximal air capture in inlet increase while increasing the α angle from 130° to 145°. Fig.56 demonstrates dependencies of normalized flow compression π/π_0 as a function of the load factor k in conditions similar to the Fig.56. One can see that flow compression in the inlet monotonically decrease while increasing the load factor. Load factor optimal for increasing the air mass flow is not optimal for flow compression increasing. Fig.57 and Fig.58 demonstrate dependencies of φ/φ_0 and π/π_0, correspondingly, as a functions of the load factor k for various α angle at value $B=3T$ for flight Mach number $M_0=6$. These dependencies are similar to corresponding dependencies obtained for M_0=8 (Fig.55,56). Thus obtained results show that at given region of MHD interaction in inlet the air capture and the flow compression noticeably depend on the value and orientation of magnetic induction and the value of the load factor.

Now we consider influence of shape and position of ionized region on characteristics of the MHD controlled inlet. Fig.59 shows dependencies of φ/φ_0 as a function of position of ionized region X_1 in x-direction for various height of the region Y_2. Ionized region is column, shown in the Fig.37b, located in $X_1 \le x \le X_1+1$ and $y \le Y_2$. Air mass flow monotonically increases while increasing the height of ionized region. For $Y_2 \ge 1.25$ the air mass flow practically doesn't depend on the height and coincides this the one for ionized region in form of band. Dependencies of φ/φ_0 upon position X_1 is more complicated. At small heights Y_2 the air mass flow monotonically increases while increasing the X_1 value. For $Y_2 \ge 1.1$ there are optimal positions of X_1 at which maximal air mass flow is achieved. The optimal value for X_1 decreases while increasing the height of the ionized region. Fig.60 shows dependencies of π/π_0 as a function of position of ionized region X_1 for various heights of the region Y_2. Conditions are the same as in the Fig.59. Similarly to the air mass flow in inlet the flow compression increases while increasing the height of the ionized region. Positions of ionized region X_1 optimal for increasing the flow compression are slightly differ from positions optimal for increasing the air mass flow.

Results of investigation of MHD controlled inlet in the case when ionized region has a rectangular shape: $3 \le x \le 4$ and $Y_1 \le y \le Y_2$ (shown in the Fig.37c) are presented in the Fig.61 and 62. The Fig.61 shows ratio φ/φ_0 as a function of bottom border coordinate Y_1 at various coordinates of the upper border Y_2 for the ionized region. One can see that the air mass flow in the inlet monotonically increases while increasing the Y_2 value. For each position of Y_2 there is optimal value of Y_1, which is greater than 0.8m in considered configuration. Fig.62 shows dependencies of π/π_0 as a function of position of ionized region Y_1 for various

coordinates of the upper border of the region Y_2. Conditions are the same as in the Fig.61. Similarly to the air mass flow in inlet the flow compression increases while increasing the Y_2 value. Positions of bottom border Y_1 for the ionized region optimal for increasing the flow compression are differ from positions optimal for increasing the air mass flow. According to the Fig.62, values of Y_1, optimal for increasing of flow compression, are less than 0.7m. Fig.63 demonstrates how φ/φ_0 and π/π_0 depend on the orientation of magnetic induction for various position of ionized region in x-direction. The ionized region has rectangular shape and it is located in $X_1 \le x \le X_1+1$ and $0.9 \le y \le 1.0$. One can see that for this configuration maximal air mass flow and flow compression are achieved at $\alpha \approx 105°$. Air mass flow in the inlet not essentially depends on the X_1 value. On the contrary the flow compression in the inlet significantly depends on the X_1. So we can conclude that shape and position of ionized region are very important factors which influence on characteristics of MHD controlled inlet.

And now we consider influence of B and q_i values on characteristics of MHD controlled inlet in the case when ionized region is the band located in $3 \le x \le 4$. Fig.64 shows the ratio φ/φ_0 as a function of magnetic induction B for various values of q_i. It is easy to see that there are optimal values of magnetic induction, depending on the power density spent on flow ionization, at which air mass flow in MHD controlled inlet achieve maximum. The optimal magnetic induction decreases while increasing the q_i. Maximal normalized relative air mass flow decreases while increasing the power density spent on ionization in the range from $0.1 W/cm^3$ to $10 W/cm^3$. So to achieve maximal air capture in MHD controlled inlet it is necessary to ensure ionization with q_i not greater than $1 W/cm^3$. Fig.65 demonstrates the ratio π/π_0 as a function of magnetic induction B for various values of q_i. Similarly to air mass flow the flow compression achieves a maximal value at some optimal magnetic induction and the optimal value of magnetic induction is decreasing function of q_i value. The maximal flow compression in the inlet is achieved at maximal power density spent on ionization. Thus both the power density spent on ionization and the value of magnetic induction are important parameters, which determine characteristics of MHD controlled inlet.

Obtained results show that MHD control allows us to modify flow field in inlet of scramjet at off-design conditions. By using MHD influence on flow we can control oblique shocks position, air mass flow and flow compression in inlet. In proper choice of region of MHD interaction, configuration of magnetic field and load factor the MHD control in scramjet inlet allows us essentially, improve inlet performance at off-design conditions.

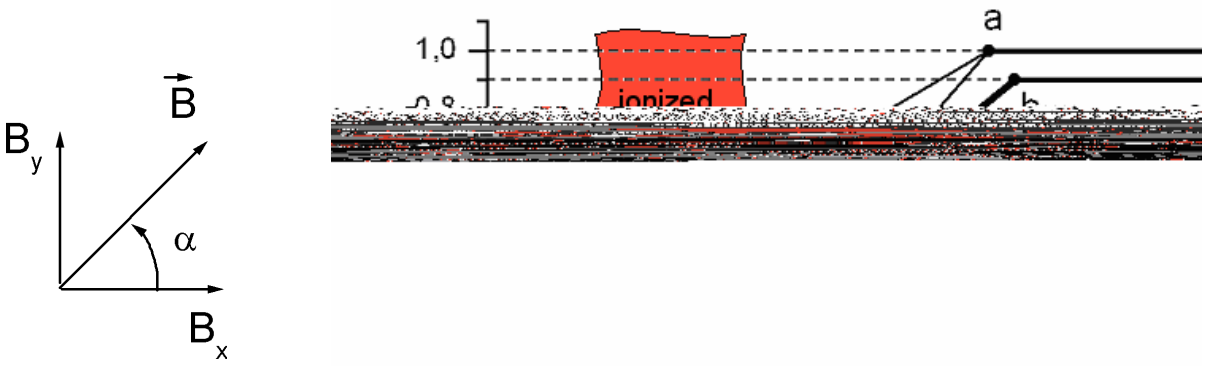

Fig.34 Geometry of MHD-controlled inlet with arbitrary region of flow ionized by e-beam, θ_N=15°, M_d=10, F_{th}=0.1.

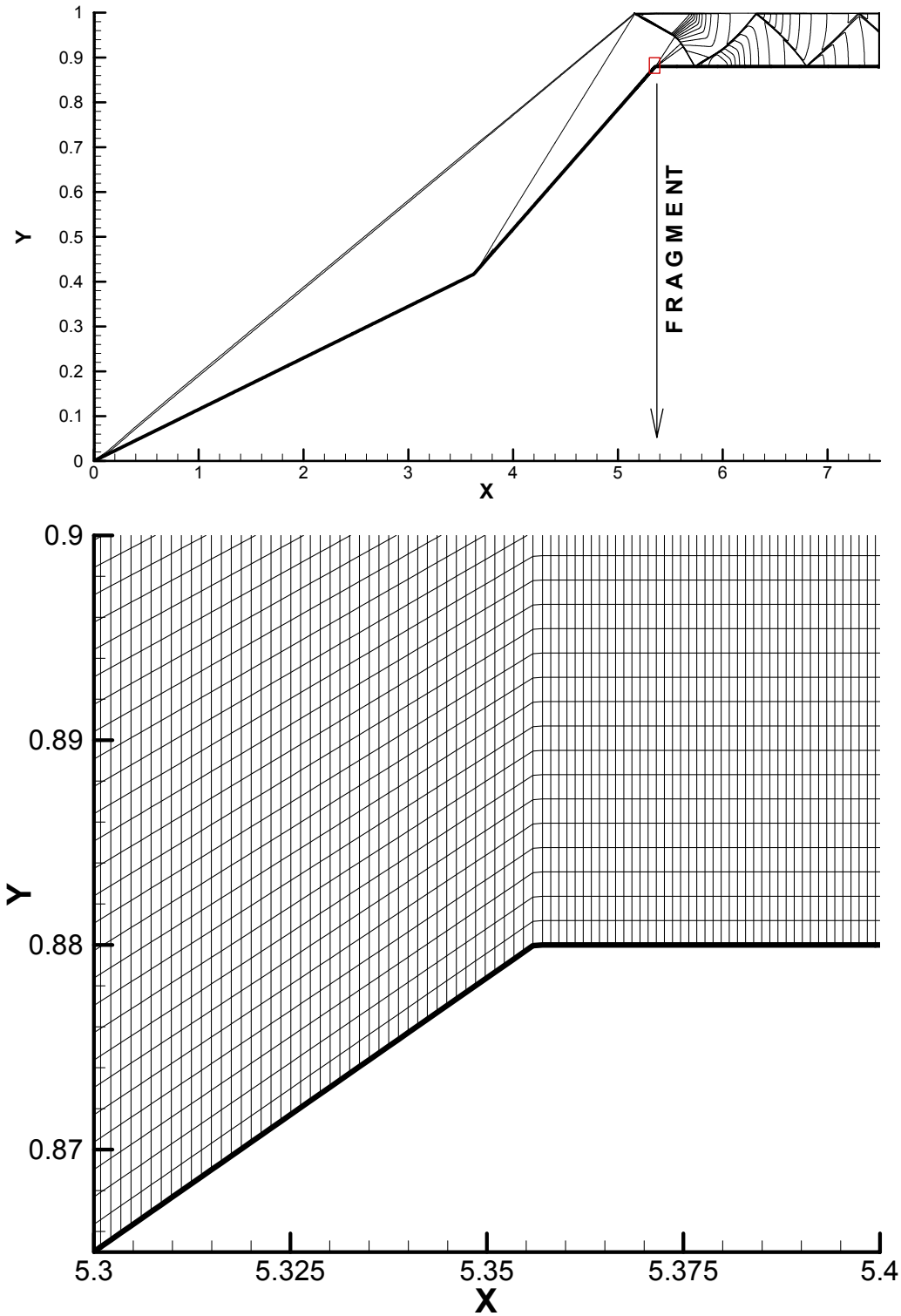

Fig.35 Pressure contours in inlet at design conditions (a) and fragment of computational grid (b) in red rectangular area marked in (a). M_d=10, M_0=10, θ_N=15°, F_{th}=0.12

a)

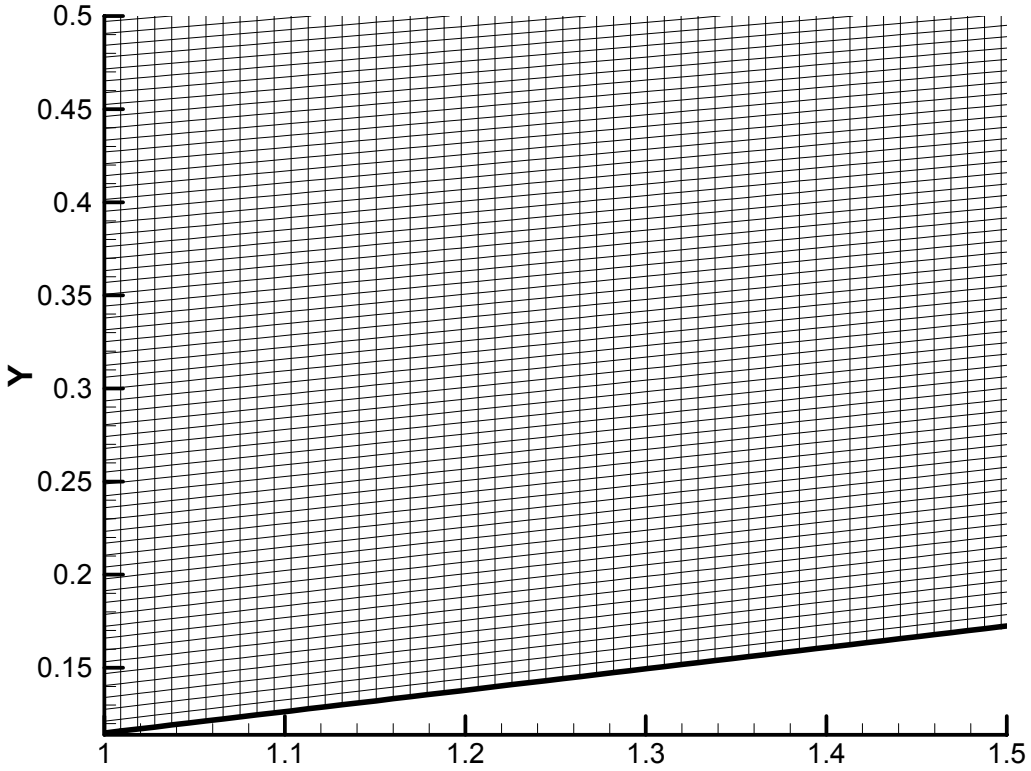

b)

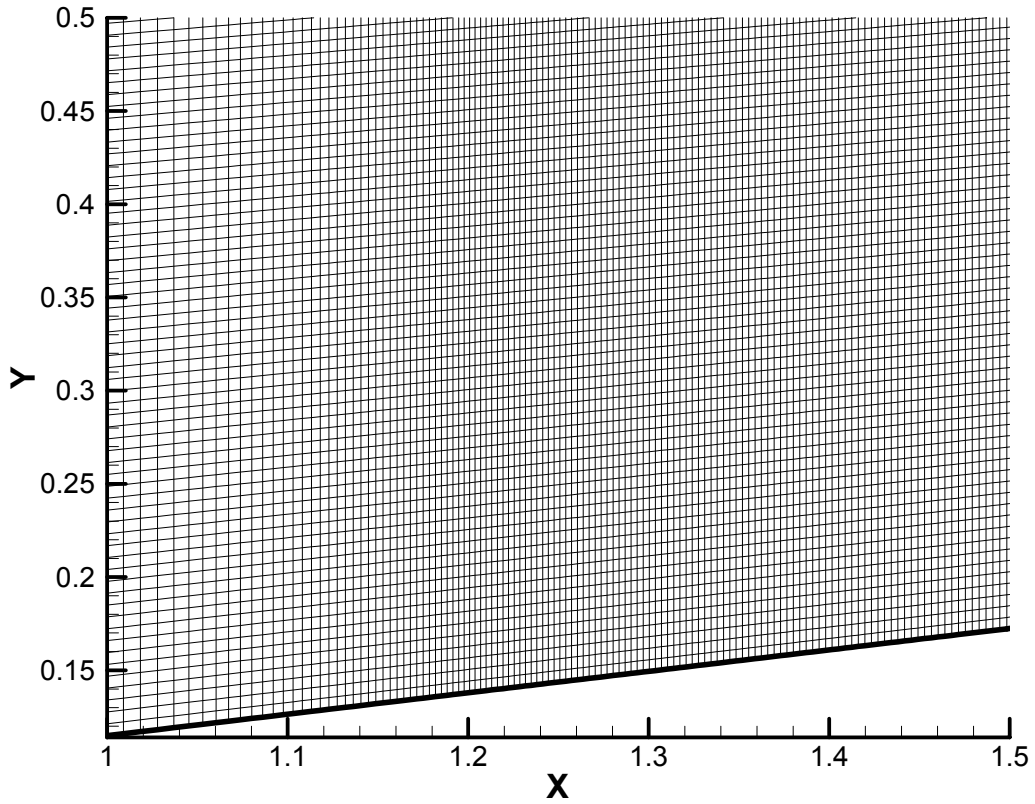

Fig.36 Fragment of computational grid in scramjet inlet without MHD generator (a) and with MHD generator located in the range $1 \le x \le 1.2$ (b). M_0=6, B=3T, q_i=50 W/cm^3.

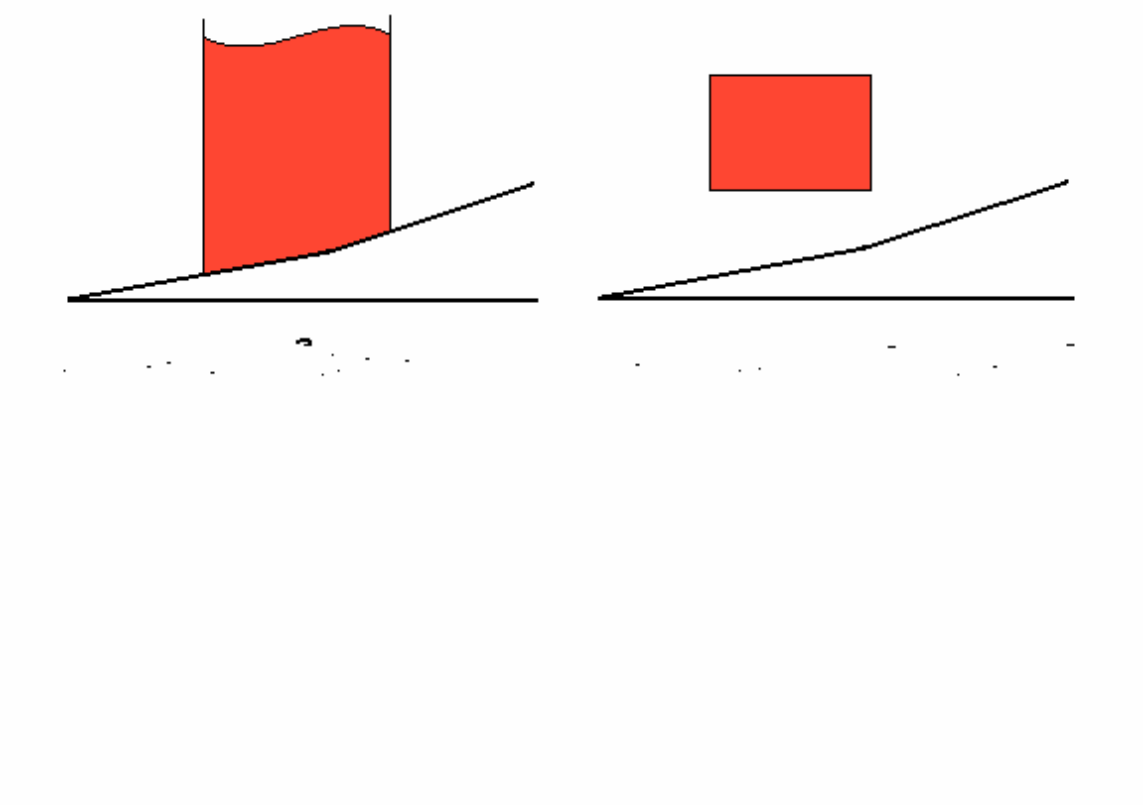

Fig.37 Simple shapes of ionized region used in calculations of flow-fields in MHD-controlled inlet

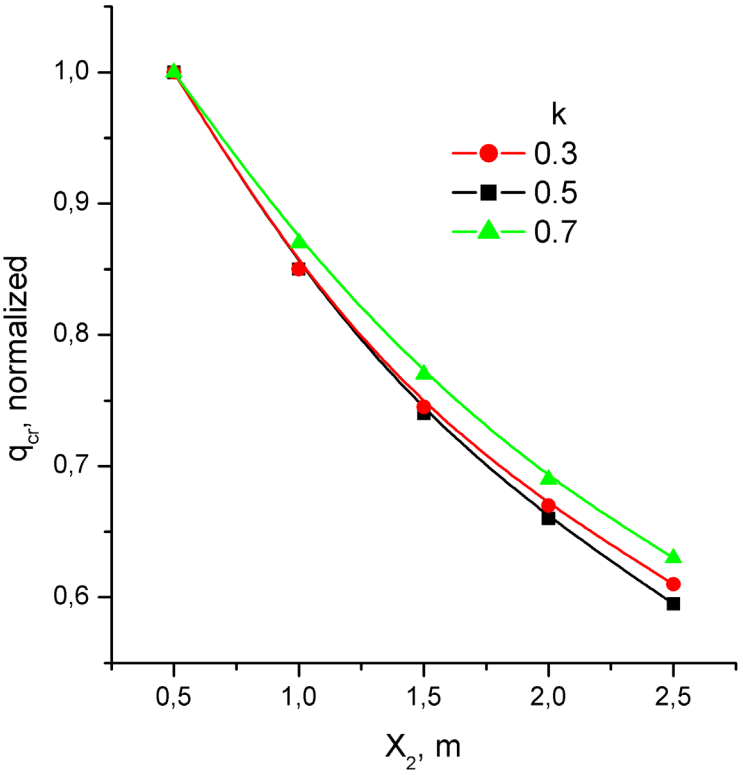

a)

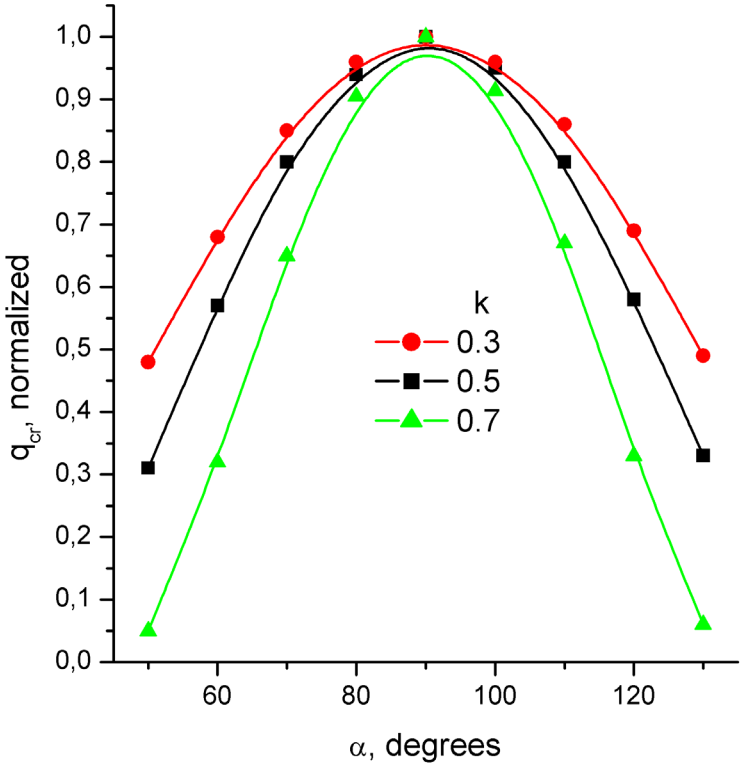

b)

Fig.38 Normalized critical power input to ionization in scramjet inlet vs length of ionized region (a) and vs orientation of magnetic field (b). $M_0=6$, $B=1T$. α=90° in (a) and x_2=0.5 m in (b).

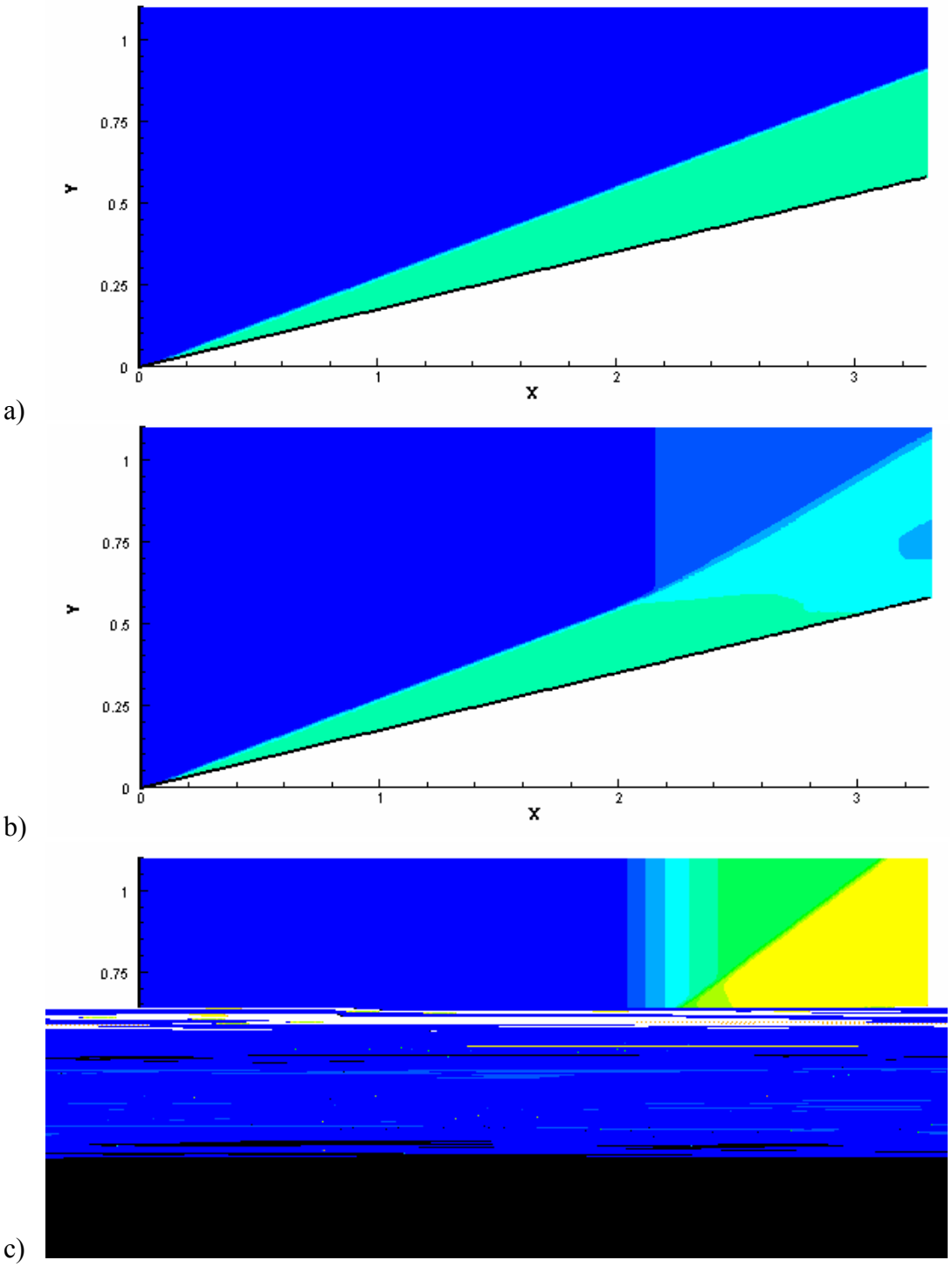

Fig.39. Pressure colors maps in stream flowing the wedge with θ=10°. M_0=8, q_i=4W/cm^3, k=0.5. a) B=0, b) B=3T, α=45°, c) B=3T, α=90°. Ionized region located in 2≤x≤2.5.

a)

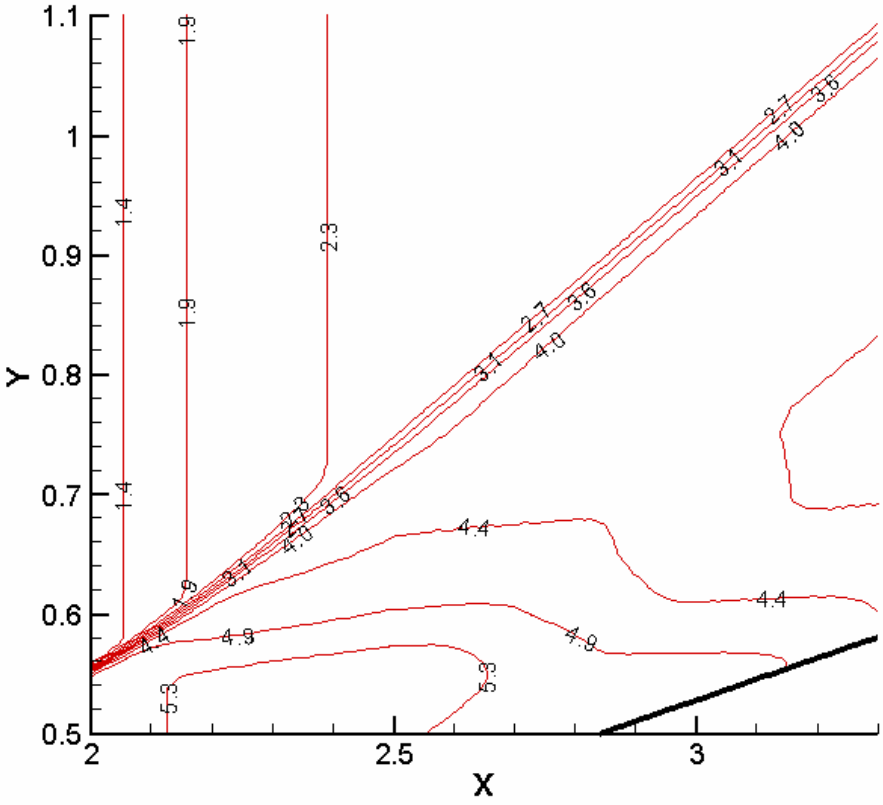

b)

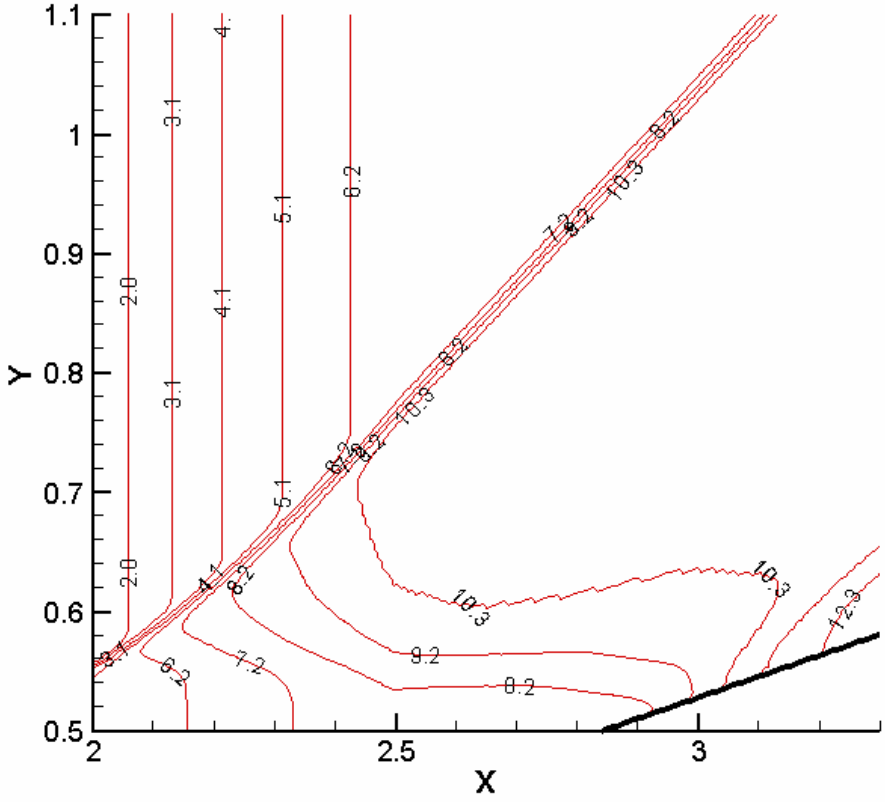

Fig.40 Pressure contours in stream flowing the wedge with θ=10°. M_0=8, q_i=4W/cm^3, k=0.5. a) B=3T, α=45°, b) B=3T, α=90°. Ionized region located in 2≤x≤2.5.

a)

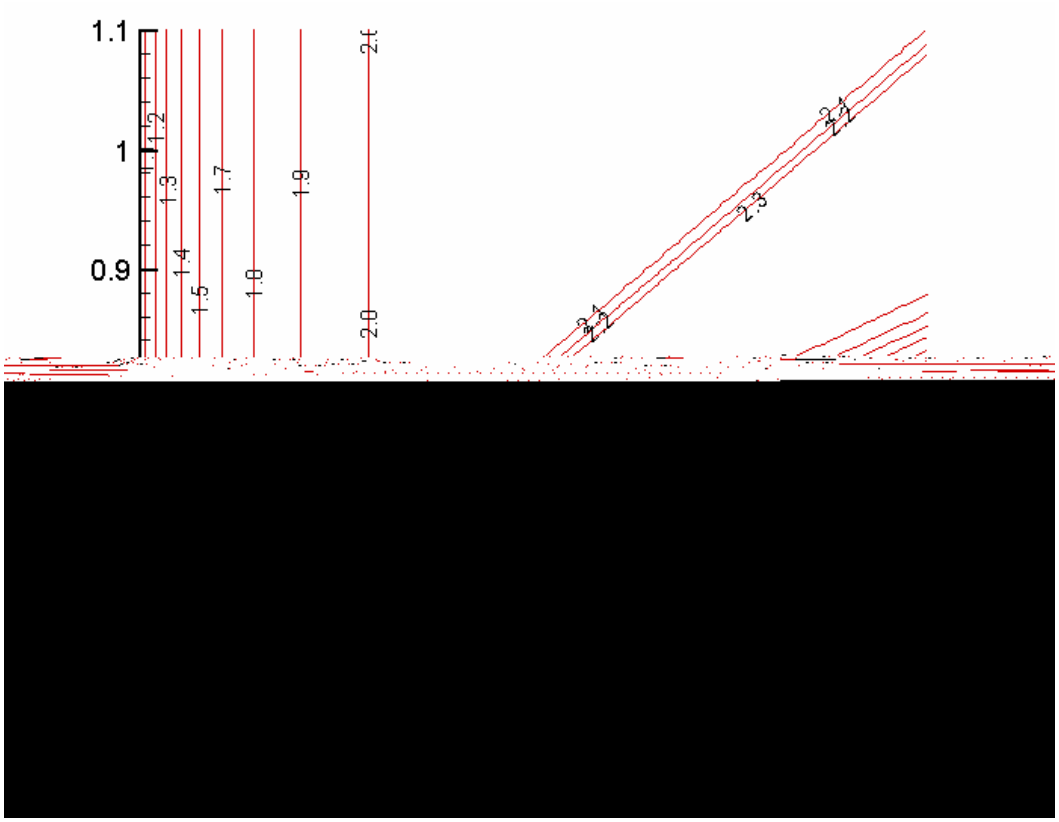

b)

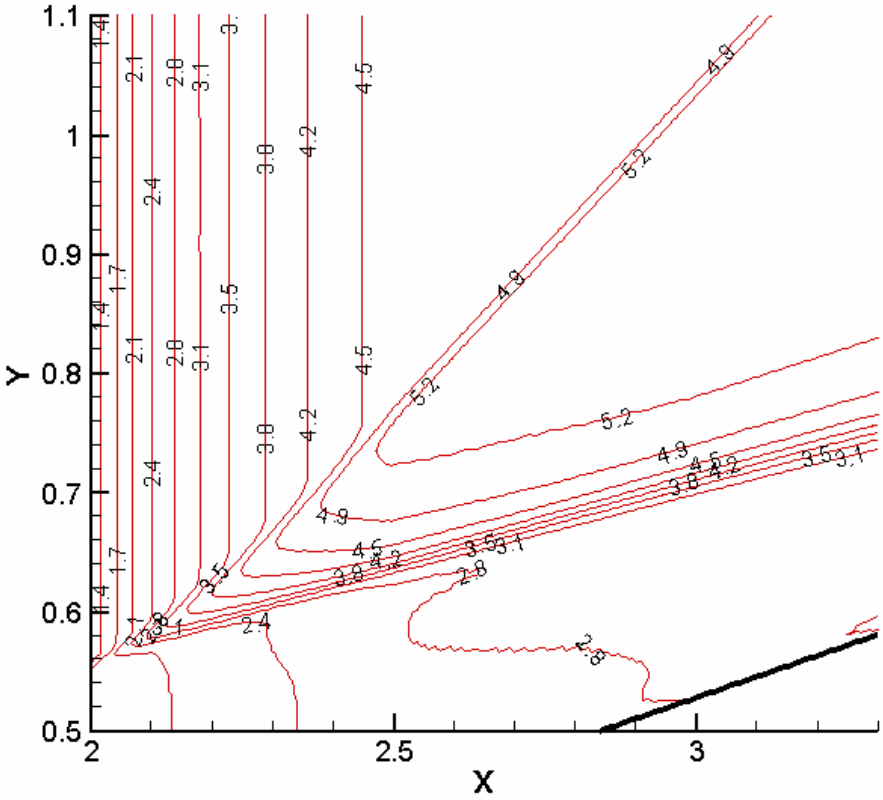

Fig.41 Temperature contours in stream flowing the wedge with θ=10°. M_0=8, q_i=4W/cm^3, k=0.5. a) B=3T, α=45°, b) B=3T, α=90°. Ionized region located in 2≤x≤2.5.

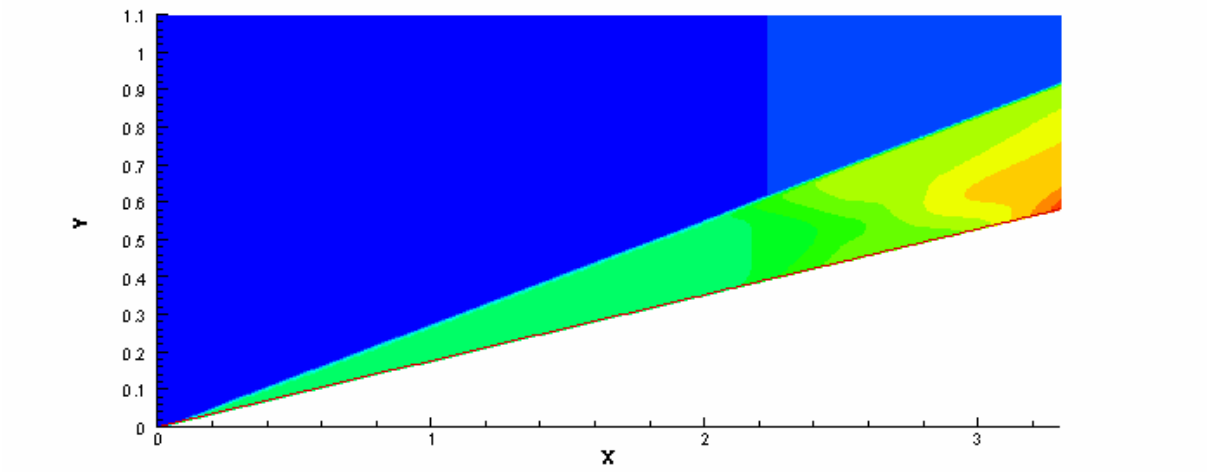

Fig.42 Pressure colors map in stream flowing the wedge with θ=10°. M_0=8, q_i=4W/cm^3, k=0.5, B=3T, α=135°. Ionized region located in 2≤x≤2.5.

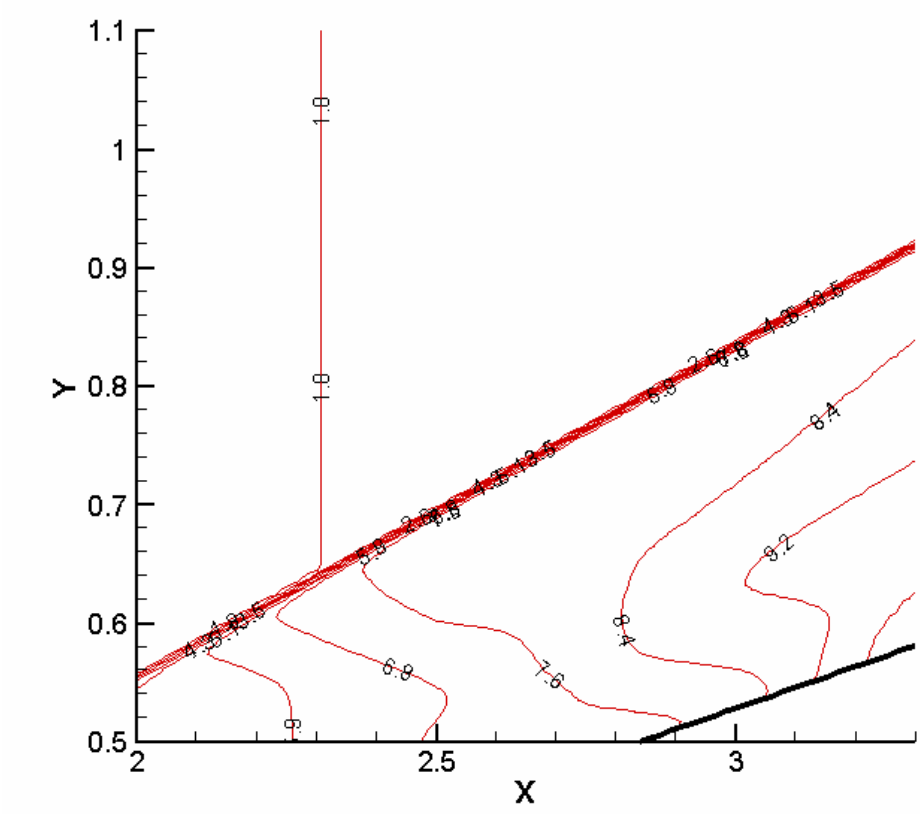

Fig.43 Pressure contours in stream flowing the wedge with θ=10°. M_0=8, q_i=4W/cm^3, k=0.5. B=3T, α=135°. Ionized region located in 2≤x≤2.5.

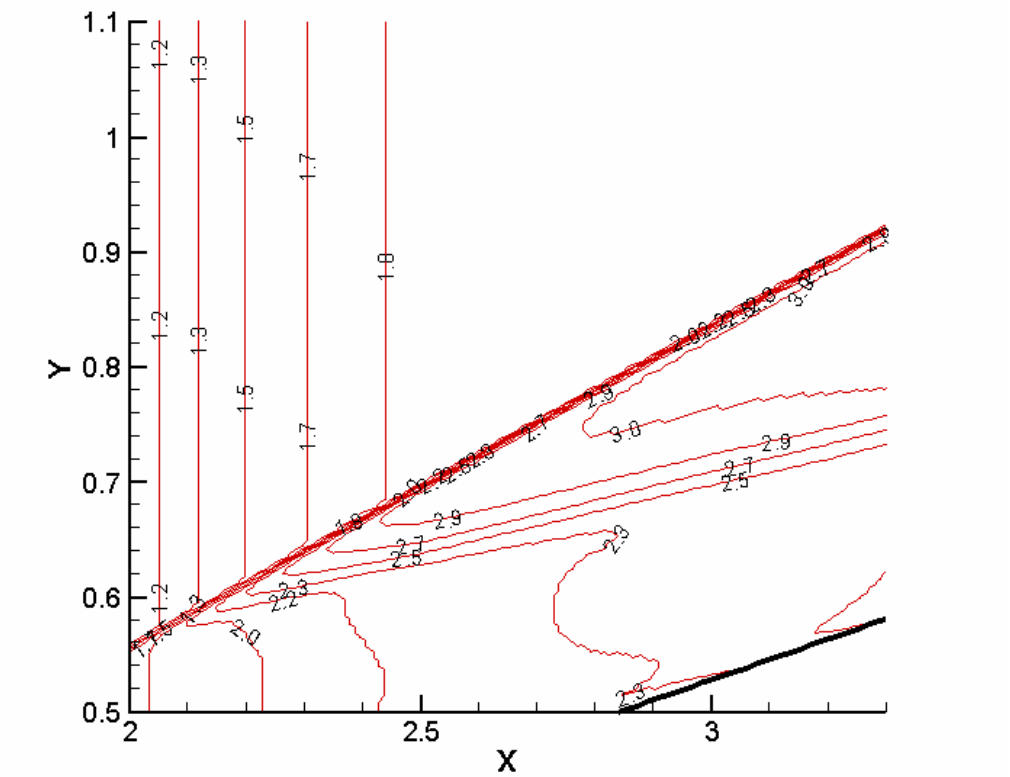

Fig.44 Temperature contours in stream flowing the wedge with θ=10°. M_0=8, q_i=4W/cm^3, k=0.5. B=3T, α=135°. Ionized region located in 2≤x≤2.5.

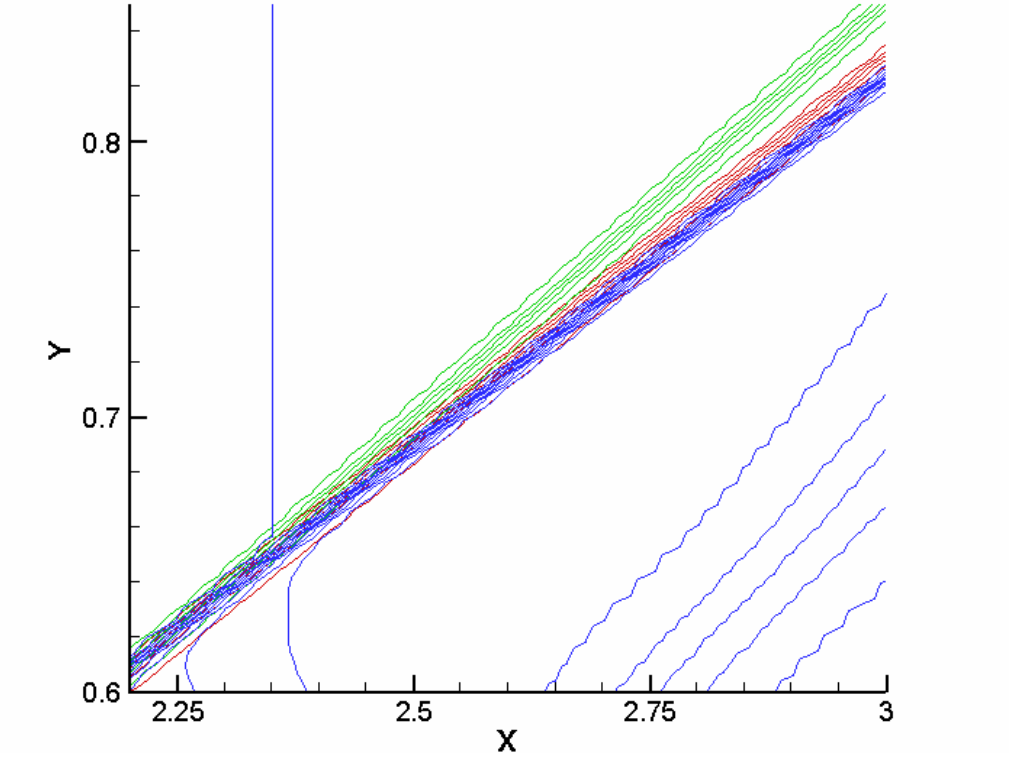

Fig.45. Position of oblique shock in stream flowing around the wedge with θ=10°. M_0=8, q_i=4W/cm^3, k=0.5. Red contours correspond to wedge without MHD control; for blue contours B=5T, α=135°; for green contours B=1T, α=45°. Ionized region located in 2≤x≤2.5.

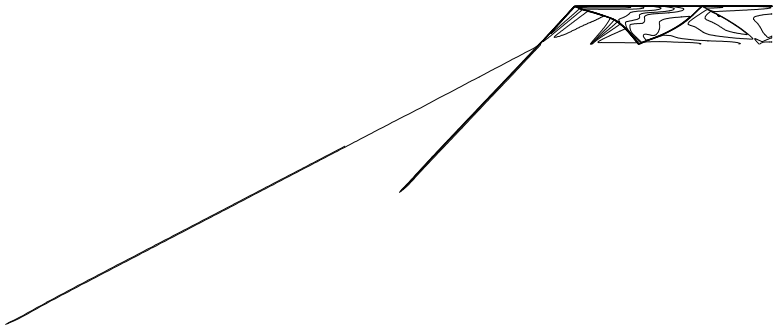

a)

a)

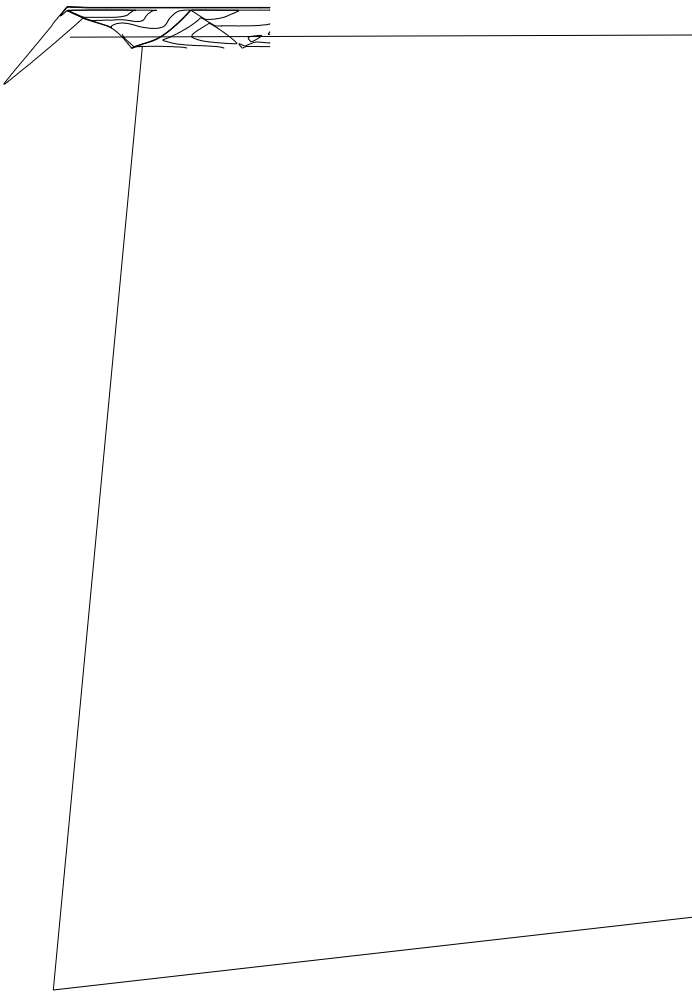

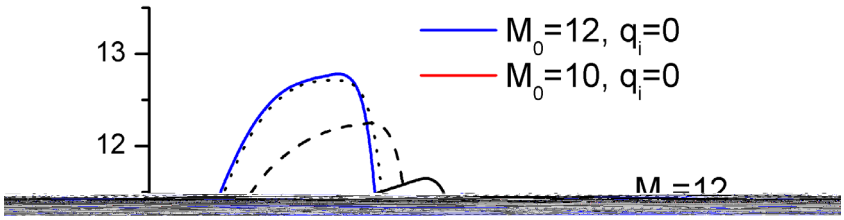

Fig.48 Density distribution across the channel at x=7.1 in MHD controlled inlet at various values of power density spent on ionization. M_d=10, θ_N=15°, F_{th}=0.12, B=1T, α=45°, k=0.5, q_i values are shown in the figure. Ionized region is located in $0 \le x \le 5$, $y \le 0.2x$.

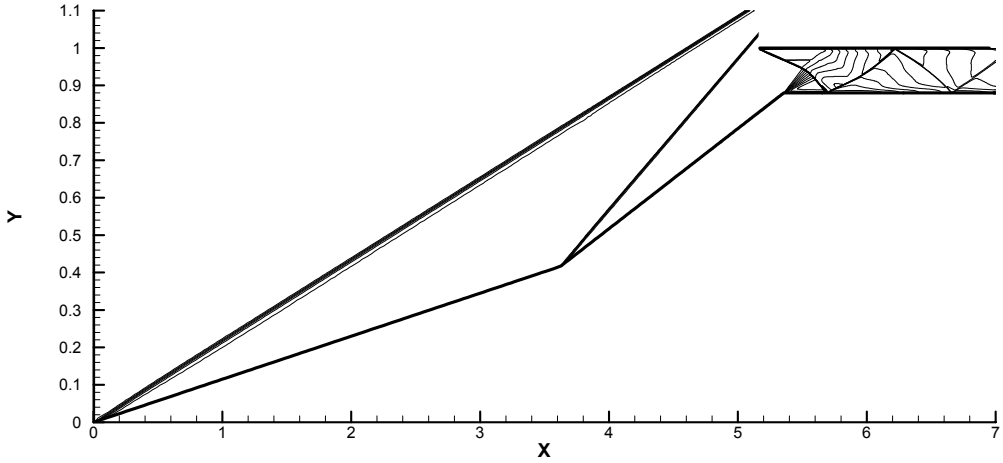

Fig.49. Mach number contours in scramjet inlet. M_0=8, M_d=10, θ_N=15°, F_{th}=0.12.

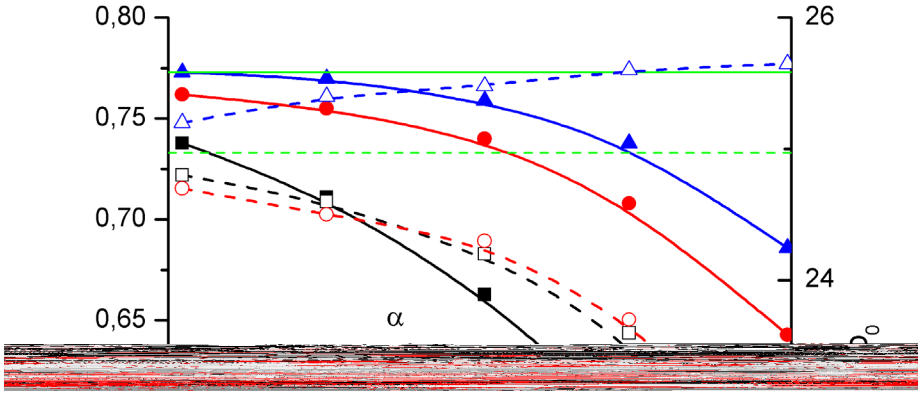

a)

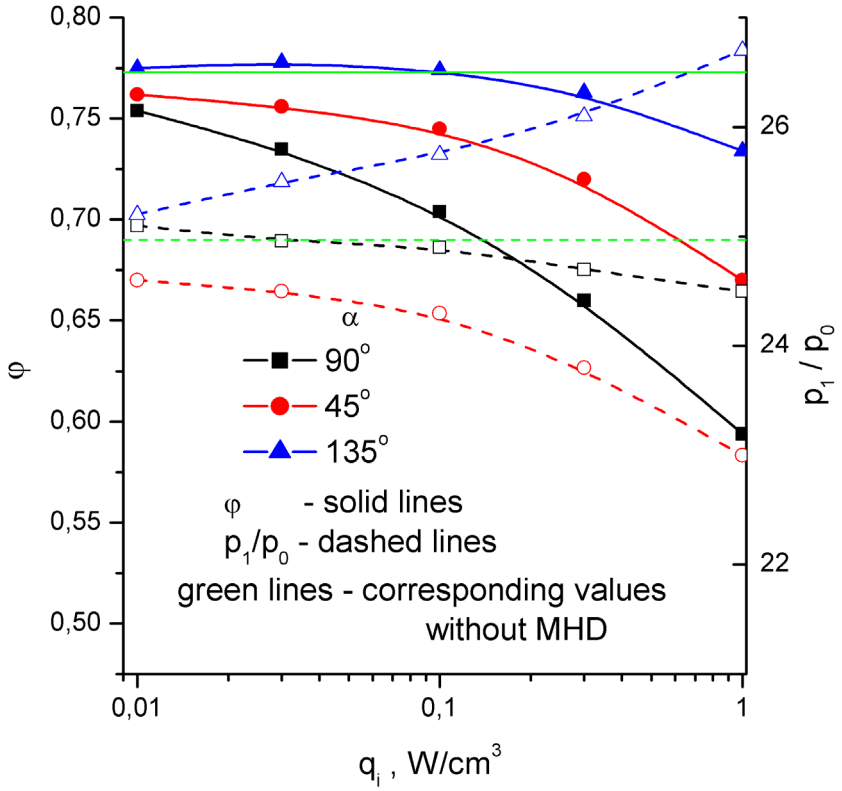

b)

Fig.50. Relative mass flow rate and pressure increase in MHD controlled inlet vs power density spent on ionization for various magnetic field orientations. Ionized region is located in $x_1 \le x \le x_1+1$. M_0=8, M_d=10, θ_N=15°, F_{th}=0.12, B=1T, k=0.5, α values are shown in the figure. (a) x_1=0, (b) x_1=1.

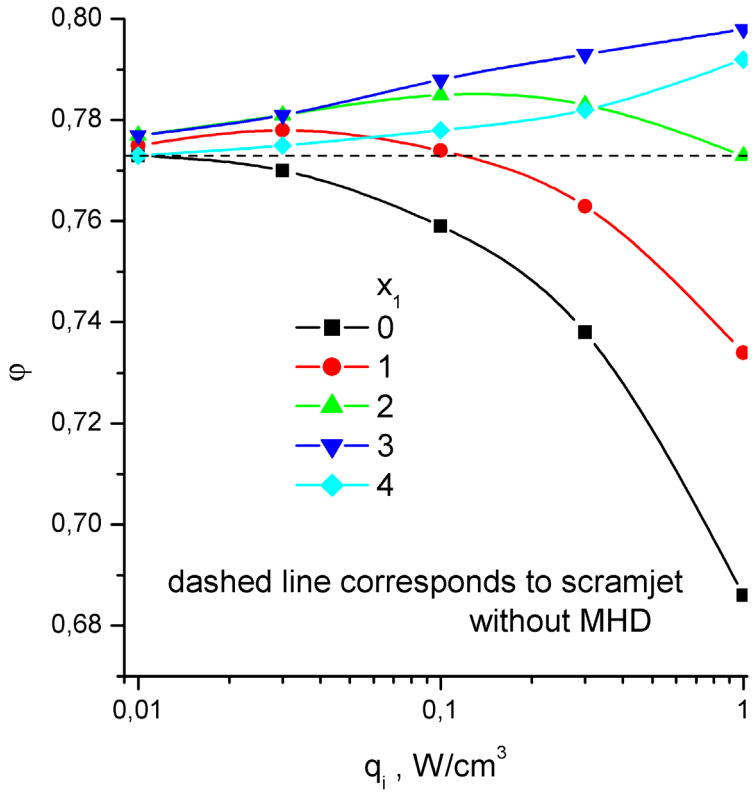

a)

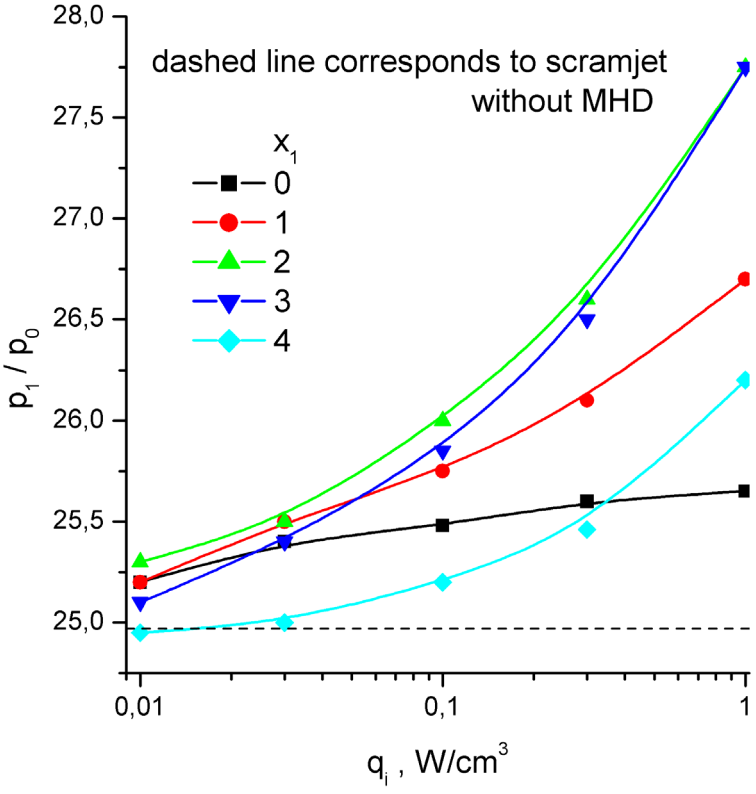

b)

Fig.51. Relative mass flow rate (a) and pressure increase (b) in MHD controlled inlet vs power density spent on ionization. Ionized region is located in $x_1 \le x \le x_1+1$. $M_0=8$, $M_d=10$, $\theta_N=15°$, $F_{th}=0.12$, $B=1$T, $k=0.5$, $\alpha=135°$, x_1 values are shown in the figure.

a)

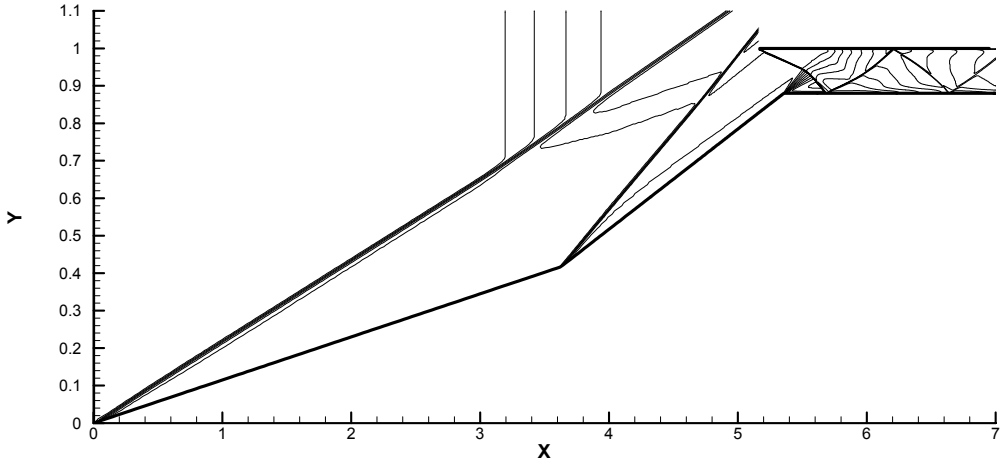
Y
X
0
1
2
3
4
5
6
7
0.1
0.2
0.3
0.4
0.5
0.6
0.7
0.8
0.9
1
1.1

b)

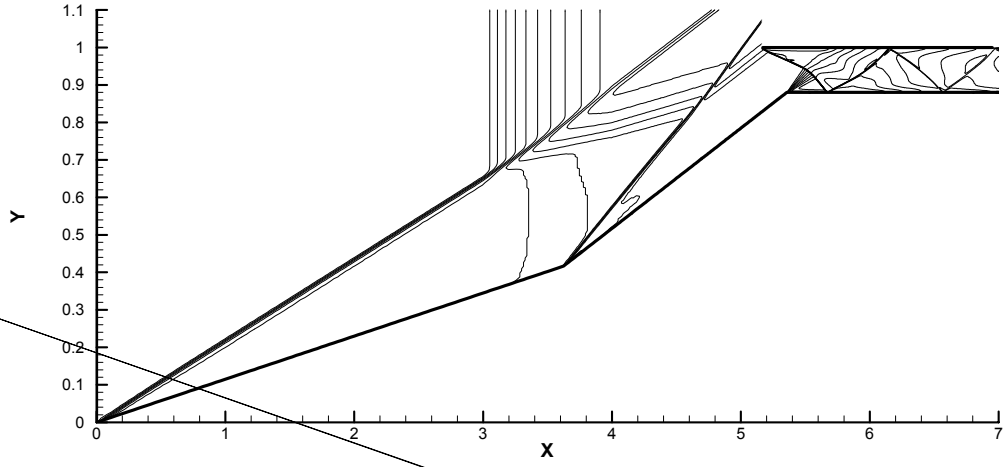
Y
X
0
1
2
3
4
5
6
7
0.1
0.2
0.3
0.4
0.5
0.6
0.7
0.8
0.9
1
1.1

c)

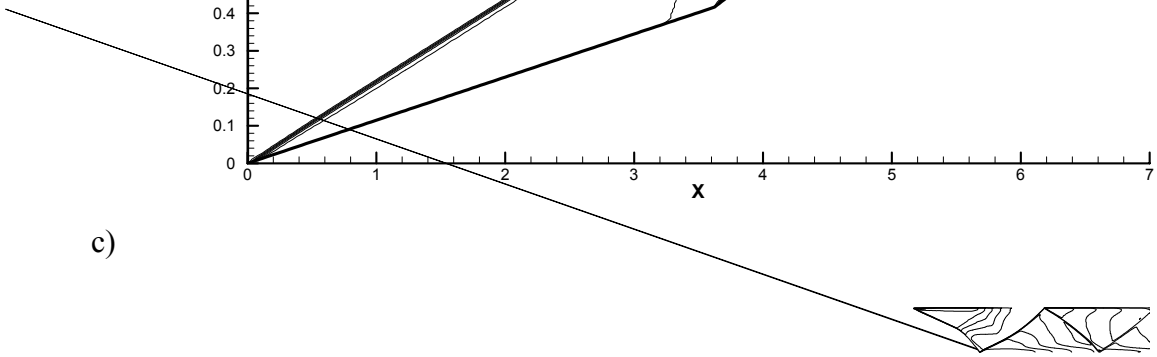

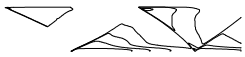

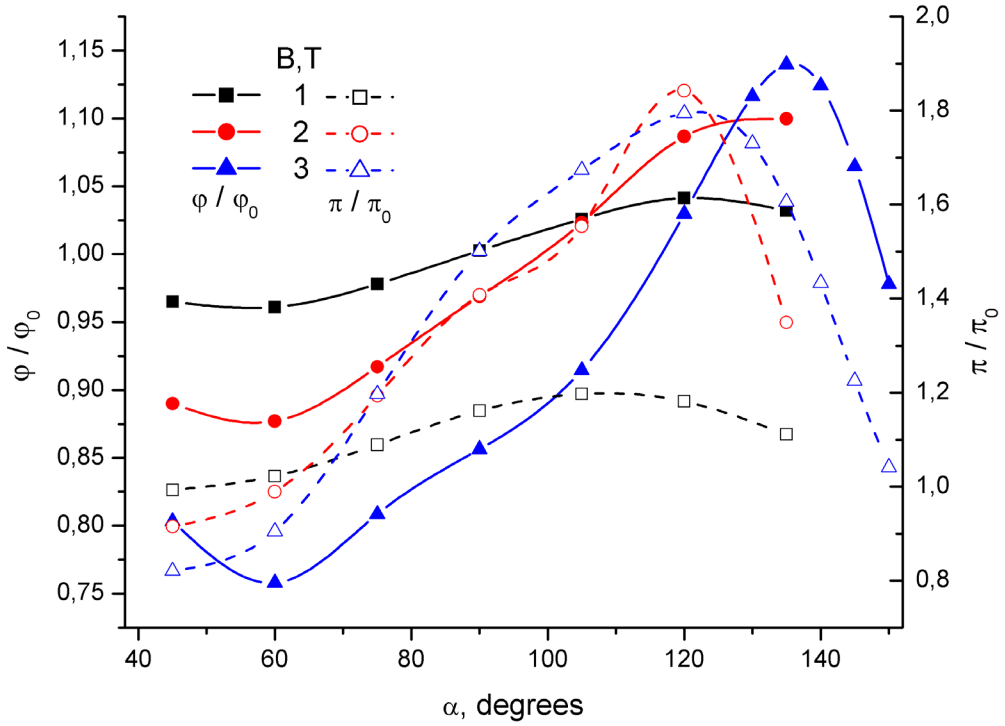

Fig.54. Normalized relative air mass flow (φ/φ_0) and flow compression (π/π_0) in MHD controlled inlet vs magnetic field orientation for various values of magnetic induction. M_0=8, M_d=10, θ_N=15°, F_{th}=0.12, k=0.5, q_i=1W/cm^3. Ionized region is located in $3 \le x \le 4$.

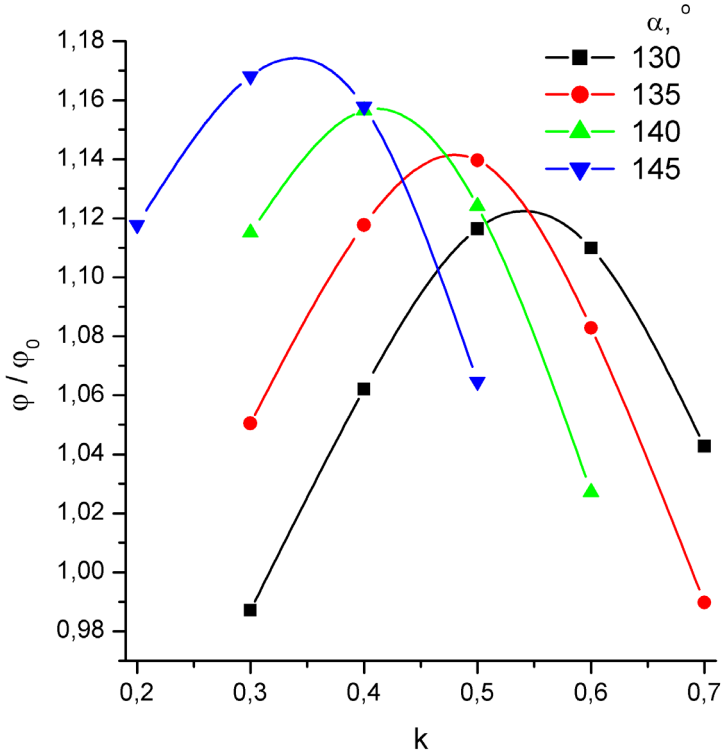

Fig.55. Normalized relative mass-flow rate in MHD controlled inlet vs load factor for various α. M_0=8, M_d=10, θ_N=15°, F_{th}=0.12, B=3T, q_i=1W/cm^3. Ionized region is located in $3 \le x \le 4$.

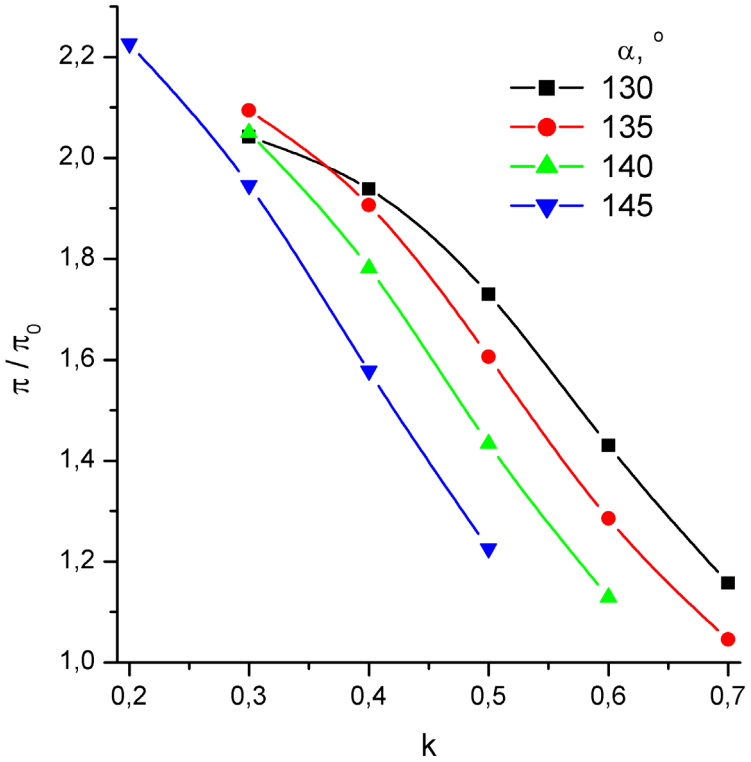

Fig.56. Normalized relative pressure increase in MHD controlled inlet vs load factor for various α. M_0=8, M_d=10, θ_N=15°, F_{th}=0.12, B=3T, q_i=1W/cm^3. Ionized region is located in $3 \le x \le 4$.

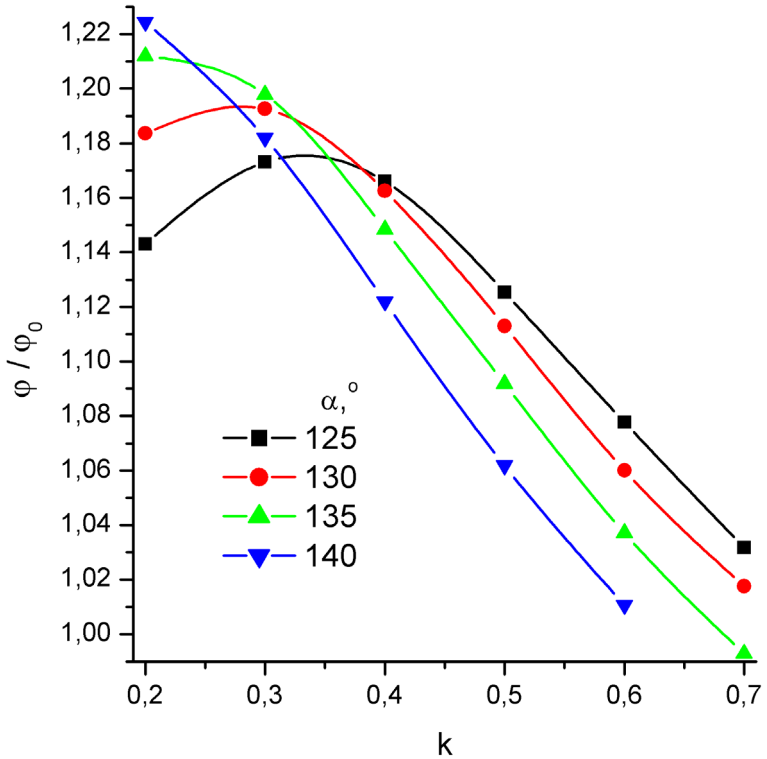

Fig.57. Normalized relative air mass flow in MHD controlled inlet vs load factor for various α. M_0=6, M_d=10, θ_N=15°, F_{th}=0.12, B=3T, q_i=1W/cm^3. Ionized region is located in $3 \le x \le 4$.

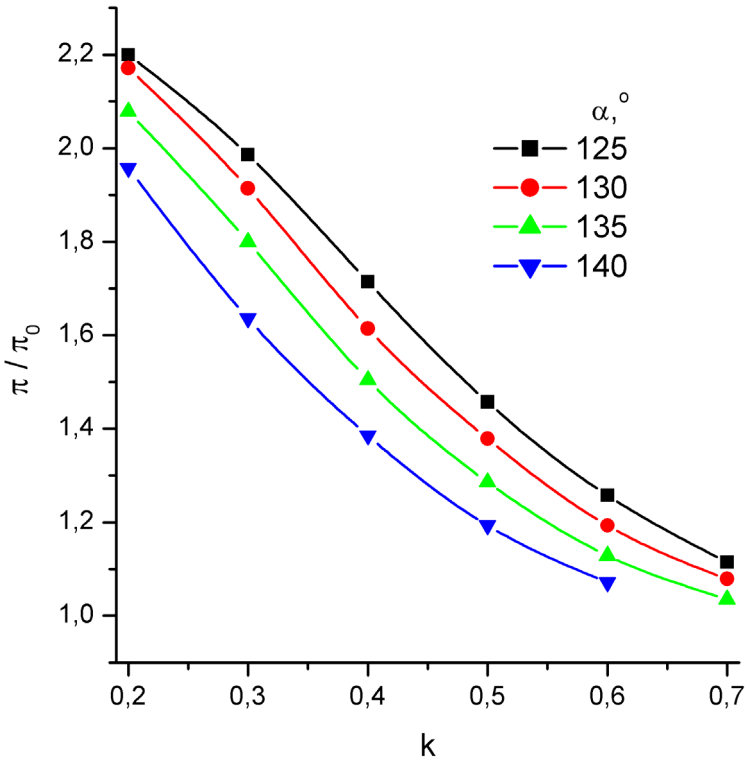

Fig.58. Normalized relative pressure increase in MHD controlled inlet vs load factor for various α. M_0=6, M_d=10, θ_N=15°, F_{th}=0.12, B=3T, q_i=1W/cm^3. Ionized region is located in $3 \le x \le 4$.

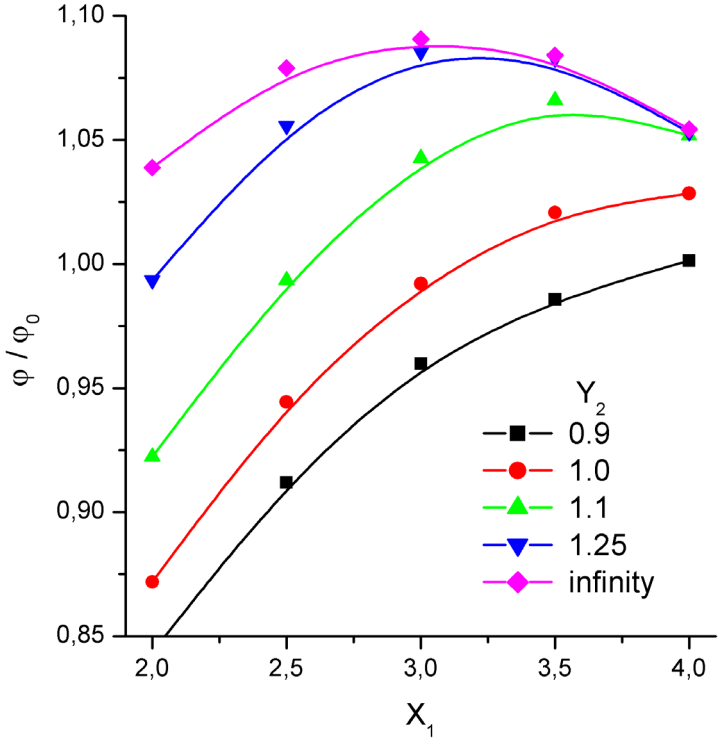

Fig.59 Normalized relative air mass flow in MHD controlled inlet vs X_1 for various height of ionized region Y_2. M_0=8, M_d=10, θ_N=15°,F_{th}=0.12, B=3T, α=135°, q_i=0.1W/cm^3, k=0.5. Ionized region is located in $X_1 \le x \le X_1+1$ and $y \le Y_2$

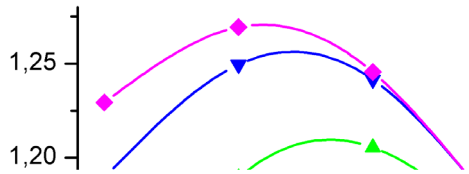

Fig.60. Normalized relative pressure increase in MHD controlled inlet vs X_1 for various height of ionized region Y_2. M_0=8, M_d=10, θ_N=15°,F_{th}=0.12, B=3T, α=135°, q_i=0.1W/ 2.0281 0 0 12.0281

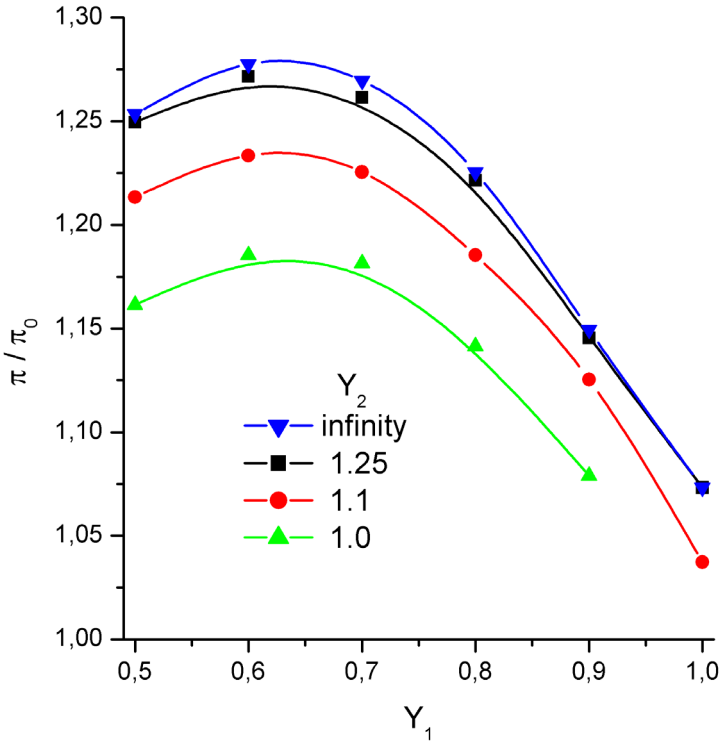

Fig.62. Normalized relative pressure increase in MHD controlled inlet vs Y_1 for various values of Y_2. M_0=8, M_d=10, θ_N=15°,F_{th}=0.12, B=3T, α=135°, q_i=0.1W/cm^3, k=0.5. Ionized region is located in $3 \le x \le 4$ and $Y_1 \le y \le Y_2$

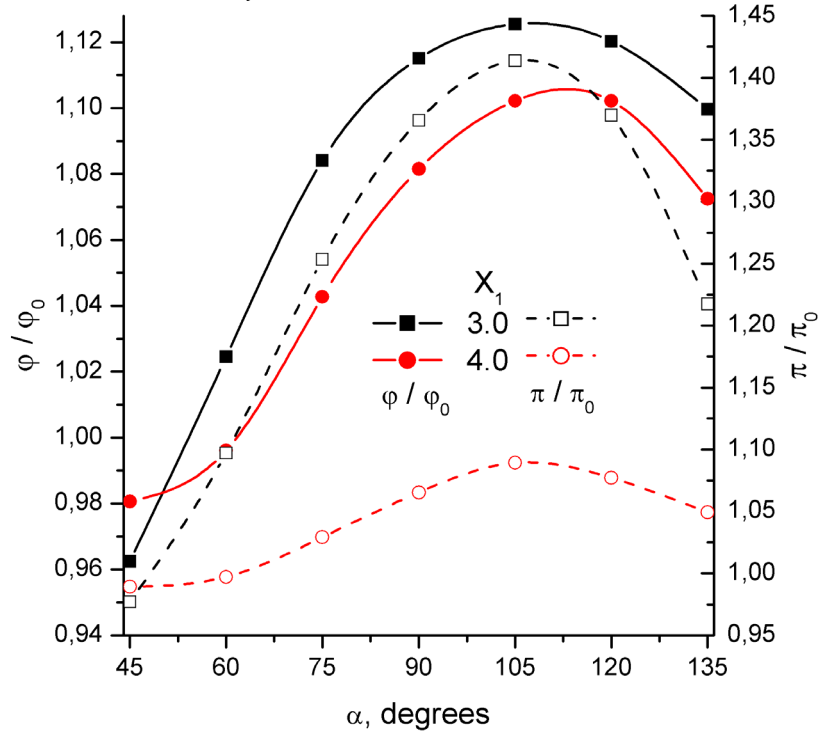

Fig.63. Normalized relative air mass flow and pressure increase in MHD controlled inlet vs α for various values of X_1. M_0=8, M_d=10, θ_N=15°,F_{th}=0.12, B=3T, q_i=1W/cm^3, k=0.5. Ionized region is located in $X_1 \le x \le X_1+1$ and $0.9 \le y \le 1.0$.

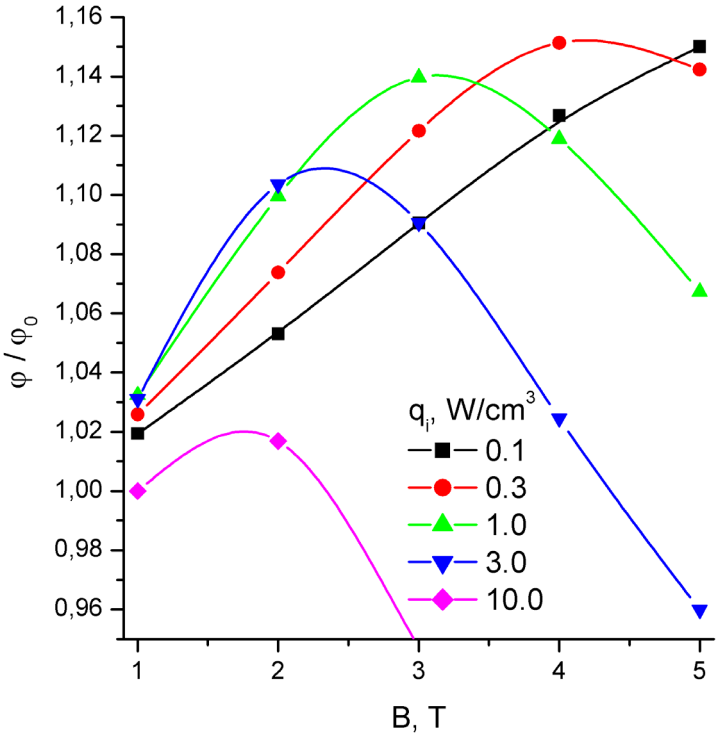

Fig.64. Normalized relative air mass flow in MHD controlled inlet vs magnetic induction B for various values of q_i. M_0=8, M_d=10, θ_N=15°,F_{th}=0.12, α=135°, k=0.5. Ionized region is located in $3 \le x \le 4$.

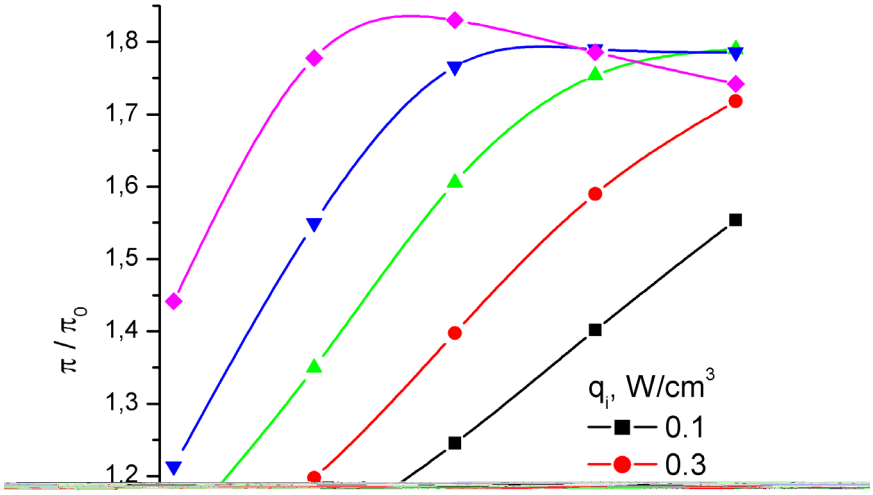

Fig.65 Normalized relative pressure increase in MHD controlled inlet vs magnetic induction B for various values of q_i. M_0=8, M_d=10, θ_N=15°,F_{th}=0.12, α=135°, k=0.5. Ionized region is located in $3 \le x \le 4$.

5. CONCLUSIONS

The main results obtained in this report are as follows:

- The model of nonequilibrium plasma sustained by e-beam is developed. Simple relations to calculations of electron concentration as a function of power density spent on ionization and flow parameters are obtained.
- Quasi-1D model of MHD generator with nonequilibrium conductivity is developed. Requirements to parameters of ionizer and magnetic systems at which nonequilibrium MHD generator operates in self-sustained mode are formulated.
- Quasi-1D model of scramjet with MHD control by internal flow is developed. Requirements for parameters of MHD generator and other subsystems of the scramjet, at which MHD control increases scramjet specific impulse, are formulated. Limitations on flight Mach number at which internal MHD generator can improve scramjet performance are obtained. Analysis of scramjet with MHD control shows that MHD generator with nonequilibrium conductivity can be used on hypersonic aircraft both for electric power production and for scramjet specific impulse increasing. Requirements for parameters of the MHD generator depend on its functionality.
- 2-D model of MHD controlled inlet of scramjet is developed. Numerical calculations of flow fields in MHD controlled inlet are carried out in a wide range of parameters variation. Obtained results show that MHD control allows us to modify flow field in inlet of scramjet at off-design conditions. By using MHD influence on flow we can control oblique shocks position, air mass flow and flow compression in inlet. In proper choice of region of MHD interaction, configuration of magnetic field and load factor the MHD control in scramjet inlet allows us essentially, improve inlet performance at off-design conditions.

Next steps need to be done in order to create more overall physical model of MHD controlled inlet. It is necessary to keep in mind real configurations of magnetic field, consider real propagation of e-beam in electrical and magnetic fields in nonhomogeneous medium taking into account processes of plasma kinetics. Influence of space charge distribution on electric field and e-beam propagation need to be considered too.

6. REFERENCES

1. Averaged Energy Required to Produce an Ion Pair. ICRU report 31, 1979
2. S.O.Macheret, M.N.Shneider and R.B.Miles, "Energy-Efficient Generation of Nonequilibrium Plasmas and Their Applications to Hypersonic MHD Systems", AIAA 2001-2880.
3. The Calculation of Electrokinetic Properties of Air and Nitrogen Plasma Excited By E-Beam. The report of Hypersonic Systems Research Institute. 1995, St. Petersburg, Russia.
4. Macheret S.O.,.Shneider M.N,.Miles R.B, Modeling of air plasma generation by electron beams and high-voltage pulses, AIAA 2000-2569
5. Kossyi I.A., Kostinsky A.Yu., Matveyev A.A., Silakov V.P., Kinetic scheme of the non-equilibrium discharge in nitrogen-oxygen mixtures, Plasma Sources Sci. Technol.,v.1,1992, p.207-220.
6. Stopping Powers for Electrons and Positrons. ICRU report 37, 1984.
7. Breev V.V., Gubarev A.V., Panchenko V.P., "Supersonic MHD generators", Energoatomizdat, Moscow, 1986 (in Russian)
8. Sheikin E.G. Analytical solution of the system of MHD equations in the quasi-one-dimensional approximation for regimes in which the flow parameters vary monotonically along the channel. Sov. Phys. Tech. Phys, v37, 1133, 1992
9. Sheikin E.G. Optimum choice of parameters for an MHD generator. Tech. Phys., v38, 741, 1993.
10. Kuranov A.L., Kuchinsky V.V. and Sheikin E.G, Scramjet with MHD control under "AJAX" concept. Requirements for MHD systems., AIAA paper 2001-2881
11. Fraishtadt V.L., Kuranov A.L., Sheikin E.G., Use of MHD systems in hypersonic aircraft, Technical Physics v.43, 1309, 1998.
12. Golovachev Yu.P., Suschikh S.Yu., "Weakly Ionized Flows in Supersonic Inlets Subjected to the External Electromagnetic Fields," in Perspectives of MHD and Plasma Technologies in Aerospace Applications, IVTAN, Moscow, March 24-25, 1999, Proceedings, p.105
13. Macheret S.O., Shneider M.N., and Miles R.B., "External Supersonic Flow and Scramjet Inlet Control by MHD with Electron Beam Ionization," AIAA Paper 2001-0492

Project Manager  **Alexander L. Kuranov**

DESCRIPTION OF VARIABLES

used in final report on the ISTC project № 2088p, "Theoretical and experimental research of capabilities of MHD technology to control gas flow with non-equilibrium ionization"

A	Cross-sectional area	m^2
a_i , b_i	Fitting parameters	
B	Magnetic induction	T
B_{cr}	Critical value of magnetic induction	T
B_{min}	Minimal value of magnetic induction	T
c_p	Specific heat at constant pressure	$J/(kgK)$
c_v	Specific heat at constant volume	$J/(kgK)$
E	Electric field intensity	V/m
e	Electron charge	C
E_b	Initial energy of electrons in e-beam	keV
F, f	Lorentz force	N/m^3
F_{th}	Relative value of the inlet throat	
g	Acceleration of gravity	m/s^2
$\overline{g_{en}}$	Averaged relative velocity of electrons	m/s
h	Static enthalpy	J/kg
H_u	Calorific value of fuel	J/kg
I	E-beam induced ionization rate	$cm^{-3}s^{-1}$
I_{sp}	Specific impulse	s
j	Current density	A/m^2
j_b	E-beam current density	A/cm^2, A/m^2
k	Load factor	
k_a	Rate constant for attachment of electrons	cm^6/s
k_c	Electron scattering rate constant	m^3/s
k_d	Rate constant for detachment of electrons	cm^3/s
L	Length of MHD generator	m
L_0	Stochiometric factor	
M	Mach number	
M_∞ , M_0	Flight Mach number	
M_d	Design Mach number	
M_{max}	Maximal flight Mach number. (MHD interaction increase specific impulse of scramjet in the case when $M_\infty < M_{max}$)	
m_e	Electron mass	kg
$\dot{m}$	Air mass flow	kg/s
N, n	Gas concentration	cm^{-3}
n_-	Negative ions concentration	cm^{-3}
n_+	Positive ions concentration	cm^{-3}
n_e	Electron concentration	cm^{-3}
N_{O_2}	Concentration of oxygen molecules in air	cm^{-3}
p	Pressure	Pa, atm
q_{cr}	Critical power density spent on flow ionization	W/cm^3, W/m^3
q_g	Power density produced by MHD generator	W/cm^3, W/m^3
q_i	Power losses by electron beam in unit of time in unit of volume (power density spent on ionization)	W/cm^3, W/m^3
q_{opt}	Optimal value of the power density spent on flow ionization	W/cm^3
q_r	Power density released in result of plasma recombination	W/m^3

$\overline{Q_{en}}$	Averaged transport cross-section of electron collisions	m^2
r	Ratio of power spent on ionization of flow in MHD generator and power produced by MHD generator ($r=W_{ion}/W_g$)	
R	Gas constant	$J/(kgK)$
S_v	MHD interaction parameter	
T	Temperature	K
t	Time	s
T_e	Electron temperature	K
T_g	Gas temperature	K
v	Flow velocity	m/s
V	Volume	m^3
W_0	Energy of flow	W
W_a	Power transferred to MHD accelerator	W
W_g	Power produced by MHD generator	W
W_i	Ionization cost	eV
W_{ion}	Power put to flow ionization in channel of MHD generator	W
x,y,z	Cartesian coordinates	
Y	Electron stopping power in air	$MeV \cdot cm^2 g^{-1}$
α	Air-fuel ratio (used in chapter 3)	
α	Angle of magnetic field orientation (used in chapter 4)	degree of arc
β	Rate constant for electron-ion recombination (used above equation 14)	cm^3/s
β	Hall parameter (used after equation 14)	
β_{ii}	Rate constant for ion-ion recombination	cm^3/s
γ	Specific heat ratio	
η, η_g	Enthalpy extraction ratio	
η_{ion}	Relative power spent on flow ionization ($\eta_{ion}=W_{ion}/W_0$)	
φ	Relative air mass flow in scramjet with MHD control	
φ_0	Relative air mass flow in scramjet without MHD control	
φ_N	Nozzle non-ideality factor	
μ	Electron mobility	$m^2/(V \cdot s)$
π	Flow compression in inlet with MHD control	
π_0	Flow compression in inlet without MHD control	
θ_N	Total turning angle of flow in scramjet inlet	degree of arc
ρ	Gas density	g/cm^3, kg/m^3
σ	Electrical conductivity	mho/m
σ_{in}	Total pressure recovery coefficient	
ξ	Factor which determines regime of MHD flow	
ψ	Factor which characterizes the MHD generator type (Faraday or Hall)	

Subscripts

x, y, z	Denotes the vector projection onto corresponding axes of Cartesian coordinates
0,1,2,3,4,5	Denotes the parameters at corresponding cross-sections of scramjet with MHD control according to the Fig.14.